The use of numerical models to determine the response of moored vessels to waves in a complex harbour geometry

MSc final project report

P.P.D. van der Ven

Delft University of Technology
August 2012

TU Delft Delft University of Technology

Version date: August 2013

The use of numerical models to determine the response of moored vessels to waves in a complex harbour geometry

MSc final project report

P.P.D. van der Ven

Delft University of Technology
August 2012

in cooperation with

Supervisors

Prof.ir. T. Vellinga	Delft University of Technology
Prof.em.ir. H. Ligteringen	Delft University of Technology
Dr.ir. M. Zijlema	Delft University of Technology
Ir. M. de Jong	Delft University of Technology
Ir. A.J. van der Hout	Deltares
Dr.ir. M.P.C. de Jong	Deltares

Contents

Preface

The present report concludes a final project performed within the master Hydraulic Engineering, specialization Ports and Waterways, of the faculty Civil Engineering and Geosciences of Delft University of Technology. The work for this thesis was carried out with cooperation of Deltares (former WL|Hydraulics).

The project, I feel, illustrates the breadth and depth of port engineering. Rather than being an isolated science, port engineering builds on adjacent engineering sciences. This is its most appealing attribute. Without a proper understanding of coastal dynamics, fluid mechanics, ship dynamics and terminal practice, one cannot design a successful terminal. This project therefore has required me to explore these aspects, going into offshore wave properties, maritime engineering and numerical modeling. Although using academic and experimental methods, including relevant but relatively small components, the present application required an engineering point of view.

Due to the many fields of study and the different perspectives I have sometimes found myself in a split, at times a frustrating position. Nevertheless, this is exactly why the subject has appealed to me and I feel fortunate to have worked on a project leaving questions to be answered and additional work to be carried out in the future. The contrary would have been worrying.

Acknowledgments

This project has been carried out under the supervision of professor ir. Tiedo Vellinga. I want to thank him and prof.em.ir. Han Ligteringen for their guidance throughout my project and interest in my progress.

Ir. Arne van der Hout has guided me most extensively, committing well beyond his obligations. I want to thank him for his interest in my project and his many and accurate comments on my report. The conversations I've had with Arne have contributed much to my progress, my understanding of and enthusiasm for the subject.

I have shared several interesting conversations with dr.ir. Marcel Zijlema and dr.ir. Martijn de Jong, whom I'd like to thank for sharing with me, step by step, their knowledge of (but not limited to) numerical modeling ins-and-outs and modeling applied to actual harbours, respectively.

The progress within this project would not have been possible without the elaborate help of dr.ir. Wim van der Molen. His updates of his numerical models were essential and his opinion on my progress helpful. Dr.eng. Paulo Rosa Santos has been an essential source of information and, moreover, provided useful comments on my work both during and after my project.

Finally, much of my enthusiasm for civil engineering has been excited during my traineeship, shortly before this final project. For this, I owe much thanks to ir. Gert-Jan Roelevink. The projects I have been involved in during that period have given me a frame of reference and forced me to think from an engineering perspective. Knowing the application of civil engineering showed me that it is worthwhile to plunge into this material.

Pepijn van der Ven
Delft, August 2012

List of symbols

Roman symbols

$\mathbf{A}$	Added mass matrix	[M]
a	Wave amplitude	[L]
$\mathbf{B}$	Linearized viscous damping matrix/retardation function	[MT^{-1}]
$\mathbf{C}$	Hydrostatic restoring matrix/spring coefficient from ship geometry	[MT^{-2}]
c	Wave celerity	[LT^{-1}]
c_g	Wave group celerity	[LT^{-1}]
D	Total water depth; $D \equiv h + \zeta$	[L]
E	Wave energy	[MT^{-2}]
$\vec{F}$	External load	[MLT^{-2}] for $F_1..F_3$ [$\mathrm{ML}^2\mathrm{T}^{-2}$] for $F_4..F_6$
f	Frequency; $f \equiv 1/T$	[T^{-1}]
$\vec{f}$	Forces acting on a fluid	[$\mathrm{ML}^{-2}\mathrm{T}^{-2}$]
G	Vessel center of gravity	
H	Wave height; $H \equiv 2a$	[L]
h	Mean water depth	[L]
k	Wave number; $k \equiv 2\pi/L$	[L^{-1}]
$\vec{k}$	Wave vector with length k and direction θ	[L^{-1}]
$\mathbf{K}$	Impuls response functions matrix	
L	Wave length	[L]
L_s	Ship length	[L]
L_0	Characteristic length of bathymetry changes	[L]
$\mathbf{M}$	Inertia matrix	[M]
n	Ratio of group velocity and phase velocity; $n \equiv c_g/c$	[-]
$\vec{n}$	Normal vector	[L]
p	Pressure	[$\mathrm{ML}^{-1}\mathrm{T}^{-2}$]
S_{ij}	Wave-related radiation stress with $i, j = x, y$	[MT^{-2}]
S	Surface	
T	Wave period	[T]
t	Time	[T]
$\vec{u}$	3D flow velocity vector	[LT^{-1}]
V	Vessel speed	[LT^{-1}]
$\vec{X}$	Ship position in SDF; $\vec{X} \equiv (x, y, z, \varphi, \theta, \psi)^T$	[L] for $X_1..X_3$ [-] for $X_4..X_6$

Greek symbols

ϵ	Measure of nonlinearity; $\epsilon \equiv a/h$	[-]
ϵ	Strain	[-]
ζ	Surface elevation	[L]
ζ^*	Reduced or effective wave elevation	[L]
ζ_{ar}	Wave elevation relative to ship motion	[L]
θ	Pitch	[-]
θ	Wave direction	[-]
μ	Measure of linear dispersion; $\mu \equiv kh$	[-]
ν	Kinematic viscosity coefficient	$[L^2T^{-1}]$
ρ	Fluid density	$[ML^{-3}]$
τ	Time	[T]
ϕ	Velocity potential	$[L^2T^{-1}]$
φ	Roll	[-]
ψ	Yaw	[-]
ω	Wave frequency; $\omega \equiv 2\pi/T$	$[T^{-1}]$
σ	Stress	$[ML^{-1}T^{-2}]$

Other symbols

D/Dt	Total differential operator	
$\vec{\nabla}$	Del, 3D vector differential operator	
∇	Displacement	$[L^3]$
$^{(1)}, ^{(2)}$	first and second order component respectively	

Abbreviations and definitions

2DH	Two dimensional, in horizontal plane	
RAO	Response amplitude operator	
CD	Chart datum	
DWT	Dead weight tonnage	[tonne]
DSPR	Directional spreading	[°]
FEUP	Faculdade de Engenharia da Universidade do Porto (Faculty of Engineering, University of Porto, Portugal)	
LF	Low-frequency; in this report $T < 25\,\mathrm{s}$	
MSL	Mean sea level	
SDF	Six degrees of freedom	
SPM	Single point mooring	
UKC	Under keel clearance	

Summary

A moored vessel can experience large motions when agitated by waves. As a result, mooring lines risk breaking, the ship becomes a dangerously uncontrolled object, but most importantly unloading and loading the ship is made impossible. From an economic perspective, it is thus important to determine vessel motions due to waves at a berth. A suitable method including this in a port design would prevent an unexpectedly high inoperativeness of a built quay. The determination of vessel motion is, however, not an easy matter; wave penetration in a harbour is not easily simulated due to its complex geometry and bathymetry. This is further complicated by the high influence of low-frequency waves. These waves, especially bound low-frequency waves, impose a strict demand on the used method.

The method used in the present thesis is a chain of the Boussinesq-type model Triton (Deltares) with the panel-method diffraction model Harberth (Van der Molen) and the time domain vessel motion model Quaysim (Van der Molen), see the figure below. This chain adequately takes into account the non-linear wave component, having an important influence on the motion and provides a complete indication of the relevant processes, using a single model chain.

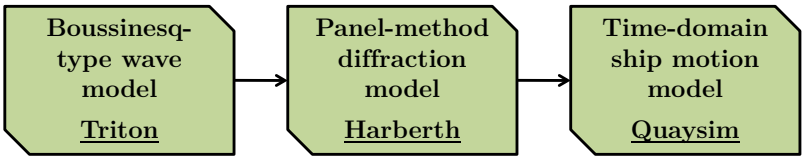

An example of the aforementioned problem is the oil berth A in the Port of Leixões, Portugal. This berth experiences a mean inoperativeness of 23%. Within the present thesis, this case has been elaborated both to obtain an insight on the origin of the problem as to assess the potential of the model chain for practice-driven engineering activities. The application of the model chain has been restricted by the limited amount of available time and the results of the validation of the diffraction and motion model.

Validation

Due to a discrepancy found between the measured and theoretically expected low-frequency energy content, the wavemodel's wave input used in the validation has been defined on the boundary using a measured timeseries. This improved the global reproduction of the low-frequency wave energy content. The imposed wave however also included the measured reflected wave. It is expected that the discrepancy, the high amount of low-frequency energy in the physical scale model basin, is due to the control of the wavemaker, in which this energy has been overestimated.

Using the vessel motion a priori, without using physical measurements for calibration, is limited too. The sensitivity for fender friction on the surge-motion, a very relevant motion for loading and unloading vessels, induces a high inaccuracy in case of uncalibrated settings.

Case study

The study regarding berth A, Leixões, shows that the quay is relatively unprotected for low-frequency waves. Their wave height is considerable with respect to the imposed low-frequency wave height (approximately 60%), particularly due to the profound shoaling towards the beach and the reflection off the beach.

An added value of the models used in the present report has been shown by including the harbour basin of the Port of Leixões. The occurrence of seiching is recognized. The energy of these eigenwaves and their nodal patterns are an indication of a significant influence of these waves on vessel motion.

Finally, the wave model indicates a current caused by wave-driven setup. The influence thereof on the quay is likely, although the magnitude of this current in reality needs to be verified.

Applicability of the method

The method used in the present report adequately takes into account the relevant wave processes. Vessel dynamics are properly accounted for too, allowing the inclusion of reflections off the quay wall and non-linear mooring line forces.

To be applicable in practice-oriented applications, improvements of the method are necessary, especially with respect to the robustness and computational speed. Nonetheless, the method has shown its added value in the presented application.

Keywords
Triton, numerical simulation, wave propagation, low-frequency waves, Quaysim, Harberth, moored vessel, diffraction model, vessel simulation, vessel motions, Leixões, Portugal

Samenvatting

Wanneer golven inspelen op een afgemeerd schip, kan dit grote bewegingen veroorzaken. Ten gevolge hiervan kunnen aanmeerlijnen breken, is het schip een gevaarlijk ongecontroleerd object, maar bovenal maakt het laden en lossen onmogelijk. Vanuit een economisch oogpunt is het dus belangrijk om scheepsbewegingen ten gevolge van golfactie ter plaatse van de kade mee te nemen in een havenontwerp. Een geschikte methode hiervoor voorkomt een verassend hoge onbruikbaarheid van een gebouwde kade. Het bepalen van scheepsbewegingen is echter niet gemakkelijk: de golfindringing in een haven is door zijn complexe geometrie en bathymetrie niet gemakkelijk gesimuleerd. Temeer omdat scheepsbewegingen veel invloed ondervinden van laagfrequente golven. Deze golven, met name gebonden laagfrequente golven, geven een zeer sterke beperking op het te gebruiken golfvoortplantingsmodel.

De methode waarvoor is gekozen in deze thesis is een koppeling van het Boussinesq-type golfmodel Triton (Deltares) met het panelenmethode diffractiemodel Harberth (Van der Molen) en het tijdsdomein scheepsbewegingenmodel Quaysim (Van der Molen), zie het onderstaande figuur. Deze koppeling neemt afdoende de non-lineariteit, die een belangrijke invloed op de beweging heeft, mee en schept een compleet beeld van de relevante processen met behulp van een enkele modelketen.

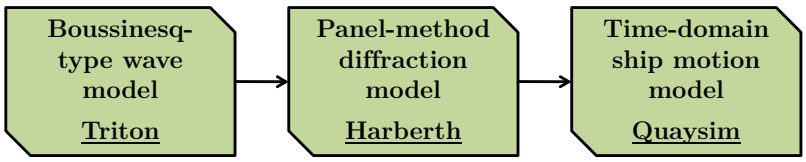

Een voorbeeld van het genoemde probleem is de oliekade A in de Haven van Leixões, Portugal. Deze kade ondervindt een gemiddelde onbeschikbaarheid van 23%. Binnen deze thesis is deze casus uitgewerkt zowel om een oorzaak van het probleem te vinden als om de potentie van de modelketen binnen het praktijkgerichte ingenieurswerk te beoordelen. De toepassing is begrensd als gevolg van de beperkte tijd en de resultaten van de validatie van het diffractie-

en het bewegingsmodel.

Validatie

Als gevolg van een discrepantie tussen verwachtingen uit theorie en metingen, gevonden in de laagfrequente band van het golfspectrum, is voor de golfinput in het golfmodel in de validatiestap gekozen voor het opleggen van een gemeten tijdserie op de rand. Hierdoor wordt de globale laagfrequente energieinhoud beter benaderd. Op deze manier was echter ook het gereflecteerde signaal opgelegd. Dat het fysieke basin veel laagfrequente energie bevat is naar verwachting te wijten aan de aansturing van de golfmaker, waarin deze energie is overschat.

Ook het sec toepassen van het scheepsbewegingenmodel is zonder fysieke calibratiemetingen beperkt. De gevoeligheid voor fender friction op de schrikbeweging, een zeer relevante beweging voor het laden en lossen van schepen, maakt dat een ongestaafde aanname hiervan een sterke onnauwkeurigheid op de resultaten legt.

Casus onderzoek

De studie van de kade A, Leixões, wijst uit dat de kadeplek relatief onbeschermd is tegen laagfrequente golven. Het optreden van havenoscillaties is aangetoond. De golfhoogte hiervan is hoog ten opzichte van de opgelegde laagfrequente golfhoogte, voornamelijk door de uitgesproken golfopstuwing richting het strand en de reflectie tegen het strand.

Een toegevoegde waarde is aangetoond door het meenemen van het havenbasin van de Haven van Leixões. De energie hiervan en het knoop-buiken-patroon zijn aanwijzingen voor een significante invloed van deze staande golven op de scheepsbewegingen.

Tenslotte wijst het golfmodel op een stroming welke door golfgedreven oploop wordt veroorzaakt. De invloed hiervan op de kadeplek is waarschijnlijk, hoewel het voorkomen van deze stroming in werkelijkheid moet worden nagegaan.

Bruikbaarheid van de methode

De methode gebruikt in deze thesis neemt de relevante golfprocessen voldoende mee. Ook de scheepsdynamica zit adequaat opgenomen in de methode, waarbij de reflecties tegen een kademuur en non-lineaire afmeerlijnkrachten kunnen worden meegenomen.

Om bruikbaar te zijn in praktijkgerichte toepassingen dienen verbeteringen te worden uitgevoerd met name op de robuustheid en snelheid van het model. Desondanks heeft de methode in de gepresenteerde toepassing zijn toegevoegde waarde kunnen laten zien.

Trefwoorden
Triton, numerieke simulatie, golfvoortplanting, laagfrequente golven, Quaysim, Harberth, aangemeerd schip, diffractiemodel, scheepssimulatie, scheepsbewegingen, Leixões, Portugal

Chapter 1

Introduction

1.1 Problem description

The purpose of a port is to hold ships still, enabling unloading and loading of a ship at berth. As loading arms do not permit too much vessel motion, a heavily moving vessel is unable to be loaded or unloaded. These operations are thus interrupted, reducing berth efficiency. When the vessel's motions amplitude increases, excessive mooring line forces cause mooring line breakage. Due to the subsequent reduced control on the moored vessel, it risks colliding with nearby ships or damaging the berthing structure and causes a hazard for quay personnel.

For these reasons, vessels are removed from the quay and sailed out of the harbour as a preventive measure in case of adverse conditions. It is clear that the subsequent inoperativeness of a berth can induce significant losses for the terminal operator. Extensive motions of moored vessels in a harbour are thus a major concern from an economical perspective as well as due to their environmental risks.

The cause of vessel motions in a harbour is a combination of the exciting wave forces and the properties of the moored vessel and the mooring configuration. In correspondence, optimizing a quay design, reducing environmental risks and inoperativeness as a result of waves to a satisfying level, one must include

- an evaluation of the wave action at the site of the berth considered
- the response of the moored ship to the waves present — an evaluation of the mooring system (and alterations)

The wave action at the berth is not easily determined as many propagation processes play a significant role in coastal and harbour zones. Furthermore, low-frequency wave penetration and possible occurrences of seiches are hard to predict but may have a severe influence.

Additionally, wave height at the berth is a very unreliable indication of berth operation limits or safety. The wave forces acting on the vessel are not simply a function of the wave amplitude. Rather, these also depend on several other parameters, as wave period, wave phasing and wave direction relative to the berthing structure have an important influence.

The resulting motions are dependent on the mooring system — essentially a damped spring-mass system, including the mooring layout, fender and mooring line properties as springs and dampers. Because of the typical low eigenperiod of this system for surge and sway motions, low frequency (LF) waves due to seiching and wave groupiness, affect the vessel's motion severely and need special attention. Furthermore, the nonlinear characteristics of the mooring system typically affect the translation of wave action to vessel motion. Even if mooring line and fender characteristics can be linearized, a vessel pushed against the fenders experiences forces much different than those acting on a ship moving off the fenders. This too induces a significant non-linearity.

The aspects mentioned above — the propagation of waves in the harbour and the response of the ship to the calculated waves — will be treated more extensively in the successive chapter.

When studying a port design or existing lay-out, it is essential to appropriately assess the mentioned aspects. Resulting ship motions and forces on mooring system elements must then be compared with design limits. This assessment can be performed using in situ or physical model measurements or by numerical modeling, each having their advantages and drawbacks.

Using physical modeling, all components are treated simultaneously as a vessel model is simply put in a wave basin. This apparently complete method, however, inherently suffers from scale and basin effects, inducing errors, e.g. eigenwaves due to basin dimensions having no correspondence to reality. Furthermore, as this method requires a laboratory basin, it is generally too expensive and time consuming to simulate a wide variety of wave conditions and mooring alternatives.

With a numerical method, one is able to evaluate numerous environmental situations, mooring lay-outs and vessels and isolate these elements to properly assess each of them. Moreover, it enables a relatively quick model set-up. Numerical modeling has been used to complement physical modeling more and more extensively throughout the last decades. However, due to the complexities — wave and vessel dynamics, harbour geometry, coastal bathymetry and nonlinear mooring characteristics must be well included — one has to turn to advanced numerical models; oversimplification might cause losing relevant aspects to a certain extent. This will be elaborated upon in Chapter 2.

1.1.1 Port of Leixões, berth A

A clear example of a terminal heavily affected by inoperativeness due to vessel motion is found at an oil terminal berth at the Port of Leixões: berth A, shown in Figure 1.1. This berth is located on the leeside and rather close to the tail end of a breakwater. Due to the effect of, in particular, diffracted and reflected waves as well as the contribution of low frequency energy, the berth experiences an inoperativeness of on average 23%, culminating to 50% during stormy months.

Berth A will be the subject of the case study within this present report.

Previous studies on berth A have had an emphasis on observations and physical modeling, the latter providing insights in the wave action around berth A and a direct coupling to vessel motion. An example of such investigation is the comprehensive work performed by Rosa Santos (2010). Physical modeling however possibly induces some unwanted artifacts and suffers limitations, as discussed above.

(a) Looking westwards, showing the harbour basin and berth A

(b) Location

Figure 1.1: Location and overview of the Port of Leixões, Portugal

It is therefore valuable to complement the previous studies with numerical simulations. Moreover, regarding the development of a generic approach to these type of issues, an application of a numerical method to a case study is extremely useful.

1.2 Applied numerical method

Within the present study, use will be made of a numerical approach. The above-mentioned components — wave propagation and vessel response — are performed in two successive steps, each step with a dedicated numerical tool. This coupling of a wave propagation model to a vessel motion model is often done when numerical models are used in this kind of application.

The method thus is a chain of numerical tools, coupled successively as shown in Figure 1.2.

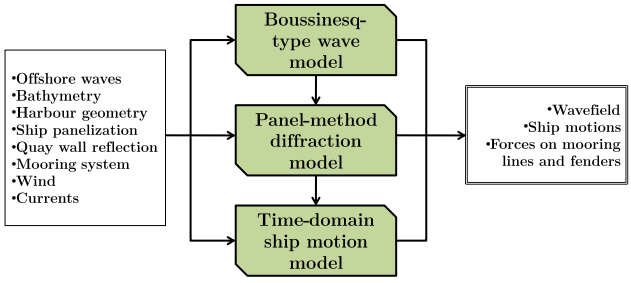

Figure 1.2: Chain of numerical tools

First, waves throughout the harbour are calculated using a Boussinesq-type — a 2D-horizontal, non-linear — wave propagation model. This model allows solving long and short wave propagation simultaneously as the short-wave forcing includes and induces LF waves. It simulates their propagation in the shore

zone and penetration into the harbour.

Within this thesis, the Boussinesq model Triton (by Deltares) is selected (see Section 2.2.2). This model includes the most relevant physics as will be discussed in Section 2.2.3.

Subsequently, Harberth (by Van der Molen) will use the obtained wavefield at the ship, represented by panels, to calculate the forces acting on the ship's hull. Diffraction around the three-dimensional hull is calculated with the possibility of including nearby structures like a quay.

Finally, Quaysim (by Van der Molen) uses the schematization of the mooring system to simulate the vessel motion. Being a time-domain model, Quaysim takes into account the non-linear properties of mooring lines and fenders.

The specifics of these models will be further discussed in Section 2.5.

The complete chain of numerical tools is then given by Figure 1.3. The other links shown in this figure are Tc-Prog (see Section 2.2.3) and Wavescat.

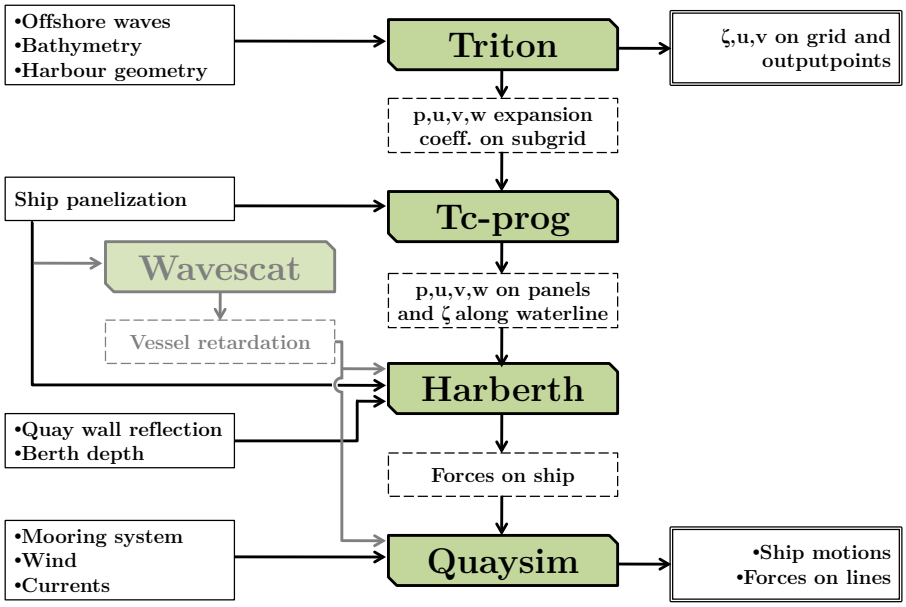

Figure 1.3: Complete chain of numerical tools indicating all numerical modules and problem elements considered, with ζ denoting surface elevation, p denoting pressure and velocity in x,y,z-direction given by u,v,w respectively

Figure 1.3 shows the physics and relevant aspects of the problem taken into account per step. Most notably, the presence of the vessel is not accounted for during the wave propagation simulation.

1.2.1 Previous applications of the method

A comparable chain method has previously been adopted by, amongst others, Bingham (2000); Van der Molen (2006); Wenneker (2006). They have applied

this method primarily to academic and laboratory physical models, using a strong simplification with respect to applications of real harbours.

Bingham (2000) describes a method combining a Boussinesq model with a diffraction model to calculate the incident waves including the harbour geometry and bottom topography but excluding the presence of the ship. The linear frequency-domain panel model WAMIT is used to calculate the hydrodynamic coefficients and the diffraction of the incident waves of which timeseries are calculated on each panel.

Pinkster and Naaijen, (2003), Wenneker et al. (2006) used a similar combination of Boussinesq and panel theory models. Using all Fourier components, whereas Bingham (2000) reduced the number of frequencies through the Haskind relations, they were able to obtain the low frequency varying drift forces as well.

De Bont et al. (2010) have coupled the Harberth and Quaysim models using a different Boussinesq model: Mike 21 BW (by DHI). This chain was also applied by Van der Wel (2011), who has later on switched to using Triton. Van der Wel's results show that Triton is able to predict the primary and LF wave heights sufficiently accurate. Furthermore, he has concluded that Triton is well able to predict possible basin oscillations (Van der Wel, 2011, p.78). Van der Wel has not been able to complete the numerical model chain with reliable wave data due to instabilities in the initial numerical wave propagation model.

1.3 Aim of the present MSc study

The aim of this report is to assess the aforementioned chain of numerical models as a method to determine the response of a moored vessel to waves, i.e. to determine if the model chain is a suitable method for this application. To this end, it is evaluated if the model chain adequately takes into account the complex geometry and bathymetry and includes incident low frequency waves and nonlinearities in wave propagation and mooring dynamics.

Furthermore, using the method to an actual harbour case will contribute to a further interpretation of the investigations regarding berth A of the Port of Leixões by modeling this harbour including its main basin. This will give an insight in the key wave propagation processes and significant wave heights at the berth. Although the current project has been limited to the above, the method chain's scope includes the determination of typical or maximum ship motion amplitudes of a vessel moored at that berth.

Applying the numerical chain method complements in the assessment of the physical processes at berth A by distinguishing real processes from those induced by physical modeling. In this manner, a better understanding of the cause of the problem at Leixões is gained. Herewith, the method can prove its added value.

The application also serves to assess the workability of the method regarding accuracy and robustness versus computational effort. This is a relevant subject for practical applications — would a port designer be able to use the method, rather than an academic only?

Recapitulating, the aim of the present report is to

- assess the applicability of the numerical model chain as a generic method

for the determination of moored vessel motions in actual harbour applications, taking into account its accuracy as well as workability

- provide an understanding of the inoperativeness issue at berth A of the Port of Leixões.

1.4 Approach

Validation

In order to obtain confidence in the method chain, a validation is performed first. Van der Wel (2011) has focused on the wave propagation in a complex geometry simulated by Triton and compared his results with physical model measurements, i.e. the first chain link. The present validation complements this research by including the second and third chain link: the diffraction and ship motion model.

The validity assessment will be done by reproducing a physical model test performed by Rosa Santos et al. (2008a). To ensure that the wavefield is represented most reliably, a relatively simple geometry will be the base of this validation. It is expected that only little deviation of wavefield is found, enabling an interpretation of simulated vessel motions specifically focused on the validation of Harberth and Quaysim. The physical model measurements will serve as comparison data.

Case study

A model of the actual harbour will be set up using a suitable schematization of boundaries and bathymetry as well as a representative wave condition. The performed validation of the model chain will attribute to an appropriate interpretation of the results of this phase.

Due to the projects confined duration, the analyses are limited to wave propagation interpretation. These contribute to a better understanding of the cause of the inoperativeness and directives for further research. The available publications from studies regarding Leixoes will be used to assess the results.

Summarizing, this present project will thus include two subsequent steps, shown in Figure 1.4.

- A validation of the method using physical model measurements.
- An application of the method to a case study.

1.5 Outline of this report

Chapter 2 introduces the relevant physics of water wave propagation and of the motions of a non-moving vessel. Additionally, more physics are concisely given in Appendix A, providing a background for wave modeling. Although these physics are presented keeping in mind the current application, the method is regarded as a generic tool to be applied in harbour zones. It is thus assessed for this purpose when it is validated in Chapter 3.

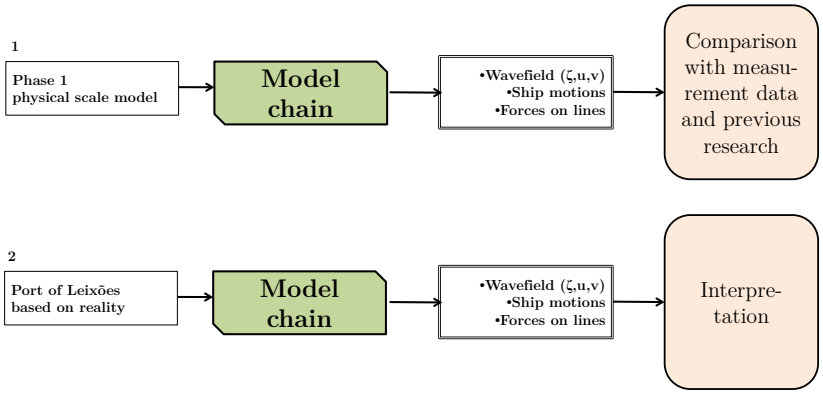

Figure 1.4: Two steps within this thesis: evaluation of the method using measurement data and application to an actual harbour case

The case study of the Port of Leixões berth A is elaborately introduced in Chapter 4. Subsequently, the model set-up and model results are treated and discussed in Chapter 5 and Chapter 6, respectively.

Conclusions both considering the generic method chain as considering the case study are given in Chapter 7, treating recommendations to further improve the method and complement the present report for both purposes.

Chapter 2

Modeling background

In the determination of moored vessel motions due to incident waves, two components are distinguishable: the propagation of incident waves into the coastal or harbour region and secondly the response of a moored vessel to these waves.

The backgrounds on modeling these two components will be treated separately in the following sections.

2.1 Wave dynamics

Determining the propagation of waves in coastal areas and harbours is a far from straight-forward task. Wave propagation of all coastal zones include, among others, generation, dissipation, shoaling, refraction and diffraction as well as nonlinear interactions. Additionally, a harbour geometry induces a higher relevance of reflections and basin oscillations. The incident wavefield, in practical applications, is multidirectional with high and low frequency wave content.

As it is required to model the wave physics adequately, an applicable wave theory is introduced and selected within following sections. An extensive and more widely applicable treatment of wave dynamics can be found in Bosboom and Stive (2012); Holthuijsen (2007); Van Rijn (2011).

2.1.1 Classification of waves

It is possible to categorize ocean waves in several ways, i.e. considering the force that generated the wave, the restoring force or the wave frequency, see Figure 2.1. The concern within this project is in gravity and infragravity waves.

2.1.2 Wave theories overview

The motion of water is well described, by the Navier-Stokes equations, elaborated upon below. Analytically solving these equations is not easily done. This holds especially when waves are concerned, in which case the position of the free surface is unknown.

Usually, approximations are necessary. This leads to various wave theories, of which some, commonly used, are shown in the overview given in Figure 2.2. The typical condition of interest is denoted in this figure.

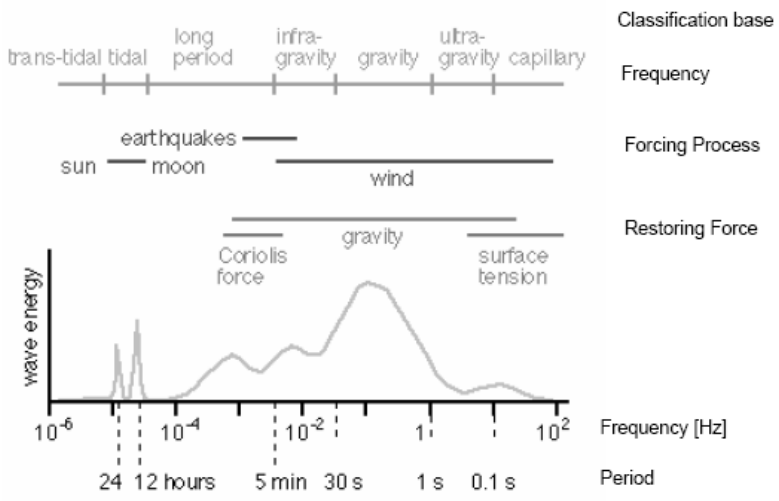

Figure 2.1: Ocean wave classification (Soler, 2006)

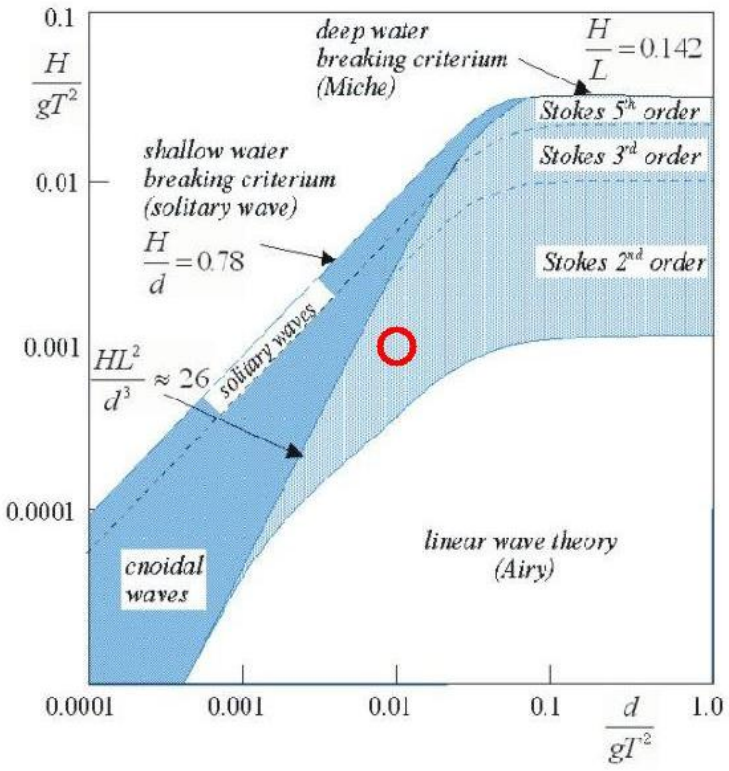

Figure 2.2: The ranges of applicability of various wave theories (Holthuijsen, 2007); marked in red is the typical condition at the Port of Leixões: $d = 20\,\mathrm{m}$, $H = 2.5\,\mathrm{m}$ and $T = 14\,\mathrm{s}$

Linear wave assumption

Assuming that the wave amplitude is small compared to the water depth, the non-linear terms of the Navier-Stokes equations can be neglected, i.e. the formulae are linearized. Further simplification, by considering an incompressible, irrotational flow lead to the the linear wave theory. Harmonic waves are solutions of these equations. This harmonic character implies that these waves do not affect one another while they travel together across the water surface.

Non-linear, evolved wave assumption

To account for the non-sinusoidal shape of a wave, it is required to take into account higher order terms. Various nonlinear theories exist, as shown in Figure 2.2.

In Stokes theory, higher order terms are added to the solution, to increasingly approximate the nonlinear equations and boundary conditions. Given below is a second-order Stokes wave, traveling in x-direction (Holthuijsen, 2007).

$$\begin{aligned}\zeta(x,t) = &\underbrace{a\cos(\omega t - kx)}_{\text{linear wave}} \\ &+ \underbrace{ka^2 \frac{\cosh(kd)}{4\sinh^3(kd)} \left(2+\cosh(2kd)\right)\cos\left(2(\omega t - kx)\right)}_{\text{second-order Stokes correction}}\end{aligned} \tag{2.1}$$

More higher-order terms can be added. However, Stokes theory of any order, as well as Deans theory, the solitary or the cnoidal wave theory, consider permanent, non-evolving waves only (Holthuijsen, 2007).

2.2 Numerical wave modeling

Navier-Stokes

The Navier-Stokes equations are partial differential equations describing the flow of fluids. It is in fact an application of Newtons 2$^{\text{nd}}$ law to an arbitrary volume within a fluid and the most complete equation of motion for the instantaneous velocities of a viscous fluid element in a gravity field, applicable most generally within the field of civil engineering.

$$\rho \frac{D\vec{u}}{Dt} = -\nabla p + \nabla \cdot \mathbb{T} + \vec{f} \qquad \text{(Navier-Stokes)}$$

In the equation above, $\vec{f}$ comprises all external forces, including gravity and rotational forces and $\mathbb{T}$ is the fluid stress tensor.

Shallow-water theory

If waves enter very shallow water, the particle motions become more and more horizontally oriented and eventually (when the water is very shallow: typically $L/h \gtrapprox 100$) all vertical accelerations may be neglected. This non-dispersive, long wave can then be described with the shallow water equations. A major

drawback of this theory is that the propagation velocity is ill-defined due to the hydrostatic pressure assumption.

Boussinesq wave theory

To solve evolving waves including higher order terms, Boussinesq-type theories are amongst the most advanced and widely accepted.

The starting assumption is that the fluid is incompressible, has constant density, is irrotational and can be described by a 3D velocity potential (Borsboom et al., 2000). The essence of Boussinesq theory, then, is to reduce this three-dimensional flow problem to a two-dimensional formulation, by approximating the vertical distribution of the horizontal velocity by a truncated polynomial expansion. The vertical profile of the velocity is subsequently represented by a single parameter.

This theory's applicability includes the transition between the shallow-water and linear regime — the wave motion is not yet horizontal and the shallow-water equations do not apply, but neither does the linear wave theory as the ratio of depth over amplitude is too small (Holthuijsen, 2007). In fact, the Boussinesq theory equations can be thought of as the shallow water equations supplemented with corrections for vertical accelerations (Holthuijsen, 2007). It includes, up to a certain accuracy (related to the dispersion, indicated by a kh-value limit), the most relevant wave dynamics. Implicitly included are shoaling, refraction and diffraction as well as nonlinear wavewave interactions. Bound and (reflected) free LF waves are described together with the primary waves, including (relative) phase information (De Jong and Borsboom, 2007). Dissipative processes such as bottom friction are modeled by parameterizations.

A simple form of the Boussinesq equations for a non-horizontal bottom read (Holthuijsen, 2007)

$$\frac{\partial \zeta}{\partial t} + \frac{\partial}{\partial x}(H\bar{u}_x) = 0 \tag{2.2a}$$

$$\frac{\partial \bar{u}_x}{\partial t} + \bar{u}_x \frac{\partial \bar{u}_x}{\partial x} + g\frac{\partial \zeta}{\partial x} = \underbrace{\frac{1}{2}h\frac{\partial^3(h\bar{u}_x)}{\partial t \partial x^2} - \frac{1}{6}h^2\frac{\partial^3 \bar{u}_x}{\partial t \partial x^2}}_{\text{corrections}} \tag{2.2b}$$

where $\bar{u_x}$ is the vertically averaged, horizontal particle velocity. Several similar equations are used, for those used in Triton, refer to Borsboom et al. (2000).

2.2.1 Available models

Table 2.1 shows categories and examples of numerical wave propagation models. The upper type of models is phase averaged and thus does not solve individual wave propagation. The lowest type, Navier-Stokes models, is the most complete description but also the most computationally expensive. Between these, numerous wave models are available, each having its approximation base (see Section 2.1.2) and use.

An elaborate discussion of currently used wave models can be found in De Jong and Borsboom (2007). This section solely serves to introduce the model used.

Table 2.1: Categories of numerical wave models (adapted from De Jong et al., 2009) with examples (De Jong and Borsboom, 2007)

Phase averaged	Spectral models		Mike 21 NSW, SWAN, Wavewatch
	Shallow-water models forced on wave-group scale		Shorecirc, Surfbeat, XBeach
Phase resolving	Potential flow models	Linear potential flow	AQWA, Diffrac, Hydrostar, WAMIT
		Fully nonlinear potential flow	
		Mild slope	PHAROS, CGWave, Mike 21 PMS, Mike 21 EMS, REF/DIF, Telemac Artemis
	Non-hydrostatic models	Single-layer	XBeach, SWASH, Weowave
		Multilayer	SWASH
	Boussinesq	Single-layer	Bouss-2D, Funwave, Mike 21 BW, Telemac Boussinesq, Triton
		Multilayer	Coulwave
	Free surface Navier Stokes models		Comflow

The most important difference is whether the model is phase averaged or phase resolving. Within this distinction, a consideration of required included physics versus computational cost must be made.

2.2.2 Selection of appropriate model

With the application within this project in mind, it is important to include both high and low frequency waves as well as their mutual phases. This is a strict demand. The individual physics can be accounted for by various numerical models. To include all at once, it is appropriate to use a Boussinesq model, a non-hydrostatic or Navier-Stokes model.

A linear, phase-averaged model is generally significantly computationally cheaper then other models. It would however not include all appropriate wave physics. On the contrary, fully 3D models would take into account the appropriate physics but take significantly more computational effort than other models.

Concerning the physical accuracy and computational demand, both non-hydrostatic and Boussinesq models seem a suitable compromise. Application of these models and comparison with Triton is outside the scope of this thesis.

Within this project, the Boussinesq-type model Triton has been selected.

2.2.3 Triton

An extensive discussion on Triton is given by Borsboom et al. (2000). Triton is a phase-resolving model developed by Deltares. It is said to have the unique property that it is both momentum and mass conservative. (Borsboom et al., 2000)

Triton is able to model wave propagation in shallow regions where nonlinear effects — shoaling, the generation of higher and lower harmonics, wave breaking, dispersion, wave-wave interaction etcetera — play an important role. Irregular multi-directional waves can be generated at an offshore boundary including bound or free LF waves.

Furthermore, as a Boussinesq-type model, Triton is expected to be able to describe the set-down beneath wave groups and to be appropriate in the investigation of harbour resonance under influence of ocean waves (Van der Wel, 2011, his reference Woo and Liu (2004))

Possible boundaries conditions within Triton are

- closed, i.e. fully reflecting
- partially reflecting
- outflow, i.e. zero reflection
- monochromatic surface elevation input
- surface elevation input through Jonswap spectrum parameters
- surface elevation input through time-series

The output provided by Triton is a timeseries of surface elevations and horizontal depth-integrated velocities.

It is not possible to model the presence of a ship within Triton. Furthermore, transmission and overtopping can not be included. Although it is expected that transmission and overtopping play a role in the wave climate at berth A at the Port of Leixões (this will be treated in Section 4.4.1), Triton is still expected to be an appropriate, adequate model for the application in this thesis.

Tc-Prog

The module Tc-Prog is used to reconstruct the velocity and pressure profile over the vertical (refer to Wenneker, 2006, Section 3.2). The results of such a reconstruction are given in Figure 2.3. This reconstruction is relevant when considering the velocities and pressure on a ship's hull through panels with a certain center x, y, z.

2.2.4 Accuracy limits of Triton

Linear dispersion, essential for the correct representation of primary waves, is modeled accurately up to $\mu \equiv kh = 3$–4. (De Jong et al., 2011, his reference Borsboom (2000)). The modeling of non-linear (difference and sum-frequency) waves is essentially limited to long (difference-frequency) waves (De Jong and Borsboom, 2007).

Furthermore, non-linear effects are represented accurately up to $\epsilon \equiv a/h < 0.25$ and $\epsilon\mu^2 < 0.25$.

Linear shoaling is simulated appropriately up to $\mu_s \equiv 1/kL_0 < 0.2$–$0.5$.

Finally, it is important to bear in mind that the reflection on partially or weakly reflecting and closed boundaries is imposed using a single kh-value. Therefore, the presence of a slope along the boundary might induce locally

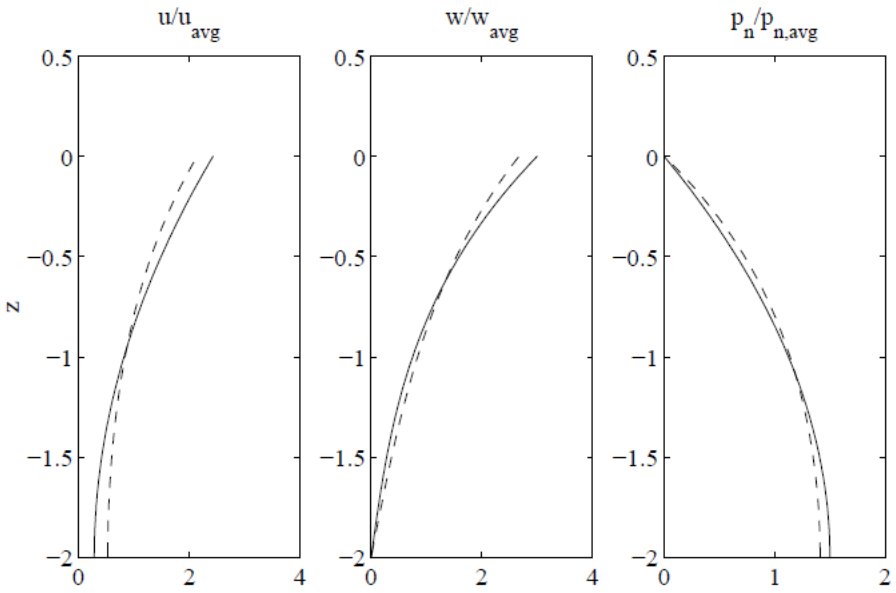

Figure 2.3: Reconstructed (continuous line) and exact (dashed line) horizontal (u) and vertical (w) velocity profiles and nonhydrostatic pressure, for a linear short wave, with $kh = 2.1$ (Wenneker, 2006, p.3-3)

inappropriate boundary conditions. Moreover, wave reflection is set for a specific frequency and expected to perform well for this sole frequency. Other frequencies are then reflected by a (slightly) larger amount.

Accuracy of LF bound waves

The accuracy limit for bound LF waves is stricter than the limit for primary waves. As shown by De Jong et al. (2011), Triton shows an underestimation of bound LF waves for higher values of kh. In this article, an extended formulation is tested, negating this underestimation, see Figure 2.4. A combination of the two formulations could therefore result in a better approximation, even for higher values of kh. The extension has, however, only been developed for 1D so far.

As the typical kh-value in the application within this project is approximately 0.64 (< 1), the representation of LF bound waves is expected to be sufficiently accurate.

Required spatial resolution

The spatial resolution of the computational grid used in Triton, or any other wave propagation model for this matter, must be sufficient to accurately represent a waveform. As a rule of thumb, 20 grid cells per wave length is often used as a requirement. This follows from the numerical time discretization of the Boussinesq equations in Triton, a Runge-Kutta scheme, inducing the following relation between the number of grid cells and the expected local numerical phase

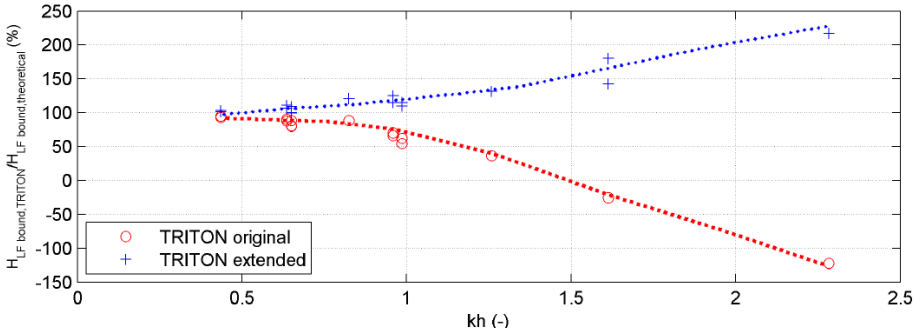

Figure 2.4: Low frequency wave height as function of $k_{\text{prim}}h$ in the original (red) and the extended (blue) version of Triton (De Jong et al., 2011)

Table 2.2: Numerical phase error due to spatial resolution calculated using Equation 2.3 (Boeyinga, 2010)

Number of cells per wave length	Expected phase error
25	1%
20	1.6%
18	2%
15	3%
10	6%
7	12%

error, used in Table 2.2. (Boeyinga, 2010, his reference Borsboom (2010))

$$\frac{\Delta x}{L} = \sqrt{\frac{3}{2\pi^2} error} \tag{2.3}$$

with $error = \frac{c_{\text{exact}}}{c_{\text{numerical}}} - 1$.

2.3 Ship dynamics

For an elaborate treatment of ship dynamics one is referred to Journée and Massie (2001b); Pinkster (1980); Van Oortmerssen (1976). This sections sole intent is to provide a theoretical base for the method used. It therefore only assesses the aspects relevant for this thesis report, e.g. is limited to a non-sailing vessel.

Any floating object experiences six degrees of freedom: surge (x), sway (y), heave (z), roll (φ), pitch (θ) and yaw (ψ), as defined in Figure 2.5. These unambiguously describe the alignment of the vessel and are given in the vector $\vec{X}$.

When one is interested in the motions of a moored vessel, one essentially considers a damped spring-mass system. In this analogy, springs represent the mooring lines and fenders (e.g. in sway-direction), dampers represent the fenders (in surge-direction) and viscous damping. Moreover, vertical motions are

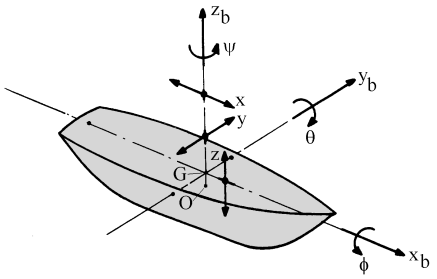

Figure 2.5: Degrees of freedom of a floating object; the body bound coordinate system $G(x_b, y_b, z_b)$ is connected to the ship with its origin at the ship's center of gravity, G; the coordinate system $O(x, y, z)$ is — in case of a moored vessel — stationary with origin O in the still water surface, at, above or below the time-averaged position of G (from Journée and Massie, 2001b)

generally dependent on the vessel shape and draught through its buoyancy and this can thus be seen as the systems main spring.

Like any spring-mass system, this moored vessel system resonates if it is forced with a frequency close to its natural frequency. Typically, the natural frequency of the horizontal motions (sway, surge and yaw) are 1–2 min — the low frequency wave and seiche period range — whereas vertical motions have natural periods of typically 5–20 s — the primary wave period range. The large eigenperiods of surge are caused by a combination of the vessel's great mass, low stiffness of the mooring lines and low damping in this surge direction. This motion is not rarely the most determinant.

An empirical relation of the significant surge amplitude with respect to the significant LF wave height is given by Ligteringen and Moes (2001).

$$\hat{x} = C_{\mathrm{x}} H_{\mathrm{s,lf}} \sqrt{\frac{gM}{h \cdot k_{\mathrm{t}}}} \tag{2.4}$$

with C_{x} usually 1–3, M is the mass of the vessel [tonne], h the waterdepth and k_{t} the stiffness of mooring system in surge direction.

2.3.1 Velocity potential

The presence of the ship changes the wavefield, e.g. waves are diffracted and reflected by the vessel and scattered by its motion. Using linearity, the velocity potential can be decomposed and can be solved using

$$\phi = \phi_{\mathrm{I}} + \phi_{\mathrm{S}} + \sum_{j=1}^{6} \phi_{\mathrm{R}}^{j} \tag{2.5}$$

in which ϕ_{I} is the potential due to the incident wave and ϕ_{S} and ϕ_{R} are due to the scattered wave and reflected wave (in all six degrees of freedom) respectively.

Pinkster (1980) has shown that in 2$^{\mathrm{nd}}$ order potential theory too the total second order problem may be split into these components.

2.3.2 Wave forces

Decomposition of forces

When the amplitudes of the motion are small — specifically, φ, θ and ψ are small — ship motions mainly have a linear character and the aforementioned superposition holds. The resulting motion in waves can then be seen as a superposition of the motion of the body in still water and the forces on the restrained body in waves, see Equation 2.6 and Figure 2.6.

$$\frac{d}{dt}(\rho\nabla \cdot \dot{\vec{X}}) = F_{\mathrm{h}} + F_{\mathrm{w}} \tag{2.6}$$

In other words, we distinguish the following forces.

1. F_{h}: The so-called hydromechanical forces and moments due to the harmonic oscillations of the rigid body, moving in the undisturbed surface of the fluid.

2. F_{w}: The so-called wave exciting forces and moments, produced by waves coming in towards the restrained body.

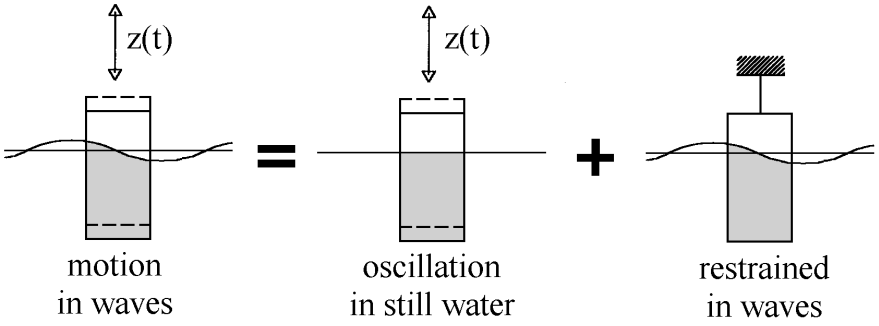

Figure 2.6: Decomposition of motion forces in a hydrodynamic reaction force (F_{h}, middle) and an exciting force (F_{w}, right) (from Journée and Massie, 2001b)

Equation 2.6 can be elaborated, e.g. to the following formula for heave (refer to Journée and Massie, 2001b).

$$m\ddot{z} = a(\ddot{\zeta}^* - \ddot{z}) + b(\dot{\zeta}^* - \dot{z}) + c(\zeta^* - z) \tag{2.7}$$

in which ζ^* is the reduced water level, a is the hydrodynamic mass coefficient, b is the hydrodynamic damping coefficient and c is the restoring spring coefficient. In this formula, the analogy with a damped spring-mass system is evident.

The term $c\zeta^*$ shown in Equation 2.7 represents the Froude-Krylov force and is due to the undisturbed wave induced pressure on the floating body.

As the vessel motions in turn exert forces on the water volume — the hydrodynamical response forces F_h, due to radiation and scattering — a correction is necessary, given as $a\ddot{\zeta}^* + b\dot{\zeta}^*$. These forces are a relatively small perturbation of the incident wave, the use of the linear free surface condition for the scattered and radiated waves is therefore justified.

1st and 2nd order forces

Loads that have the same frequencies as the waves and are linearly proportional in amplitude to the wave amplitudes are known as first order wave forces. Second order forces, analogously, are proportional to the square of the wave amplitudes. These load components have frequencies both higher and lower than the frequencies of the waves.

Second order forces are the product of two first order quantities (e.g. the first order force and motion) or due to the second order wave exciting force. Van der Molen (2007a); Van Oortmerssen (1976) use the following subdivision.

I	The relative waveheight contribution
II	The contribution of squared velocities
III	The contribution of displacements times pressure gradients
IV	The contribution of ship rotations times inertia forces
V	The contribution due to second order potentials

These are apparent in the following formula for 2nd order forces.

$$\begin{aligned}\vec{F}^{(2)} = &- \underbrace{\int_{\mathrm{wl}} \frac{1}{2}\rho g {\zeta_r^{(1)}}^2 \cdot \vec{n} \cdot dl}_{\mathrm{I}} \\ &- \underbrace{\iint_{\mathrm{S_0}} -\frac{1}{2}\rho |\vec{\nabla}\phi^{(1)}|^2 \cdot \vec{n} \cdot dS}_{\mathrm{II}} \\ &- \underbrace{\iint_{\mathrm{S_0}} -\rho(\vec{X}^{(1)} \cdot \vec{\nabla}\frac{\partial}{\partial t}\phi^{(1)}) \cdot \vec{n} \cdot dS}_{\mathrm{III}} \\ &+ \underbrace{\vec{\alpha} \times (M \cdot \ddot{\vec{X}}_{\mathrm{G}}^{(1)})}_{\mathrm{IV}} \\ &- \underbrace{\iint_{\mathrm{S_0}} -\rho(\frac{\partial}{\partial t}\phi_{\mathrm{w}}^{(2)} + \frac{\partial}{\partial t}\phi_{\mathrm{d}}^{(2)}) \cdot \vec{n} \cdot dS}_{\mathrm{V}}\end{aligned} \tag{2.8}$$

in which $\vec{\alpha}$ is the angular motion vector, S_0 the hull's surface and X_{G} is the position of the center of gravity of the body in the fixed system of axes, $O(x, y, z)$. For moments a comparable formula is used.

The 2nd order forces contain time-varying components as well as a non-zero mean component, known as the wave drift force. This drift force causes a vessel, floating freely in waves, to tend to drift in the direction of propagation of the waves.

The mean wave drift force on a ship is

$$\bar{F} = \frac{1}{16}\rho g \zeta_{\mathrm{r}}^2 \cdot L_{\mathrm{s}} \tag{2.9}$$

in which ζ_{r} is the waveheight relative to the ship motion.

2.3.3 Response to waves

Considering the aforementioned decomposition of forces, assessing the response of a vessel one needs to

- determine the (1^{st} and 2^{nd} order) wave exciting forces in the absence of motions induced by these forces
- determine the hydrodynamic reaction forces (added mass and damping)
- determine the motions due to these forces.

The hydrodynamic reaction forces can be determined using a free decay test, i.e. performing an analysis of the response of a vessel due to an initial offset in a single degree of freedom and in absence of any other excitation.

Free floating vessel

In many cases the ship motion has a mainly linear character. This holds especially for unmoored vessels. This linearity means that, at each frequency, the different ratios between the motion amplitudes and the wave amplitudes as well as the phase shifts between the motions and waves are constant. As a consequence, resulting motions in an irregular wavefield can be found by superposing responses of all wave components, having different amplitudes, frequencies and possibly propagation directions. When the wave spectrum and vessel response characteristics are known, the response spectra and the statistics of these responses can thus be found by using the amplitude ratios (Journée and Massie, 2001b). These ratios as a function of frequency are called the response amplitude operator (RAO), examples of which are shown in Figure 2.7. Three zones can be distinguished; the peak zone is dominated by damping terms, the left and right tails by spring terms and mass terms respectively (Journée and Massie, 2001a, Figure 5.11).

Applying this RAO, one implicitly assumes linearity.

Moored vessel

According to Pinkster (1980), moored vessels show a more pronounced effect of 2^{nd} order forces. This, and the fact that mooring systems are typically nonlinear (forces are dependent on deflection) means that the response spectrum does not need to look much like the incident wave spectrum at all. Rather, it can contain energy at entirely different frequencies. Simply applying the RAO therefore is inadequate, a non-linear method to assess vessel motions is required.

2.4 Diffraction models

Forces on the vessel are calculated first, from the wave induced velocities, surface elevation and pressures. These forces will subsequently be used in the vessel motion model.

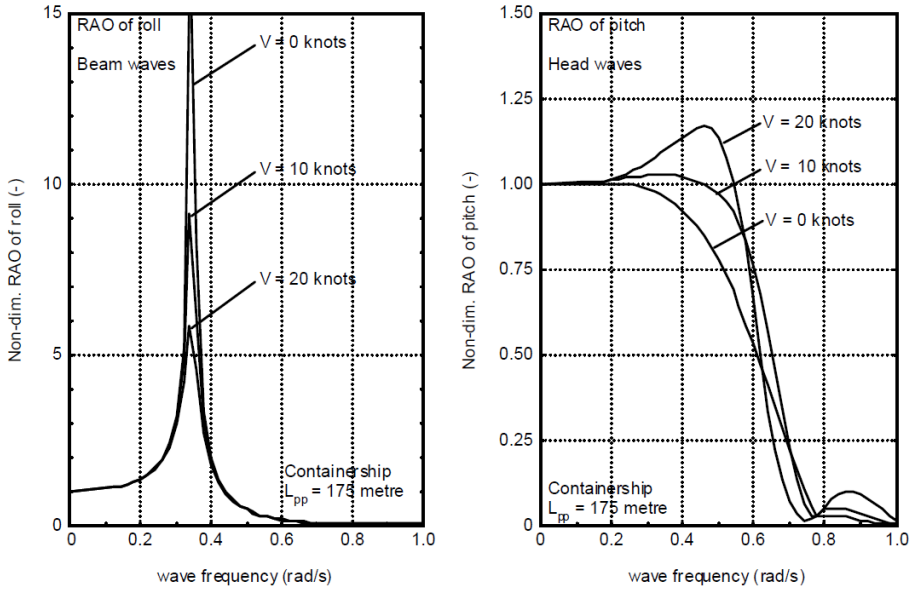

Figure 2.7: RAO of a containership of length $L_{pp} = 175\,\mathrm{m}$ in stationary and sailing conditions (Journée and Massie, 2001a)

2.4.1 Panel theory

Whereas strip theory builds up the hull using circular parts in the length direction of the vessel, panel theory builds up a hull using typically 500–1500 panels, see Figure 2.8. The panels are small enough to assume that the sources and doublets strength as well as the fluid pressure is constant over each element. No restrictions are imposed on the shape of the body. The forces and moments on the vessel are calculated using the principle below.

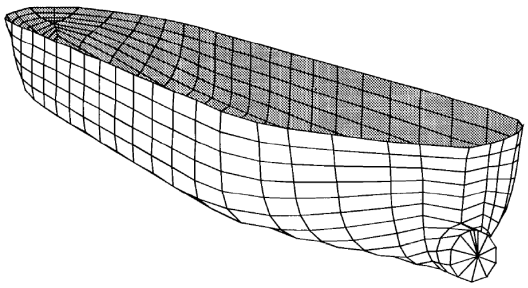

Figure 2.8: 3-D panel representation of a hull form of a crude oil carrier (Journée and Massie, 2001b)

$$\vec{F} = -\iint_{\mathrm{S}} p \cdot \vec{n} dS \tag{2.10a}$$

$$\vec{M} = -\iint_{\mathrm{S}} p(\vec{x} \times \vec{n}) dS \tag{2.10b}$$

Irregular frequencies

Panel methods are the most commonly used method to analyze the linear steady state response of large structures in regular waves. An aspect to be kept in mind is the possible appearance of so-called irregular frequencies. An irregular frequency is a frequency at which the solution matrix for the radiation or scattered potentials is singular or near-singular. This affects the results in time-domain, best observed in the retardation functions where a non-decaying oscillation may be present. Full removal of the irregular frequencies in time-domain computations is not possible. The effect may however be decreased by using a panelization in which the number of panels (especially the number of panels in y and z-direction) is chosen sufficiently large and the time step sufficiently small. (Van der Molen, 2007b).

2.4.2 Harberth

Harberth is a linear time-domain panel method developed by Van der Molen (2007b).

This model calculates or reads the hydrodynamic coefficients — the added mass and retardation functions of the ship moored at the quay (De Bont et al., 2010). A timeseries of the forces on the vessel is calculated through a straightforward, fully time-domain method, enabling the calculation of the motions of a moored ship due to first and second order wave forces. The vessel is restrained, i.e. the forces are calculated on a non-moving body.

Harberth takes into account the multi-directional, irregular and inhomogeneous character of the wave field in a harbour (Van der Molen, 2006). The Froude-Krylov forces are obtained by integrating the pressures due to the incident wave on the panels. The diffraction force due to scattering of the incident wave by the presence of the ship is then computed, at which Harberth is capable of including a quay (assumed infinitely long) in the panel schematization (Van der Molen and Wenneker, 2008). This also includes reflections against the quay wall of waves scattered by the ship. This property is an added value of Harberth compared to other diffraction models.

The equations driving Harberth are given by Van der Molen (2006, Section 4.2). The main assumption of Harberth is that the vessel is stationary or, equivalently, not affected by a significant constant current.

2.4.3 Wavescat

Wavescat is used to obtain the retardation function of the vessel for the present study (see Figure 1.3). Although this is incorporated within Harberth itself, irregular frequencies within the retardation function influenced the response of the vessel. To solve this a schematization of the vessel including an upper lid has been made and considered using Wavescat.

2.5 Ship motion models

Numerous vessel motion models are available: Termsim (Marin), BAS (Deltares), Ship-moorings (Arcadis Alkyon), TIMIT (MIT), Anysim, Optimoore and many more.

The basis of most vessel motion models is the Cummins equation (Cummins, 1962), given below (from Journée and Massie, 2001b, Section 6.5.1), in which the added mass, damper and spring coefficients are given by matrices **A**, **B** and **C**, respectively. This equation shows an evident similarity with Equation 2.7.

$$(\mathbf{M}+\mathbf{A})\ddot{\vec{X}}(t)+\int_0^\infty \mathbf{B}(\tau)\dot{\vec{X}}(t-\tau)d\tau+\mathbf{C}\vec{X}(t)=\vec{F}(t) \qquad \text{(Cummins)}$$

2.5.1 Time-domain versus frequency-domain

As has been discussed in Section 2.3.2, if the system is linear, the response of the system can be studied in the frequency domain. However, in a lot of cases there are several complications due to which this linear assumption is invalid, for instance non-linear viscous damping, forces and moments due to currents, wind, mooring lines and second order wave loads. If the system is nonlinear, the superposition principle and thereby the frequency domain approach is inappropriate. In that case one must solve the equations of motion in the time domain.

Since the importance of non-linearities is emphasized, the main criterion for the current application on the vessel motion model is that it solves the vessel motion in time-domain.

2.5.2 Quaysim

Quaysim is a time-domain ship motion simulation model developed by Van der Molen et al. (2010). It is used to compute the ship motions and mooring line forces of a ship moored at a quay or a jetty due to waves, current and wind by integrating the force timeseries.

The effect of radiated waves formed by the oscillations of the ship is included using impulse response functions. The interaction of the ship with non-linear mooring lines and fenders is also included. In this way the non-linear response of the moored ship can be computed.

Wind and current are accounted for using specific modules. The output also includes timeseries of forces on and/or along the mooring system components.

2.6 Motion limits

The maximum allowable ship motions are given in Table 2.3 for different ship types. Although given here as a single value, in practice this is dependent on the loading equipment and the experience of the crane driver. Furthermore, the loading process is not stopped immediately after exceeding a certain motion amplitude. Rather, the process slows down first and is only stopped if the productivity has become very low with respect to the capacity. Oil tankers allow relatively large movements, but the strength of mooring lines remains as a limiting condition.

Table 2.3: Maximum allowable ship motions (Van der Molen, 2006, his reference Bruun (1985), PIANC (1995))

	surge [m]	sway [m]	heave [m]	roll [°]	yaw [°]
Tanker	2.5	2	1.5	4	2
Ore carrier	1.5	0.5	0.5	4	2
Grain carrier	0.5	0.5	0.5	1	1
Container carrier	0.5	0.3	0.4	1.5	0.5
Ro/ro ship	0.3	0.2	0.1	n.a.	n.a.
General cargo ship	1	0.5	0.5	3	2

2.6.1 Mooring lay-out guidelines

According to the Oil Companies International Marine Forum (OCIMF), the ship mooring system should be arranged as symmetrical as possible about the amidships point of the ship, as it is more likely to ensure a good load distribution than an asymmetrical arrangement.

OCIMF (2008, p.14) further recommends

- breast lines should be orientated as perpendicular as possible to the longitudinal center line of the ship and as far aft and forward as possible
- spring lines should be orientated as parallel as possible to the longitudinal center line of the ship
- the vertical angle of the mooring lines should be kept to a minimum.

The ship motion is very sensitive to the pretension of mooring lines; higher pretension induces less movements — at the cost of higher loads on the line (Van der Molen and Wenneker, 2008). This is supported by model measurements performed by Rosa Santos et al. (2009). By slackening or tensioning of lines it is also possible to move the natural frequency of moored vessel system away from a significant wave or harbour resonance frequency (Van der Molen and Wenneker, 2008).

Chapter 3

Validation of model chain

The goal of this chapter is to validate the numerical model chain described in Section 1.2 as a method to determine the wave propagation and the response of a moored vessel. To this end, it has to be shown that this method performs the following tasks.

1. Represent the wavefield (ζ,u,v,w,p) in a complex harbour lay-out appropriately.

2. Simulate the movements of a moored vessel in such a wavefield with sufficient accuracy.

The most favourable conclusion would be that all relevant phenomena and physics are accounted for and available measurement data are accurately reproduced.

3.1 Previously performed research

The validation is based on the data gathered by Rosa-Santos during the physical modeling of the Port of Leixões berth A. Specifics of these model tests are given in Appendix B.

Rosa Santos et al. (2009) have numerically modeled the ship motions too, using a different numerical method. His results thereof do not coincide with the physical model results although the dependency of the significant oscillation amplitude on the primary wave peak period is similar to that of the physical model. A reasonable similarity is shown only for heave and pitch whereas from physical measurements it follows surge and sway are most significant with respect to the limits as stated by PIANC, see Table 2.3.

An earlier validation has been performed by Van der Molen (2006). This thesis was based on laboratory representations of a basin. Further research on and appliance of this method on real harbour applications was amongst his recommendations.

3.2 Approach

The requirements listed above will be assessed separately, i.e. the wavefield represented by Triton is evaluated first, subsequently the vessel motions modeled by Harberth and Quaysim are evaluated. These separate assessments are not fully independent as the wavefield determined by Triton is used to determine the vessel motion, also illustrated by Figure 1.3.

Because of this dependency, it has been decided to base the assessment on the phase 1 physical simulations performed by Rosa-Santos, a rather simple geometry, see Figure 3.1. Van der Wel (2011) has already indicated the appropriateness of Triton considering more complex geometries, further supporting this decision.

A more complete overview of the properties of the tests considered is given below.

- Phase 1 lay-out.
- MSL (CD+2 m).
- The asymmetrical mooring layout.
- Extra pretension (245–265 kN on breast lines).
- Low friction coefficient on fenders.
- Waves of $H_s = 1.5$ m and with period T_p 12, 14 and 16 s; inducing typical kh-values of 0.6–0.7.

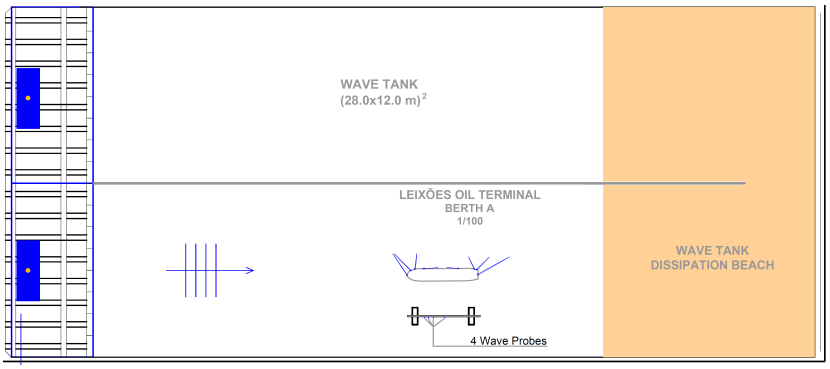

Figure 3.1: Physical model set-up during phase 1 (Rosa Santos, 2010)

Thus, the phase 1 lay-out — essentially a rectangular basin of uniform depth with an energy absorbing beach at its end — will be represented in this chapter. Wave and velocity output data will be compared with the available data of physical measurements at probes 1–4. Subsequently, ship movements will be calculated using Harberth and Quaysim, allowing a qualitative comparison with the measurement data.

3.2.1 Available data

The comparison data used in this chapter is gathered during the physical model tests performed by Rosa Santos. These data comprise

1. surface elevation data of four probes along a line parallel and close to the berthed vessel, see Figure 3.1
2. vessel motion data from the Qualisys motion capture system
3. records of forces on mooring lines and fenders
4. paddle positions timeseries and the free surface elevation timeseries imposed at the wavemaker

Analyses of available data

Analyses of the data is discussed more elaborately in Appendix B. The most important conclusions of these analyses are listed below.

- The bound wave compensation induces an unrealistic amount of LF wave energy in the imposed surface elevation (see Figure B.4).
- The LF waveheight $H_{\mathrm{m0,lf}}$ measured at the probes 1–4 is high compared to theory, approximately 17 cm for $T_{\mathrm{p}} = 12\,\mathrm{s}$ (approximately 11% of $H_{\mathrm{m0,full}}$), 23 cm for $T_{\mathrm{p}} = 14\,\mathrm{s}$ (15%) and 27 cm for $T_{\mathrm{p}} = 16\,\mathrm{s}$ (18%).
- Eigenwaves have occurred in the physical model tests.
- The surge amplitude seems most critical with respect to motion criteria, with approximately 1.2–1.6 m significant amplitude.
- Horizontal ship motions are typically in the 40–100 s range.
- Mooring lines perpendicular to the vessel experience the highest forces; overall forces affecting the lines range 110-330 kN.
- Fenders experience approximately 800 kN forces.

3.3 Set-up

3.3.1 Triton

The model domain used is in accordance with the physical model tests, i.e. half the basin. The grid cell size is $dx = 4\,\mathrm{m}$ by $dy = 12\,\mathrm{m}$. This inequality decreases the required run time and does not induce a significant discrepancy, as has been confirmed by a comparison run. This can be expected as a quasi-2D case is considered.

The first eigenmodes of a model with these dimensions in the longitudinal direction, taking into account the sloping bathymetry, are 2.2 and 4.4 mHz (in prototype scale). Additionally, eigenmodes in the transverse direction are possible, in which the first harmonics are 11.1 and 22.2 mHz. If basin seiching would be present, these frequencies would be most expected.

The bathymetry defined is shown in Figure 3.2 and uses MSL as reference level. A beach slope is included to allow wave shoaling. Tritons wave breaking module is not activated. However, dissipation does occur as a numerical effect of the finite spatial resolution. It has been verified by a comparison run that no significant variance was introduced by using the breaking module.

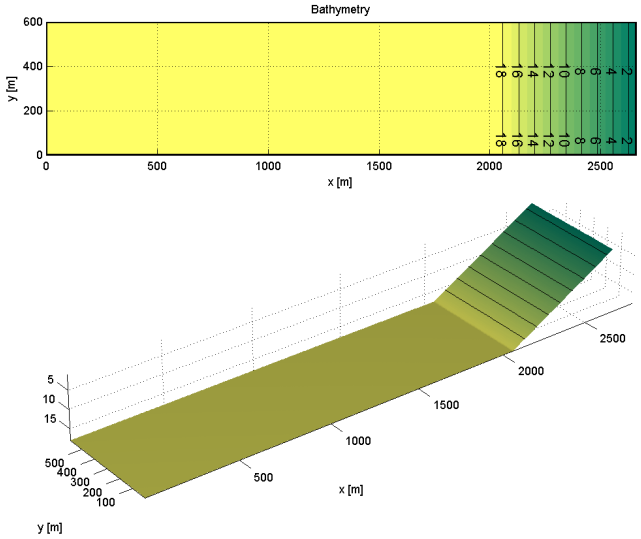

Figure 3.2: Waterdepth [m], relative to CD+2 m (MSL)

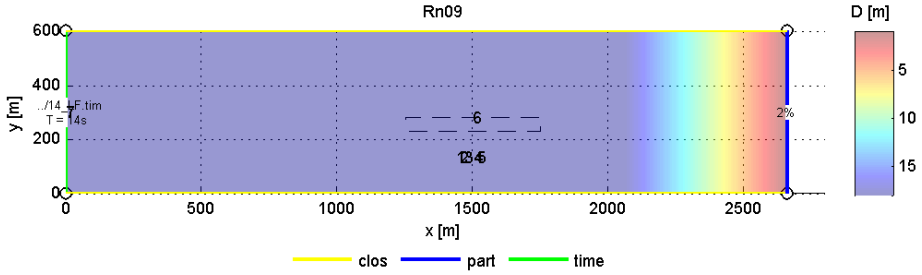

Figure 3.3: The model set-up used in this phase, showing the bathymetry and output locations. The boundary types are given, where yellow, blue and green denote closed boundary, partially reflecting boundary and incident wave through timeserie-file respectively. The black dotted line indicates the grid at which the Taylor expansion coefficients are written as output data, to be used during the reproduction of the depth profile, as discussed in Section 2.2.3.

On both the upper and lower side a closed boundary is imposed, see Figure 3.3, in agreement with a basin and desirable in case of perpendicularly traveling waves. On the western boundary a wave is imposed, see below. Dissipation of waves on the shore has been complemented by imposing a mere 2% relection on that end.

Table 3.1 shows the length of the runs used. Accounting for a cut-off period of 600 s, a record of 500 waves has been pursued. The measurement record was comparable of length. The timestep used is $dt = 0.1$ s.

Wave input

Three variations of wave input have been used during wave modeling.

- JONS Using a Jonswap spectrum with $H_{m0} = 1.5$ m, $\gamma = 3.3$, colinear waves with direction $\theta = 270\,^{\circ}$N.
- J+LB Using this Jonswap spectrum and adding low frequency bound waves conform Van Dongeren et al. (2003), based on Herbers et al. (1994).
- PRB1 Using the measured water level elevation at probe 1 of the associated physical measurement and imposing this timeseries as a unidirectional wave on the western boundary.

These have been used for wave periods $T_p = 12$, 14 and 16 s.

Table 3.1: Length of runs [s]

	T_p		
	12 s	14 s	16 s
JONS, J+LB	6600	7600	8600
PRB1, MEAS	6186.20	7252.90	8212.90

3.3.2 TcProg, Harberth, Quaysim

The schematization of the vessel used in TcProg and Harberth is given in Figure 3.4, using 672 panels. This schematization has been created in accordance with the main vessel dimensions.

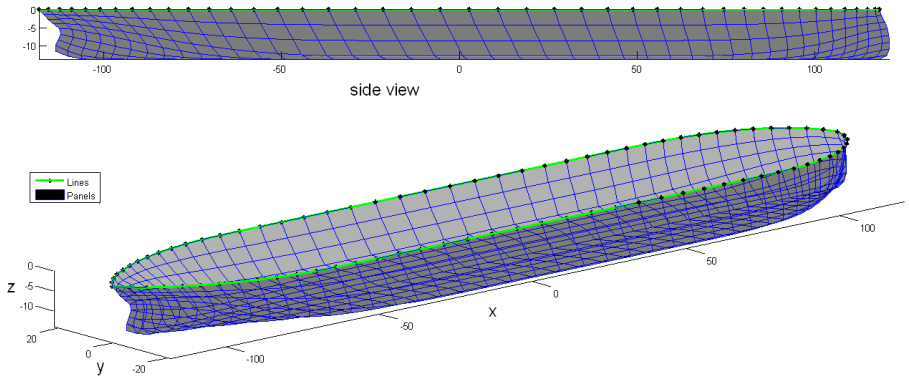

Figure 3.4: Hull schematization used in Harbeth and TcProg

In Quaysim, the ship dimensions and mooring lay-out are reproduced most accurately to agree with the scale model. Fender and mooring line characteristics are set, as well as mooring line pretension and fender friction. The

mooring line stress-strain relations are linear, in accordance with the measurement hardware used. These values are taken from measurements performed on the physical scale model, see Appendix B.

3.4 Results and discussion

3.4.1 Wavefield as input for vessel motions

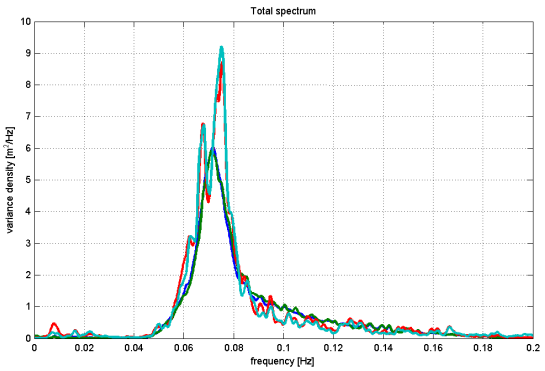

Figure 3.5: Modeling of phase 1, showing the agreement of primary wave spectra; considering output of the run for $T = 14\,\mathrm{s}$ at probe 1; using primary spectrum (blue; mostly coinciding with the green line), primary spectrum including LF waves conform Van Dongeren (green), using waterlevel measured at probe 1 as input (cyan) and the corresponding measurement (red)

Table 3.2 and Figures 3.5 and 3.6 show some of the resulting wave spectra of the modeling of phase 1 and measurement data of the physical model. It can be seen that the primary energy content, $H_{\mathrm{m0,full}}$ agrees well. Although PRB1 does not give an exact Jonswap-shaped spectrum, it does resemble the measurement, as the red and cyan lines essentially overlap, i.e. the measurement does not reseamble a Jonswap spectrum. The overestimation of total waveheight seen from PRB1 (see Table 3.2) is likely due to the fact that reflected waves are included in the imposed surface elevation timeseries. This discrepancy is however only in the order of 3%.

Most important to note is the discrepancy between the amount of LF energy from MEAS and PRB1 versus JONS and J+LB, see Figure 3.6. It seems that the measurements contain excessively high energy at low frequencies. This has been noted in the analyses of the available data. Apparently, when reproducing the measurements using a Jonswap spectrum (with or without including the theoretically calculated bound wave in the input timeseries), the resulting LF waveheight is ill-estimated: approximately half of what has been measured.

This discrepancy is not related to the uncertainty within the realization of the input timeseries, i.e. the relative deviation exceeds by far the uncertainty due to phasing realization, which is further discussed in Appendix C.

Most probably the amount of LF energy found in the measurements is due to basin oscillations. Considering that the run lengths are comparable, it would be expected that this oscillation would be triggered in the Triton run too, but

Table 3.2: Results from simulation $T_p = 14\,s$, at probe 3

	Full spectrum				LF part of spectrum (Figure 3.6b)			
	JONS	J+LB	PRB1	MEAS	JONS	J+LB	PRB1	MEAS
H_{m0} [m]	1.52	1.52	1.64	1.59	0.11	0.11	0.27	0.22
T_p [s]	13.94	14.17	13.31	13.15	125.0	1400	123.2	62.18
$T_{m-1,0}$ [s]	13.14	14.83	15.26	14.09	104.5	485.2	98.32	73.92
$T_{m0,1}$ [s]	11.84	11.77	12.41	12.27	63.25	97.59	62.09	53.72
$T_{m0,2}$ [s]	11.33	11.28	11.77	11.66	55.53	70.34	53.76	48.66

this is seen to be hardly the case (the blue and green lines share some peaks with the red and cyan lines, but their amplitude is very limited). In Appendix B it has been shown that the surface elevation imposed through the wavemaker contains much more LF wave energy than can be expected from theory. This has likely caused the seiching amplitude measured.

The excessive LF wave energy occurs in three distinct ranges, 7–10 mHz, 15–18 mHz and 21–25 mHz. The most profound is in the first range, with 100–160 s periods. Taking into account that ship motions are typically in the range 40–100 s (0.010–0.025 Hz; see Section B.7) it is assumed the impact of LF energy found on the resulting ship motion in this range will be limited. The other ranges mentioned are less overestimated in measurements too, but will likely affect the vessel motions.

When incident waves are defined using measurements at probe 1, the spectrums peaks seem to be reproduced adequately. In this case, as can be seen from Table 3.2, the LF waveheights $H_{m0,lf}$ (in which the low-frequency range is defined 0–0.04 Hz) are slightly overestimated by Triton. Furthermore, periods are consistently higher from Triton simulations than from measurements.

Comparing JONS with J+LB, the difference being the inclusion of bound waves in the timeseries, it shows that the amount of LF wave energy does not differ significantly. Due to the force disequilibrium of a wavefield without bound waves, low-frequency waves are generated as free components. It must be noted however that the distribution of this energy over the lower frequency range is different, i.e. the proper inclusion of bound waves induces more energy at the very low frequencies. Furthermore, as the LF waves are free, the phases of these waves deviate from those of the properly added LF bound waves as well as from those imposed during physical modeling.

It is concluded that the results from PRB1 are sufficiently close to measurements to use as an input for vessel motions computations.

3.4.2 Vessel motion and mooring line forces

The wavefield data from Triton simulations serves as input for the subsequent steps in the method chain, as discussed in Section 1.2. Use has been made of the results of runs PRB1 to approach the wavefield during measurements as far as possible. Below, a discussion of the run considering a condition of $T = 14\,s$ is given.

The forces on the vessel body are shown in Figure 3.7. It can be seen that the calculation is stable and has no increasing or decreasing trend.

A first run of Quaysim and evaluation is made using the mooring system parameters known from literature, taking the friction coefficient, mooring line

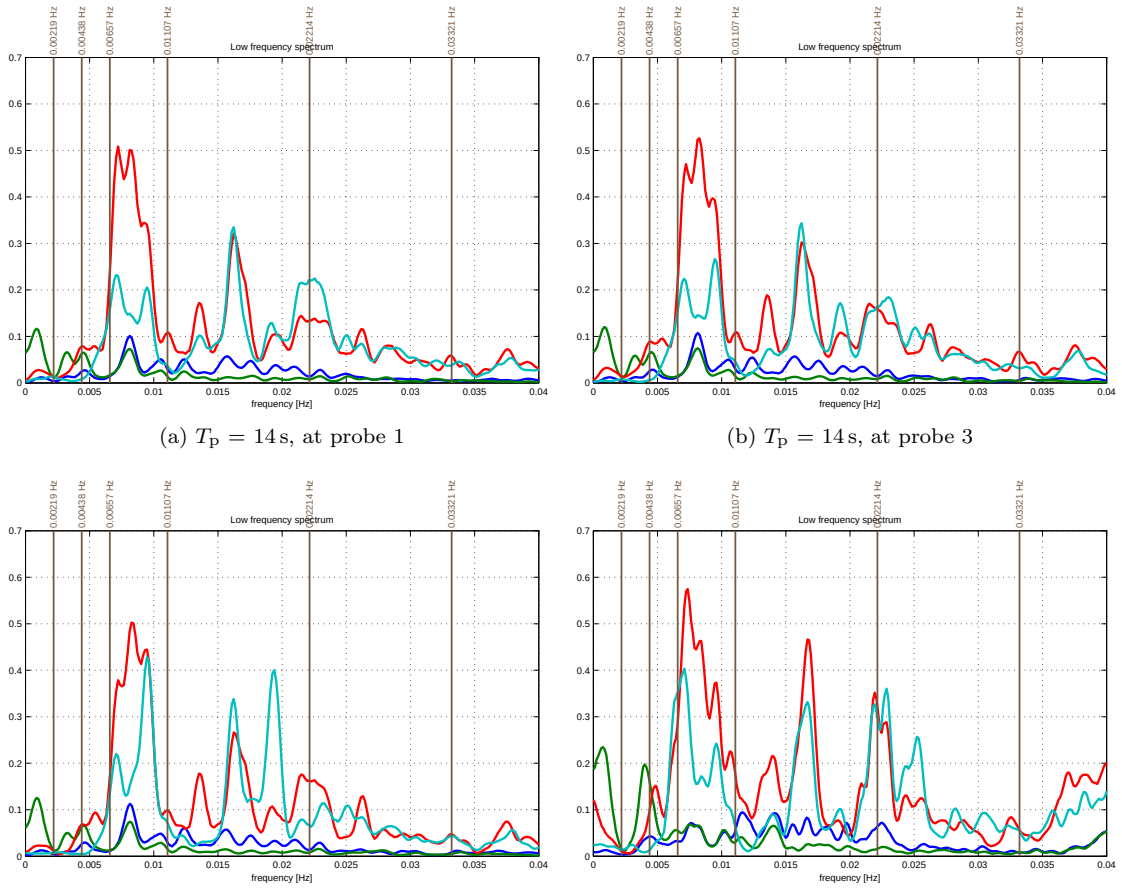

(a) $T_\mathrm{p} = 14\,\mathrm{s}$, at probe 1

(b) $T_\mathrm{p} = 14\,\mathrm{s}$, at probe 3

(c) $T_\mathrm{p} = 14\,\mathrm{s}$, at probe 4

(d) $T_\mathrm{p} = 16\,\mathrm{s}$, at probe 3

Figure 3.6: Modeling of phase 1, showing LF part of spectrum; using primary spectrum (blue), primary spectrum including LF waves conform Van Dongeren (green), using waterlevel measured at probe 1 as input (cyan) and the corresponding measurement (red); vertical lines indicate the first eigenmodes of the basin

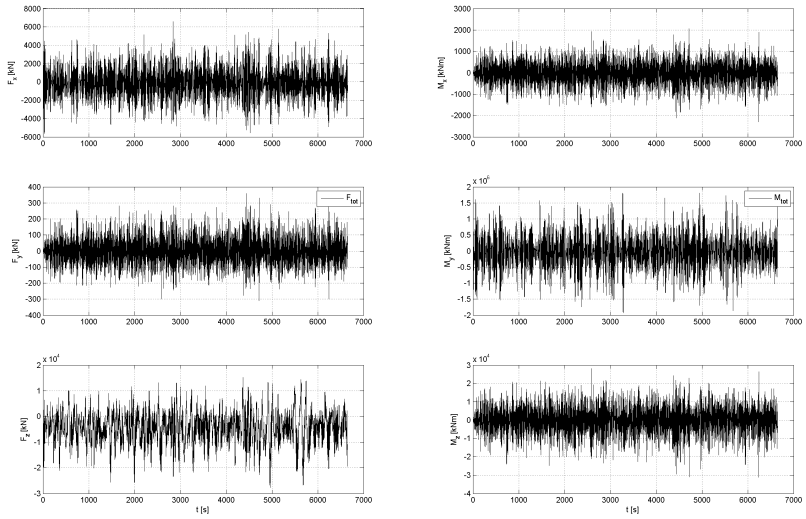

(a) Forces (b) Moments

Figure 3.7: Resulting force timeseries in all six directions, obtained by Harberth, based on PRB1

Table 3.3: Significant motion (defined as $4\sqrt{\text{variance}}$) of run considering $T = 14\,\text{s}$ before calibration

	Surge [m]	Sway [m]	Heave [m]	Roll [°]	Pitch [°]	Yaw [°]
Simulation	2.989	0.750	0.336	0.169	0.787	0.394
Measurement	1.532	0.919	0.384	0.826	0.408	0.825
Difference	+95%	-18%	-12%	-80%	+93%	-52%

pretension and charateristics according to measurements performed on the physical setup. The motions obtained from Quaysim are evaluated through spectral analyses, see Figure 3.8 and compared to measured motion spectra (Figure B.5). A concise comparison is given in Table 3.3.

Keeping in mind the relevance for ship (un)loading, the horizontal motions surge, sway and yaw are most important. Whereas the simulation results show an overestimation of surge by 99%, sway and (to a lower degree) yaw are underestimated. The former is dependent most significantly on fender friction. Since mooring lines keep the vessel on the fenders, their lay-out and tension has an influence as well. The eigenperiod of surge from simulation is higher than the measured eigenperiod (the blue peak is right of the most left green peak). This eigenperiod is essentially determined by the stiffness of the mooring system and the vessel's mass and added mass. Yaw, on the contrary, shows an underestimation of the eigenperiod, possibly due to an overestimated mooring line stiffness. The narrow peak of yaw motion shows in the surge spectrum as well.

The three peaks shown in the low-frequency band of the heave motion show for both measurement as simulation results. These three peaks, at approxim-

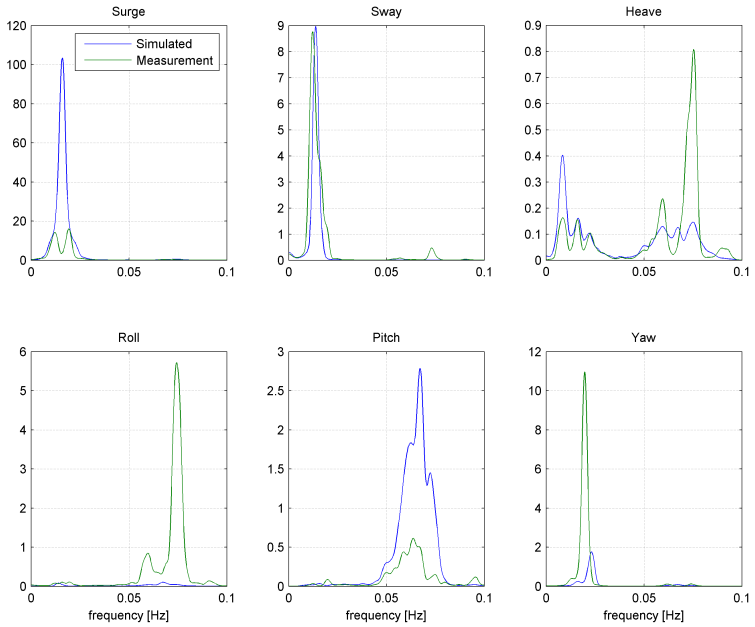

Figure 3.8: Motion spectra resulting from Quaysim (blue) and measurements (green) for condition $T = 14\,\mathrm{s}$

Table 3.4: Adjusted parameters for calibration

Parameter		Original	Adjusted
Break elongation mooring line	1 [-]	0.0505	0.0562
	2	0.0417	0.058
	3	0.0467	0.050
	4	0.0472	0.0520
	5	0.0454	0.0936
	6	0.0455	0.090
	7	0.0417	0.0603
	8	0.0344	0.068
Fender reaction force [kN]		1000	800
Fender friction coefficient [-]		0.12	0.25
Viscous damping coefficient for yaw [-]		0.027	0.00

ately 8, 16 and 22 mHz can be attributed to the LF wave energy, as discussed earlier.

The underestimation of roll and sway might be attributed to the occurrence of sloshing (transversal waves) in the model basin. It is possible that these waves are ill-resolved by Triton due to the limited resolution in y-direction. A comparison run with a higher resolution did, however, not show a significant difference. The sloshing in the physical basin might have been caused by incident wave being less unidirectional than assumed in the Triton run.

Another influence on sway is given by the fenders reaction force, pushing the vessel off the fender after impact.

The motions in roll and pitch are sufficiently small that the discrepancy between the measurements and the model results are not determining. The heave motion seems overestimated on first sight, but considering our interest in low-frequency motions, the simulation is quite accurate.

A statistical analysis of mooring line forces shows that the breaking force of 2×640 kN is occasionally exceeded, especially for mooring lines 3 and 4, indicating a high force pushing the vessel backwards, not unlikely in the case of head-on waves.

Calibration

It has been pursued to calibrate the model input to further approach the measurements. As discussed above, relevant parameters are the fender friction, the fenders reaction force and the mooring line stress-strain characteristic. Changes made are shown in Table 3.4. Based on an analysis of the first run, fender friction was increased, the fender reaction force was decreased and mooring line stiffness was adjusted through the break elongation per mooring line.

The calibration was based on condition $T = 14$ s. Results are shown in Tables 3.5 and 3.6. It has been attempted to improve the correspondence of mooring line forces.

As can be seen from Figures 3.9, 3.10 and 3.11, the simulation does improve. However, it must be concluded that the simulation is still not reliable, as deviations do occur for the different conditions tested. Specifically, it can be seen that higher energy conditions are more profoundly overestimated.

Table 3.5: Significant motion of the run for $T = 14\,\mathrm{s}$ after calibration

	Surge [m]	Sway [m]	Heave [m]	Roll [°]	Pitch [°]	Yaw [°]
Simulation	2.217	0.755	0.334	0.177	0.780	0.424
Measurement	1.532	0.919	0.384	0.826	0.408	0.825
Difference	+45%	-18%	-13%	-79%	+91%	-49%

Table 3.6: Significant mooring line force of the run for $T = 14\,\mathrm{s}$ after calibration

Mooring line	1	2	3	4	5	6	7	8
Simulation	368.9	602.9	683.6	1018.5	554.3	300.7	441.4	354.1
Measurement	150.3	269.3	337.0	269.2	213.8	322.7	270.8	282.7
Difference	+145%	+124%	+103%	+278%	+159%	-7%	+63%	+25%

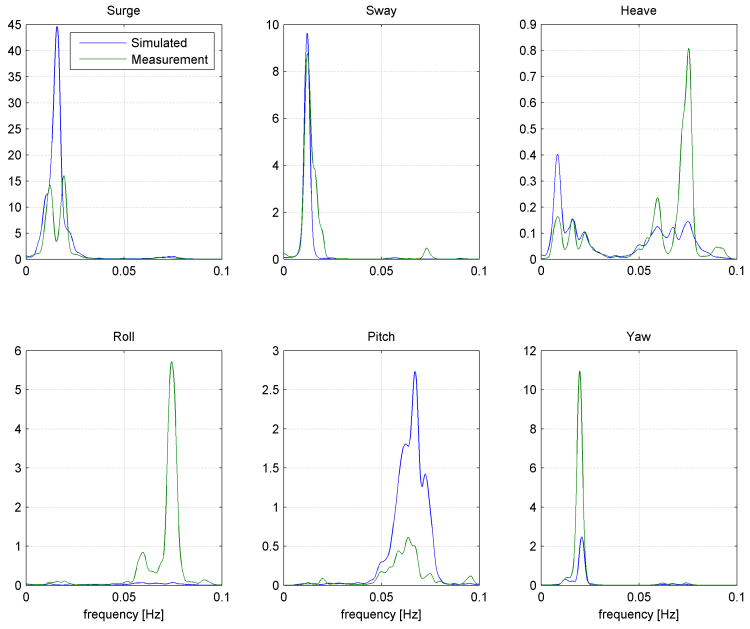

Figure 3.9: Resulting motion spectra after calibration for $T = 14\,\mathrm{s}$

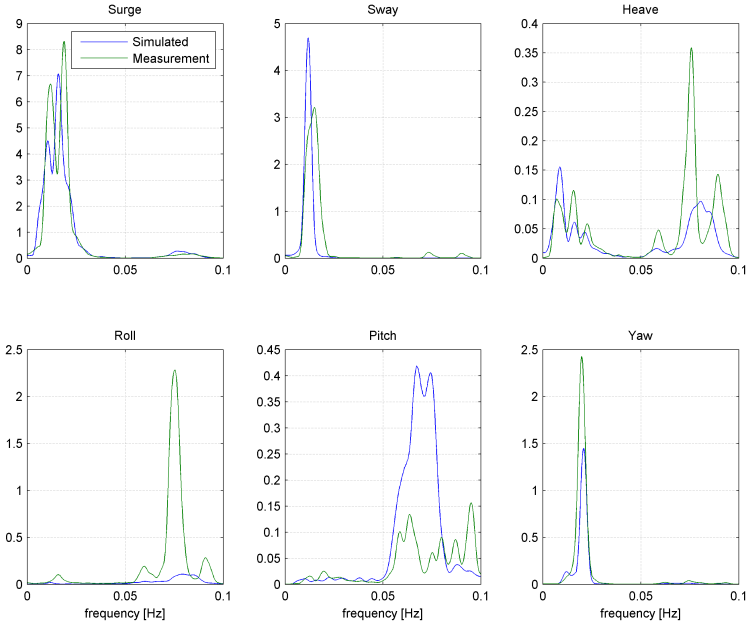

Figure 3.10: Resulting motion spectra after calibration for $T = 12\,\mathrm{s}$

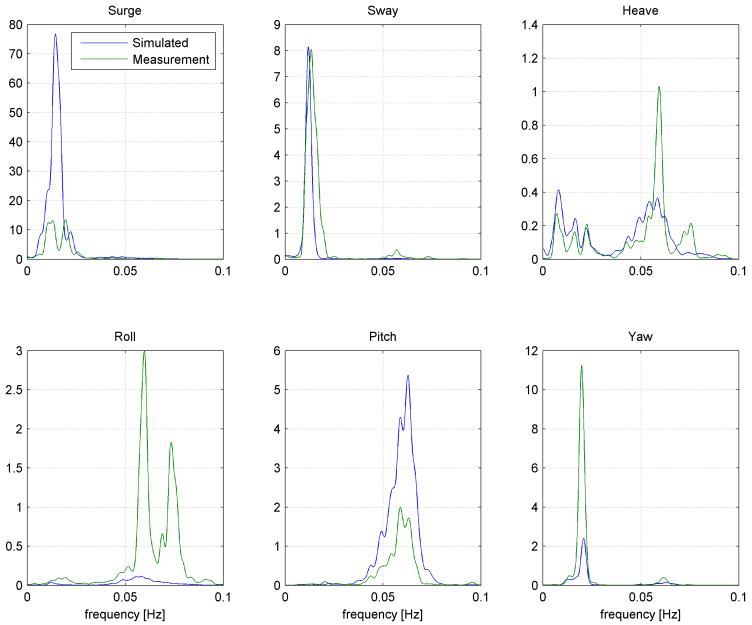

Figure 3.11: Resulting motion spectra after calibration for $T = 16\,\mathrm{s}$

Due to time restrictions, a better calibration could not be performed within this project.

3.5 Conclusion

An important discrepancy is found in the wavefield simulated by Triton, compared to the waverecords measured. A high amount of LF energy seems to be present in the physical model tests, presumably due to eigenwaves triggered. Underlying cause of these eigenmodes may be found in the excessive amount of LF energy imposed in the physical model, although this must be further explored to ensure this hypothesis.

It is expected through the overlapping frequency ranges of these LF waves and natural frequencies of vessel motions that this excessive amount of LF wave energy has had an affect on vessel motions amplitude. This has subsequently been shown from the Quaysim results.

It has been decided to proceed to the chain elements Harberth and Quaysim using the model results of PRB1, in which measurements of a probe were imposed as boundary condition. The wavefield is modeled appropriately, shown above. This approach ensures the best accordance with measurements and thus a more isolated evaluation of Harberth and Quaysim.

The model does show the important aspects influencing the motions, considering the most important, horizontal motions. However, deviations in the significant value are clear. Even after calibration the model results are not truly reliable. A more extensive calibration needs to be performed.

Although many more conditions were tested during the physical measurements, it has not been pursued to reproduce these using the presented model chain. Due to the discrepancy found in the LF wave energy, it is recommended to perform a similar validation but based on a different physical model test as future research.

This does however indicate the difficulty found when modeling vessel motions using Harberth and Quaysim. Even when parameters are measured and lay-out has been documented, the system shows to be very sensitive to deviations thereof. Estimating ship motions based purely on numerical modeling is therefore highly discouraged. Rather, numerical simulations must be (extensively) calibrated using prototype or physical model measurements.

Chapter 4

Port of Leixões, berth A

> "In January 1974, a tanker of 137,000 DWT experienced surge motions of 10 to 15 m and sway motions of 3 to 4 m. During this event, five mooring lines were broken. The analysis of wave records in that period shows the presence of waves with periods ranging from 2 to 4 minutes and heights of approximately 50 cm." (Campos Morais and Abecasis, 1978)

4.1 Introduction

The Port of Leixões is located in the north of Portugal. Its one the most important ports of the country. Annually, its oil terminal handles over $7{\cdot}10^6$ tons of cargo.

This oil terminal is composed of three berths, as can be seen in the aerial photograph, Figure 4.1. Berth B and C, used for refined products, are located in the harbour basin and offer a depth of CD-10 m and CD-6 m respectively. Berth A — the berth of interest — is located along the ports northern breakwater, near the harbour entrance, in relatively unsheltered water. Alongside this berth the depth is approximately CD-16 m, facilitating oil tankers up to 100,000 DWT.

Between 1990 and 2003 berth A was inoperative during on average 23% of the time (Rosa Santos et al., 2008a). Inoperativeness is specifically high during the months of January and December, reaching on average 50%, as shown in the graph, Figure 4.2. It must be noted that also the time that dredging or maintainance caused the unavailability of berth A is included in these figures. Nevertheless, in general it is stated that the operational and security conditions are not assured, on average, about 20% of the time.

In case of critical environmental conditions, (un)loading operations have to be stopped as soon as possible. The ship is kept in position by tugboats and, if necessary, additional mooring lines. If these measures prove insufficient, the oil tanker needs to leave the berth. Although nowadays weather forecasts are available 3–5 days ahead, this situation still occurs (Rosa Santos et al., 2008a).

The conditions at berth A are supposedly particularly influenced by the overtopping of and transmission through the ports northern breakwater and diffraction around this breakwaters head. Moreover, resonance phenomena may play a significant role in the wave action at this berth. Finally, the vessel's

Figure 4.1: Satellite picture of the Port of Leixões area, showing the oil terminal and its three berths (© GeoEye; DigitalGlobe)

motions are influenced by the the mooring system and fenders. (Veloso Gomes et al., 2005)

These aspects will be treated in the subsequent sections.

4.1.1 Historical development Leixões

An overview of the historical development of the Port of Leixões is given in Figure 4.3.

The Port of Leixões undertook expansion projects in the 1930's and 1970's. In the late 1990's the port has been adopted to be able to handle Panamax container vessels.

A more recent development is the SPM (single point mooring) system that has been installed offshore of the Port of Leixões in 2006, at a depth of CD-28.5 m. This system is intended to facilitate oil tankers up to 150,000 DWT, the biggest that demand Leixões, having a draft up to 17 m. This SPM can be used during adverse weather conditions also, it does however only facilitate unloading operations.

The existing Leixões northern breakwater has a crest at CD+15 m. Its approximately 700 m long tail was initially constructed as a submerged breakwater (1940) but was later reinforced into an emerged rubble-mound breakwater (1969). It is along this part of the northern breakwater that berth A is located. After a severe storm in the 70's, damaging the emerged breakwater, the breakwater was reconstructed and further protected by a new submerged breakwater on its seaward side.

These developments too can be seen in Figure 4.3.

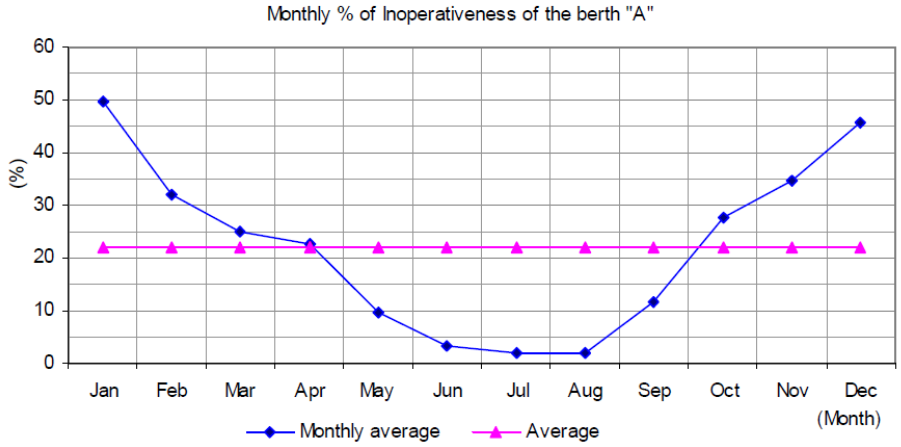

Figure 4.2: Monthly percentage of inoperativeness of berth A, 1990–2003 (Rosa Santos et al., 2008a)

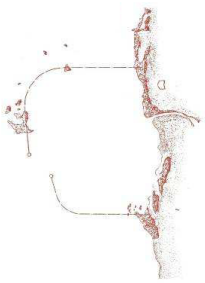

(a) 1890

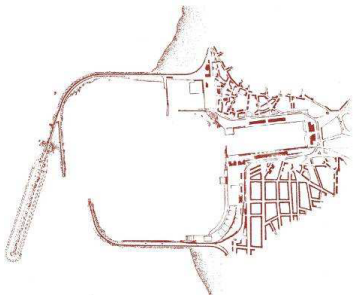

(b) 1940, showing the submerged breakwater with crest CD+1 m and dock 1, constructed between 1937–1941

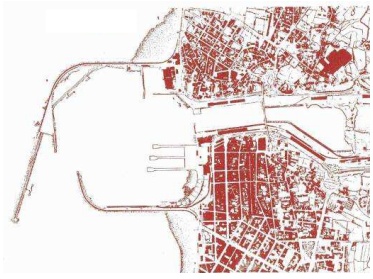

(c) 1969, showing the emerged northern breakwater and berth A

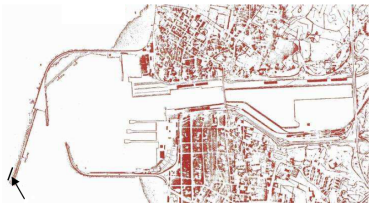

(d) 1980, showing the completed dock 2 of which construction started in the 1950's and the location of the submerged breakwater on the seaward side (indicated by an arrow)

Figure 4.3: Historical development of the Port of Leixões (images from Rosa Santos et al., 2008a); (Campos Morais and Abecasis, 1978)

4.2 Environmental conditions

In the vicinity of the Port of Leixões tides are of the semi-diurnal type, reaching amplitudes that range between 2–4 m, see Table 4.1. CD denotes a few centimeters above LLW, lowest low water level (Campos Morais and Abecasis, 1978). The meteorological tides outside enclosed water bodies are small (0.2 m to 0.6 m).

Table 4.1: Tidal range (Rosa Santos et al., 2008a)

High tide	CD+4 m
MSL	CD+2 m

The wave climate is highly energetic. The main storms come from the North Atlantic, mainly between the months of October and March. Wave directions between west and northwest prevail (Rosa Santos et al., 2010b). Waves from southwest do not occur very often, and their significant wave height is usually small compared to waves coming from the other directions.

Analysis of Leixões wave buoy data (since 1996 installed at 41 °19'N 8 °59'E, at 83 m waterdepth) between 1981–2003 indicate (Rosa Santos et al., 2008a)

- a typical offshore waveheight $H_s = 2.5$ m with a probability of exceedance of 73%
- that most frequent wave periods are in the range 7–12 s.

4.2.1 Inoperativeness conditions

An analysis (Rosa Santos et al., 2008a; Veloso Gomes et al., 2005) of wave records has shown that berth A's inoperativeness is predominantly caused by offshore waves of over 2.5 m in height having wave periods of 8–20 s. Furthermore, studies have concluded that mainly waves coming from a direction between west (270°) and northwest (315°), i.e. approximately perpendicular to the northern breakwater, affected the operativeness (Rosa Santos et al., 2008a). Terminal operators and ship pilots have stated that the most problematic sea states occur when waves approach from the west (almost perpendicular to the northern breakwater). These waves can diffract around the head of the breakwater more easily. (Rosa Santos et al., 2010a,b)

The conditions associated with inoperativeness are shown in Figures 4.4 and 4.5.

In general berth A is operational when the deep water waveheight is less than 2.5 m and for wave periods of 7–15 s (Veloso Gomes et al., 2005).

4.2.2 Extreme conditions

During storms, significant offshore waveheights may exceed 8 m and wave periods can be of the order of 16–18 s, with the storm persisting for up to 5 days (Rosa Santos et al., 2010b). Furthermore, extreme storm events include deep water waveheights exceeding 20 m and deep water wave periods reaching 25 s (Veloso Gomes et al., 2005).

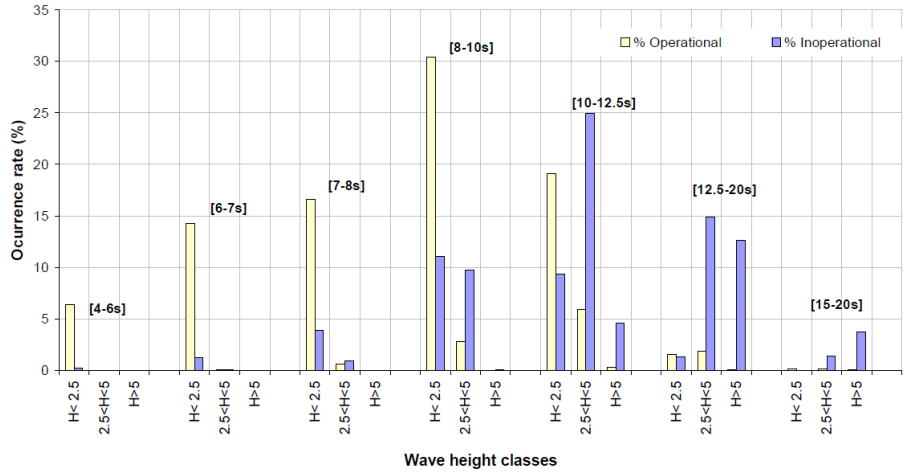

Figure 4.4: Distribution of berth A inoperativeness by wave height and wave period classes (Rosa Santos et al., 2008a)

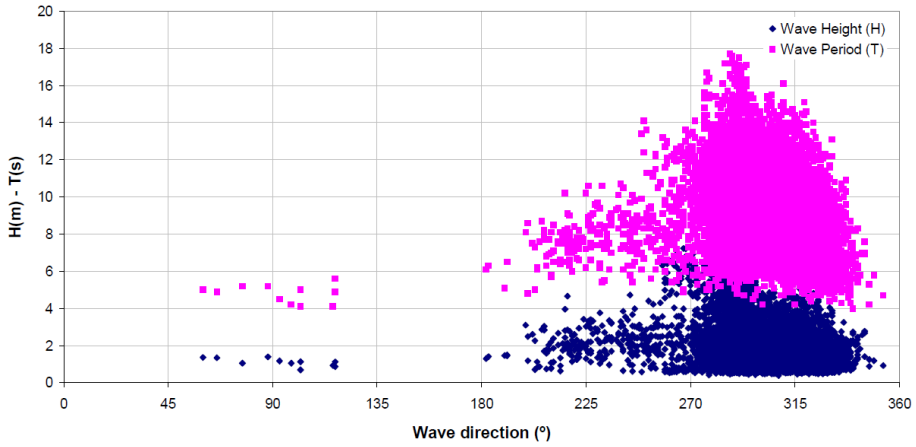

Figure 4.5: Berth A inoperativeness offshore conditions (Rosa Santos et al., 2008a)

Extreme events as a function of return period (T_R) were assessed by Veloso Gomes et al. (2005). Table 4.2 shows their findings, supplemented by data from Veloso Gomes et al. (2009). The latter have determined the extreme conditions based on buoys within 100 km of Leixões as the buoy close to Leixões has less than 20 years of registered data.

Table 4.2: Extreme wave conditions

T_R [year]	T_p [s]	H_s [m]	H_{max} [m]	
1		7–8	12–13	(Campos Morais and Abecasis, 1978)
10	12.0–23.2	11.1		(Veloso Gomes et al., 2009)
10		12.7	20.3–22.9	(Veloso Gomes et al., 2005)
50		13.3	21.3–24.0	

Close to the berth, results of numerical simulation as well as ship pilot reports show that during high tide waves of 2.5 m may be expected due to certain offshore wave conditions (Veloso Gomes et al., 2005).

4.2.3 Long waves

Rosa Santos et al. (2008a); Veloso Gomes et al. (2005) state that in the Leixões harbour area two ranges of low-frequency waves often occur: the first one with periods ranging 2–5 minutes and the second with periods ranging from 15–20 minutes. Campos Morais and Abecasis (1978) report the presence of waves with periods 4, 8, 16, 20 and 40 minutes having significant amplitude.

Based on the primary wave energy statistics, Rosa Santos (2010, p.381) deduces that an offshore LF waveheight of 10–15 cm occurs approximately 65% of the time.

So far, no measurements of long waves have been performed. The port authority has data from a tidal gauge enabling a limited extraction of low-frequency data. This has however not yet been executed. (Rosa Santos, 2012a)

4.3 Bathymetry

The bathymetry near the port is given in Figure 4.6, taken from admiralty charts.

4.4 Port lay-out

As discussed, berth A is located on the leeside of the northern breakwater of the Port of Leixões. The proximity of berth A to the breakwater head implies that the climate at the berth is significantly influenced by diffracting waves around, overtopping waves over and transmitted waves through the breakwater. These will be discussed below.

Another probable effect of the current port lay-out is the occurence of seiches, e.g. Campos Morais and Abecasis (1978) have hypothesized a resonant area along berth A, shown in Figure 4.8. This triangular wedge is supposed to have a resonance period of approximately 133 s.

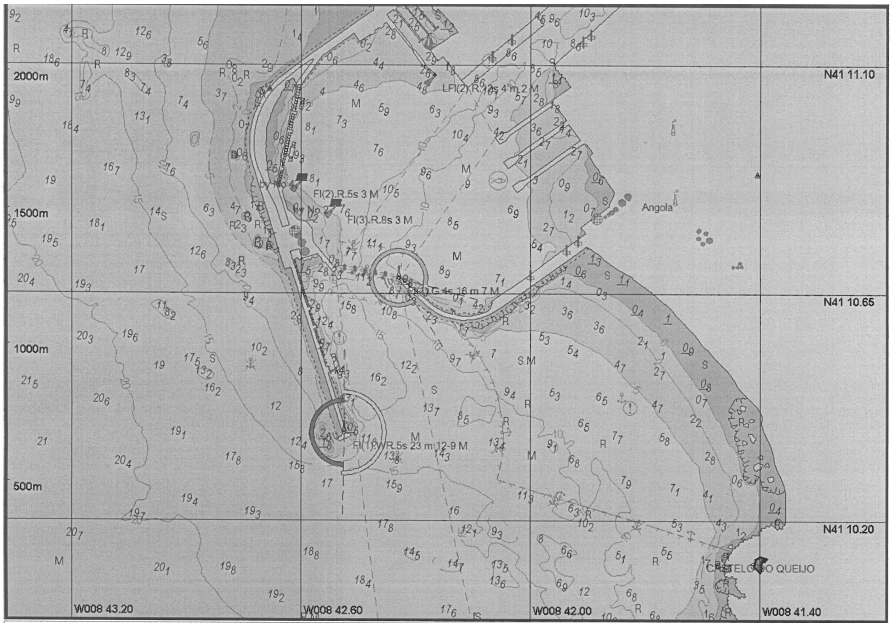

Figure 4.6: Leixões area bathymetry [m] (© Chartworx)

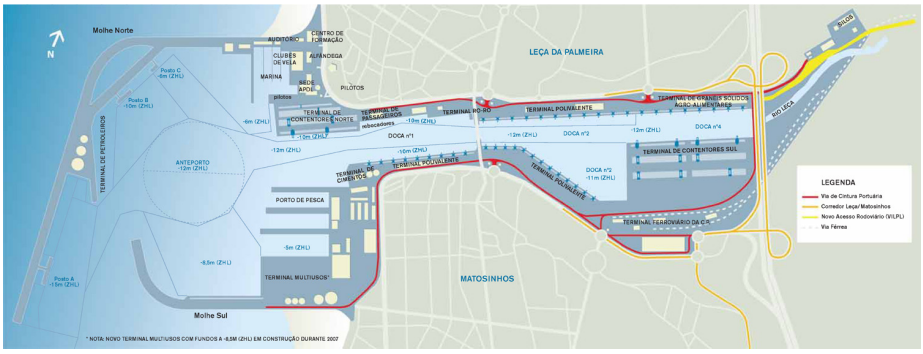

Figure 4.7: Port layout (© APDL)

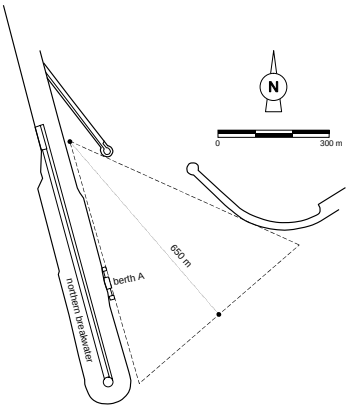

Figure 4.8: Hypothetical resonant area (adapted from Campos Morais and Abecasis, 1978)

4.4.1 Overtopping and transmission of the northern breakwater

Overtopping events affect the berth A in two different ways. The wave conditions in the vicinity of the berth worsen by the overtopping water, affecting the berthing, most importantly by pushing the vessel off the fenders. Secondly, the access to the berth through the northern breakwater in order to release the mooring lines in emergency situations is made difficult.

Veloso Gomes et al. (2009) have physically modeled the overtopping of the breakwater. From this, it can be concluded that during adverse conditions (H = 12.3 m and T_p = 20 s) the overtopping is severe: $Q \approx 40\,\mathrm{L/s/m}$'.

An analysis of the bathymetry evolution lead to the supposition that sediments are able to cross the breakwater core induced by water movements (Veloso Gomes et al., 2005). This supposition is supported visually by pilots and terminal operators noticing water and sand flows coming from the breakwater normally at the stern of the ship during adverse sea conditions. Because of the history of the breakwater — it is built up in several phases using different materials, see Section 4.1.1 — it is not possible to accurately determine the permeability conditions of the structure. However, the presence of the 90 tonne concrete blocks on the armor layer of the old submerged breakwater is enough to conclude that the structure is permeable to sediments as well as water currents.

4.5 Berth properties

Berth A, shown in Figure 4.9, can accommodate vessels up to 100,000 DWT carrying crude oil and other refined products. The jetty structure of berth A consists of two breasting dolphins, equipped with a pneumatic fender and double mooring hooks. In this arrangement eight mooring legs are used with double mooring lines, see Figure 4.10. The largest oil tankers are usually moored using

steel mooring lines with a synthetic mooring tail (usually nylon). The breaking strength of these mooring lines is typically of the order of 90–100 t and their maximum energy absorption capacity is approximately 135 t·m.

Figure 4.9: Berth A (Rosa Santos, 2010)

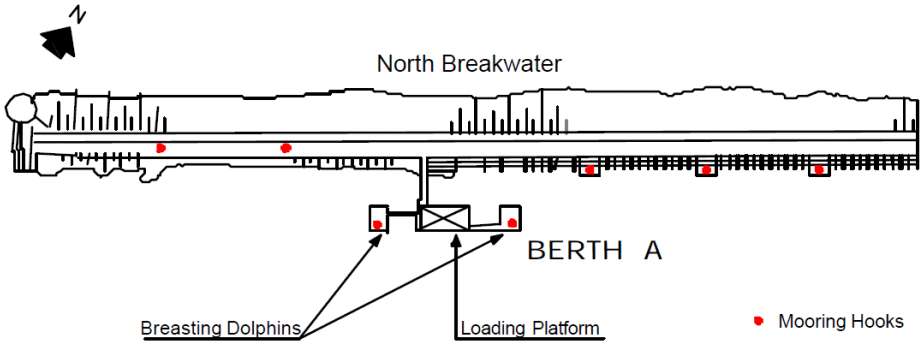

Figure 4.10: Sketch of berth a mooring lay-out (Veloso Gomes et al., 2005)

The pneumatic type fender berth A is equipped with, see Figure 4.11, has been pointed out as a possible drawback issue. These fenders have a typical high recoiling behavior This means that almost all the energy transmitted to the fender, either during the berthing or after each impact while the ship is moored to the berthing structure, is transmitted back to the oil tanker and only small energy dissipation occurs in the fender. When the vessel is pushed off the fender, the friction in surge direction decreases drastically.

4.5.1 Studied mooring system elements influence

As a possible intervention on the oil tankers mooring system, the use of pretension on the ship breast lines was assessed. This measure causes the oil tanker to be pulled against the installed pneumatic fenders, taking advantage of the fender friction characteristics to reduce the moored ship motions, especially surge. Based on physical model tests, it was concluded that increasing breast lines' pretension effectively reduces these motions, specifically those in the horizontal plane. The best results were obtained when high pretension forces were combined with high friction fenders. In this case, reductions of 35 and 60% can

Figure 4.11: Berth A's fender (Rosa Santos, 2010)

be achieved (Rosa Santos et al., 2010a). The influence on the ship sway motions is less significant but still important.

Another possible adaption, a modification of the mooring layout in accordance with the OCIMF recommendations (as mentioned in Section 2.6.1), was found to have only a negligible influence on the moored ship response.

Finally, water depth was identified as an important factor controlling the response of the moored ship through the underkeel clearance (UKC) (Rosa Santos et al., 2010b).

Chapter 5

Model set-up

5.1 Model purpose

Using physical models one is limited by the dimensions of the basin. Although a numerical models extent is also limited due to the computational effort, it allows easier variation and far more set-up freedom. By modeling the Port of Leixões numerically one is thereby able to distinguish real processes from those induced by physical or numerical modeling.

Van der Wel (2011) has recommended to take into account the inner harbour basin of the Port of Leixões rather than limiting the domain at the harbour entrance. In this way, eigenmodes developed in the numerical model can be expected to have a correspondence to reality instead of being due solely to modeling limitations. Furthermore, a numerical model with this extent provides data that can be well used for an interpretation of physical processes at the Port of Leixões.

The purpose of the model presented in this chapter is thus to gather data enabling such an interpretation and ensuring the noticed phenomena are occurring in reality.

The analyses presented in Chapter 6 are based primarily on two set-ups, denoted as LG05 and LG06. The latter uses closed boundaries along the breakwaters and basin. This model is intended to provide a better insight in the effect of reflections and eigenmodes, due to the breakwaters and basin perimeter, specifically. The two set-ups will be introduced below.

5.2 Model extent

The extent of the numerical model used in this phase can be seen in Figure 5.1. Its dimensions are 2,568 m left to right by 2,084 m. The incident wave boundary is approximately 1.2 km from the breakwater, the southern boundary approximately 0.7 km from the breakwaters tip.

The model boundaries have been simplified significantly to enlarge the robustness of the model by avoiding instabilities as encountered during previous runs (not discussed in this report), most notably in the corners of the boundary. The schematization to this end uses as many grid-aligned boundaries as

(a) Physical model (b) Present numerical mdoel

Figure 5.1: The extent of the numerical model presented in this chapter versus the extent of the physical model used by Rosa Santos (2010), both projected on an aerial view (© GeoEye; DigitalGlobe)

possible. As a result, the orientation of the southern breakwater differs from reality.

The models left-right direction is tilted 18 ° counterclockwise from the east-west direction in reality, i.e. upwards is pointing in a NNW-direction. This is done to align the northern breakwater with the grid and coincides with Rosa Santos' phase 2 physical model orientation, as can be seen from Figure 5.1.

The most important difference is the inclusion of the ports main basin, as shown in the figure. Futhermore, the beach has been reproduced on a more accurate location, whereas during physical modeling the beach was located closer to the quay. Finally, a difference can be found in the dimensions of the model, the present numerical model boundaries are further offshore and away from the breakwater.

Computational settings

The simulation length chosen is 11800 s. The timestep applied in calculation is $dt = 0.1$ s. The computational grid resolution is $dx = dy = 4$ m. Wave breaking and run-up, modules of Triton, have not been applied.

5.3 Bathymetry

The bathymetry used, shown in Figure 5.2 is based on admiralty charts of the Leixões port area (see Figure 4.6). In order to further avoid the mentioned instabilities, it has been pursued to minimize slopes at the boundaries, either along or perpendicular to the boundary. Furthermore, a minimum depth of CD-2 m is maintained for the same reason.

5.4 Boundary conditions

The boundaries are shown in Figure 5.3, again indicating the bathymetry and showing the output points. All diagonal boundaries are represented by staircase boundaries. Triton includes a cut-cell method (refer to Wenneker and

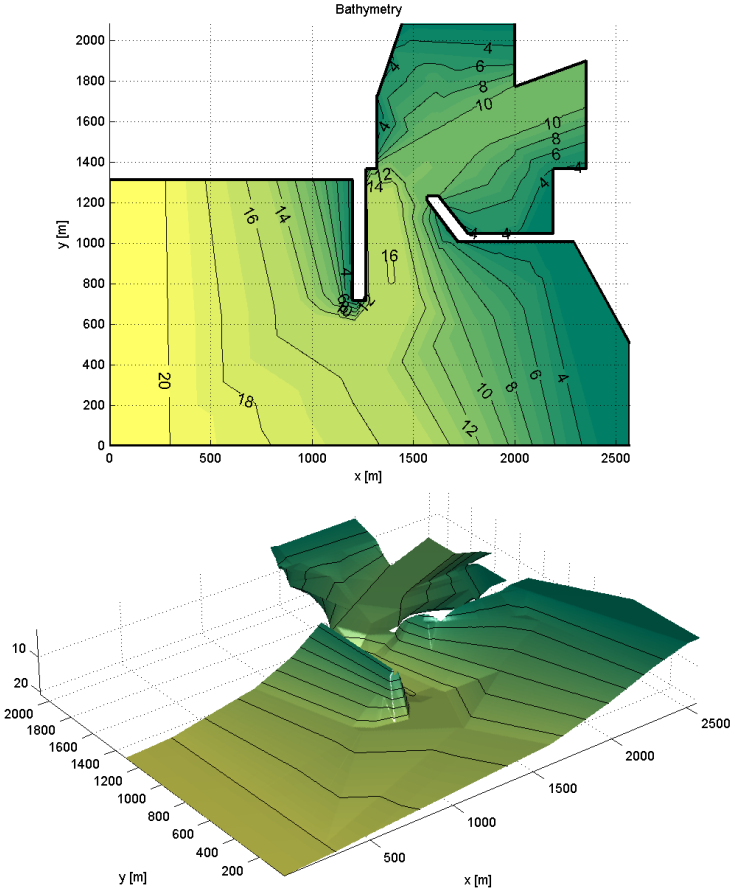

Figure 5.2: Bathymetry, depth with respect to CD

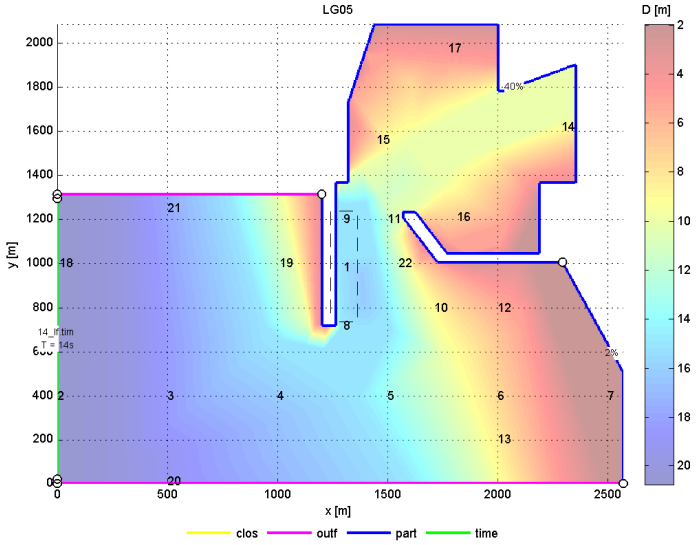

Figure 5.3: The model set-up used, showing the bathymetry and output locations. The boundary types are given, where yellow, pink, blue and greed denote a closed boundary, open boundary, partially reflecting boundary and incident wave through timeseries-file, respectively; the black dotted line indicates the grid at which the Taylor expansion coefficients are written as output data, to be used during the reproduction of the depth profile

Borsboom, 2005), a more appropriate method to model diagonal boundaries. This approach has not been used in the present runs as this easily induces instabilities.

The boundaries perpendicular to the incident wave have been defined as outflow, since the wave come in obliquely to the domain. A closed boundary would reflect these outgoing waves. For the same reason, the northern boundary has been chosen open too, thus enabling the wave energy to exit the domain as in reality.

Reflection parameters of LG05 are based on Van der Wel (2011, pp.63–67) in which a numerical model of phase 2 (see Appendix B) has been compared to corresponding measurements. A theoretical basis for reflection parameters is given in Appendix A. The second model (LG06) has been run with closed breakwater and basin boundaries, i.e. 100% reflection. As previously mentioned, this model allows a more specific interpretation of eigenmodes as these occur more pronounced. Furthermore, the importance of basin reflections is assessed more easily. It is expected that the reflection coefficient of the basin circumference in reality is between these two values, i.e. 40% reflcetion off vertical quay walls expectedly provides an underestimation in the harbour basin area.

	LG05	LG06
Beach	2%	2%
Breakwaters, basin boundaries	40%	100% (closed)

		Primary	Carrier	Bound
Waveheigth H_{m0}	[m]	2.50	2.31	0.10
Period $T_{m0,1}$	[m]	11.8	13.1	53.4
Mean direction	[°]	274.74	274.74	274.35
Spreading *DSPR*	[°]	15.2	15.6	36.5
Number of components		3200	617	380072

Table 5.1: Imposed spectrum at depth $H = 20\,\text{m}$

5.4.1 Waves

On the western boundary, a wave is imposed through a time series of surface elevation. This series has been created based on a Jonswap spectrum with $\theta = 274.5\,°$, directional spreading $DSPR = 15\,°\text{N}$, $H_{m0} = 2.5\,\text{m}$, $T_p = 14\,\text{s}$ and a peak enhancement factor $\gamma = 3.3$.

Bound waves have subsequently been added using Van Dongeren et al. (2003), as will be further discussed in Appendix A. Doing this, for practical reasons it has been assumed that only pairs of the most energetic of the primary waves induce bound LF waves. In the present study these components are referred to as carrier waves and each contains 10% or more of the maximally energetic component, the same threshold as used by Van Dongeren et al. (2003). It has been assumed that this approach does not induce an underestimation of the LF energy.

Table 5.1 shows the main properties of the primary, carrier and bound spectrum. Note that the directional spreading of the bound waves is larger than that of the original spectrum, as is expected from literature. Compared to the colinear case studied by Rosa Santos et al. (2008a); Van der Wel (2011), the bound low frequency wave height in the present set-up is lower, precisely due to and as expected from the directional spreading of the primary waves.

The input timeseries are generated with a sufficient frequency resolution to obtain accurate estimates of the spectral shape after postprocessing. Furthermore, a ramp-function has been applied to decrease the spin-up time. A cut-off period is used to allow this spin-up.

The resulting time series of wave elevation of one location along the western boundary (point $(x, y) = (0,20)$) is then shown in Figure 5.4.

Correspondence of imposed wave conditions to inoperativeness conditions

The waveheight and period are in the same order as those chosen during the physical research performed by Rosa Santos et al. (2008a). Observing Figure 4.5 and considering that these data are recorded by a buoy at 83 m waterdepth, it can be concluded that $H_{m0} = 2.5\,\text{m}$ and $T_p = 14\,\text{s}$ at CD-20 m are quite severe conditions and inoperativeness occurs typically for milder conditions than these.

Furthermore, as statistics show that inoperativeness occurs typically for waves with $\theta = 270$–$320\,°$, and pilots and terminal operators observe most critical conditions when $\theta \approx 252\,°$ (see Section 4.2.1), the chosen wave direction is considered representative. Regarding the directional spreading no information has been published. As a lower *DSPR* of primary induces a higher LF significant

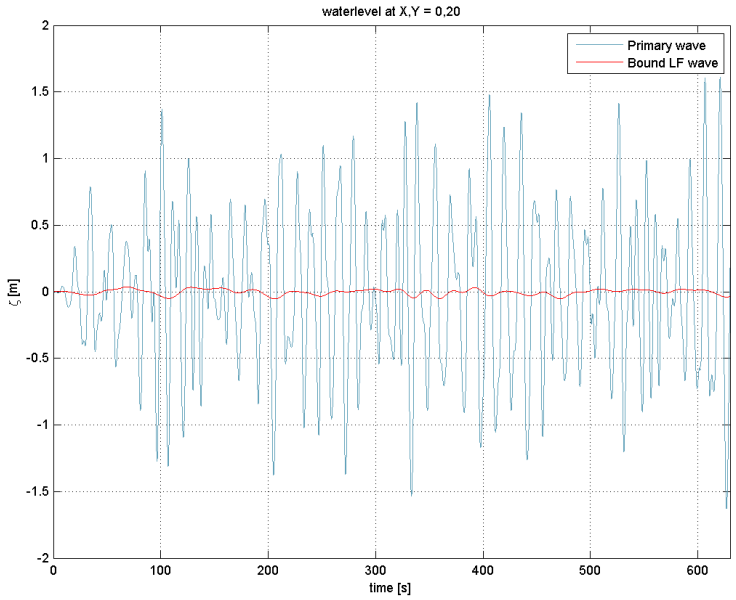

Figure 5.4: First part of generated timeseries

waveheight, $DSPR = 15\,^\circ$ is expected to be reasonable (corresponding to typical swell conditions) and not to underestimate the LF energy content.

The low-frequency wave height of approximately 10 cm on the incident wave boundary is in accordance with the typical values given by Rosa Santos (2010) (see Section 4.2.3).

As discussed earlier, transmission and overtopping is not possible to be included in Triton. Their influence is estimated to be sufficiently negligible for the current assessment.

In conlusion, it is assumed that the conditions imposed in these model runs are representative for the problem at hand and in accordance with previously performed studies.

Chapter 6

Results and discussion

In this chapter, results from runs LG05 and LG06 will be shown and discussed. These runs have been introduced in the precedent chapter; LG05 used breakwater and harbour basin reflection parameters of 40% whereas LG06 used closed boundaries.

This chapter aims to provide insight in the wave processes at the Port of Leixões relevant for a moored vessel at berth A. Due to the lack of confidence in the subsequent steps of the method, as treated in Chapter 3, Harberth and Quaysim have not been applied. When a more elaborate calibration of the latter model has been performed, this will very well be possible. Because of the restricted time within the thesis, this is beyond the present scope. Rather, to increase the knowledge of relevant wave processes found in the wavefield near the berth, the wave analyses of the case study have been emphasized.

Van der Wel (2011) has shown that Triton reproduces the physical scale model basin wave conditions with a good agreement. His results were influenced by the limited dimensions of the basin. The full-scale calculations performed in the present report is expected to complement his findings.

6.1 Primary wave climate

The primary wave energy at berth A is governed by shoaling and diffraction of waves. Reflection is expected to have a less significant effect since primary waves are typically dissipated at the beach, unlike LF waves.

Figure 6.1 shows an instantaneous surface elevation at the end of the run. Diffraction and shoaling can easily be identified and follows expectations.

Figure 6.2 shows the significant waveheight in the full domain resulting from the Triton runs using 40% reflection on breakwaters and harbour basin boundaries. The significant waveheight $H_{\mathrm{m0,full}}$ at the berth is approximately 19 cm, clearly only a small part of the incident primary waves with $H_{\mathrm{m0,full}} = 2.5\,\mathrm{m}$.

The angle of incidence $\theta = 274.5\,^{\circ}\mathrm{N}$ can easily be recognized as the significant waveheight decreases visibly along a line starting in the upper left of the domain, towards the breakwaters tip. Although it seems that this line does not exactly hit the breakwaters tip, a diffraction patterns on the leeside of the breakwater is evident.

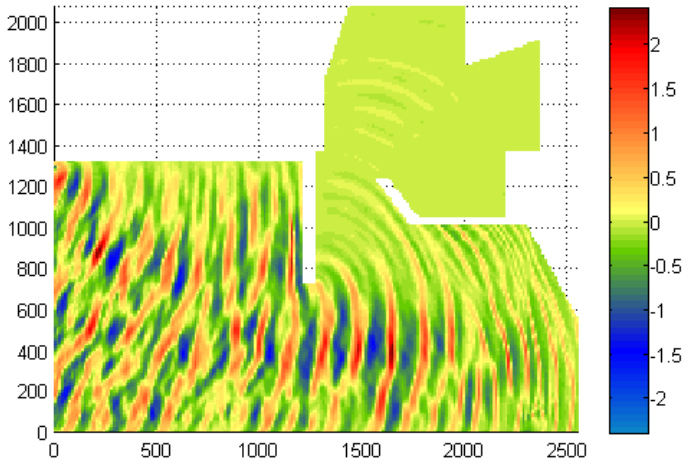

Figure 6.1: Instantaneous waterlevel elevation [m] at the end of run LG05, showing shoaling and diffraction

It has been pursued to improve the runs accounting for the above, by imposing a wavefield on the northern boundary too. These runs, however, caused instabilities near the breakwaters tip. One could alternatively extend the western boundary further north. However, as the instability is expected to be caused by waves with too high an amplitude, the instability might occur using this alteration as well. This instability is an unwanted feature of the boundary conditions presently implemented in Triton (and not necessarily found in other Boussinesq-type models).

An odd feature found in this image is the low significant waveheight along the southern boundary. As this boundary is defined an open boundary, it is expected that primary waves (to which period the boundary condition had been adapted) are not affected at all by its presence. However, it can be seen that little energy is found within approximately 30 m of this boundary. Other applications of Triton, outside this project, have shown simular results. It is understood that the boundary conditions perform best in accordance with settings for perpendicularly propagating waves. The low wave energy near the boundary could indicate that the boundary is construed as a nodal point due to the above deficiency. In this case, the boundary would act as a reflecting boundary and would therefore bounce energy towards the harbour entrance rather than letting it pass out of the system. This excessive amount of energy does however not show in the figure. It is therefore concluded that energy is simply dissipated along the boundary. This is desirable if completely parallel progressing waves are considered. The obliquely propagating waves seen here are detrimentally affected in the same manner.

Finally, it is notable how the significant waveheight seems to decrease along the wave propagation, starting at the incident boundary. Although dissipation is expected, especially in the surfzone, it can be seen that the wave energy content decreases gradually over the entire domain. Dissipation can occur due to the limited spatial resolution, as waves cannot be resolved when these are too

short with respect to the grid cell size. One would thus expect that the shown decrease of energy is most profound in the high frequency band. Analyzing the spectra of points along a line of propagation towards the shore, it can be seen that this is not the case. The decrease of waveheight along the domain is therefore not due to the spatial resolution. The mechanism causing this energy reduction has not been identified within this project as the impact thereof is estimated to be limited to primary waves.

In conlcusion, some shortcomings are found. Overall it can however be noted that the most important primary wave phenomena at Leixões, diffraction around the breakwaters tip and shoaling towards the shore, are apparent in this model.

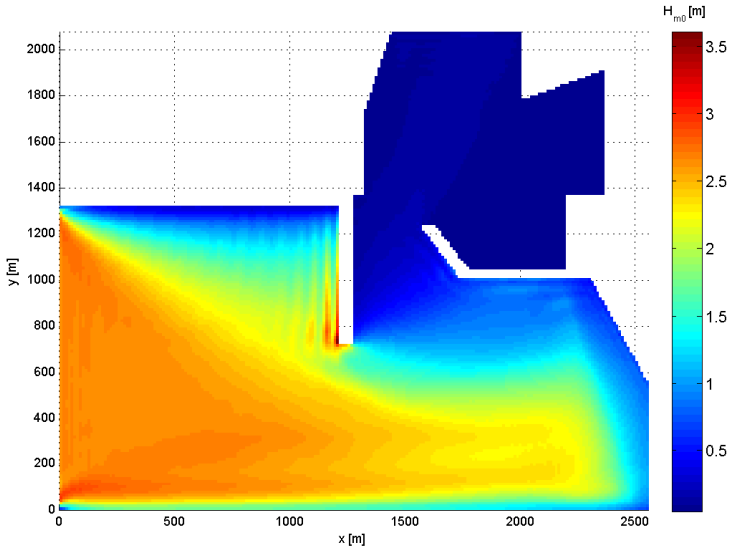

Figure 6.2: Full spectrum waveheight $H_{\mathrm{m0,full}}$ (from LG05)

6.2 Low frequency waveheight

It has been concluded above that berth A is well protected against the attack of the primary waves. However, the relative waveheight of low frequency waves at berth A is high; whereas primary wave energy hardly propagates to berth A, low frequency energy does, through reflection and diffraction.

Figure 6.3 shows the significant low frequency waveheight in the entire domain. It can be seen that, of the approximately 10 cm at the incident boundary, 6 cm $H_{\mathrm{m0,lf}}$ is found at berth A. This shows that even the leeside of a breakwater, in a lay-out as found in Leixões, is relatively ill-protected from LF waves. Moreover, it is important to note that this range of periods, 25–200 s, also includes natural frequencies of some important degrees of freedom of the vessel considered.

A phenomenon clearly seen in the figure is the profound shoaling of LF waves. When comparing with Figure 6.2, it is evident that the low frequency waveheight increases more rapidly when waves propagate shorewards. Although

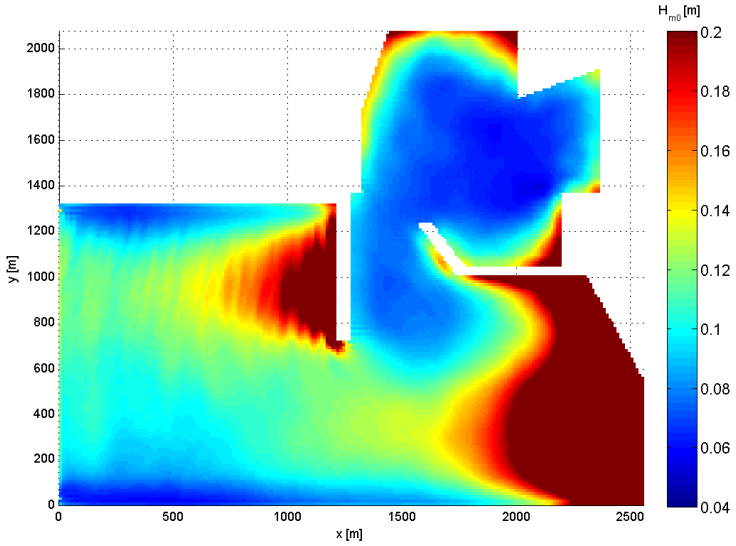

Figure 6.3: Low frequency (T =25–200 s) waveheight LG05

the colormap of the figure has been truncated to allow a better resolution, it can be seen that low frequency waveheights reach well over 20 cm.

Finally, in the corners of the harbour basin, high amounts of LF energy are found. These are due to the eigenwaves in the basin and illustrate the relative importance of these eigenmodes, which will be treated more elaborately below, within the total amount of LF wave energy.

6.3 Harbour oscillation

Assessing harbour oscillations is not typically performed using Triton. Other models are available, e.g. PHAROS (a mild slope model, see Table 2.1), developed specifically for this purpose (hence its name: program for harbour oscillations). This model uses a monochromatic, low frequency incident wave without the forcing primary waves. The output shows the response amplitude over input amplitude. In this manner, a spatial image of seiche patterns is obtained, showing gain of amplitude and locations of nodes and anti-nodes.

Although Triton is developed for different purposes, eigenwaves, when occuring, will develop. When considering a single output point's spectrum, eigenwaves will possibly show as a peak. Subsequently, when considering all output points in a computational grid, one can spatially show the energy content of a single, specific frequency on all grid points. Thus, it enables an analysis of harbour oscillations and seiching patterns in the basin much like PHAROS or other dedicated models do. This is the approach adapted for the current analysis, i.e. the following steps are taken.

- Generate sufficiently long wave records on the grid, in time domain, to allow a required frequency resolution, taking into account the spin-up time of the system.

- Apply a Fourier transform analysis for all points on the grid.
- Show the amplitude of a single (LF) component on all grid points.

For the purpose of harbour oscillations, a run is used with closed (i.e. 100% reflecting) boundaries along the breakwaters and harbour basin boundaries: LG06 (as introduced in Chapter 5).

Avilez Valente (2007, Chapter 6 and Annex B) has performed studies regarding harbour oscillations at the Port of Leixões, in view of the development of a terminal within the harbour basin. This study too uses a mild slope model with a limited number of periods as an input. His conclusions and figures serve as a validation of the results of the present analysis.

The main difference between the present approach and Avilez Valente (2007) or an approach like using the PHAROS model is that the latter apply monochromatic LF waves and a limited number thereof, at distinct, predefined frequencies. The results show a relative amplitude, i.e. do not indicate the absolute energy with which the oscillation occurs. This absolute energy is related to the amount of LF wave energy at the incident boundary. The approach of this present study takes into account the complete, more realistic spectrum. This does thus include primary waves as well as an appropriate amount of LF wave energy in various LF wave components at once. Its results are thus absolute energy contents.

This spatial approach of the assessment of LF energy negates much of the issues found when analyzing a single points spectrum, as is done more usually from Triton output. The uncertainty within a single realization of a spectrum is treated in Appendix C. The grassiness (unsmoothness) of such a single spectrum makes it ambiguous to attribute certain peaks to eigenmodes whereas others of same order of magnitude are left undeclaired. The present approach focusses more on patterns due to seiching and therefore is less influenced by the grassiness, i.e. the spatial image shows relative energy content and thus nodes and anti-nodes whereas a single spectrum shows absolute content of a single point. Moreover, a node too can heavily affect a (moored) vessel as precisely that location experiences a maximal slope and velocity. A node does however not show as a peak in a single points spectrum and would therefore not be detected easily.

Figure 6.4 shows an example of the output of the presented approach and compares this with a mode found by Avilez Valente (2007). Triton seems to be able to predict the eigenmodes of the harbour basin appropriately, as the correspondence of nodal and anti-nodal locations is apparent. Other modes tested by Avilez Valente (2007) are found in the Triton run analysis too. Given that both the bathymetry as the boundaries modeled in the setup of the present study are significantly simplified, it is remarkable that the eigenmodes within this model show such an overall resemblance with those resulting from the more appropriate model performed by Avilez Valente (2007).

Above all, it can be noted that the eigenwave patterns seem to be governed by the harbour basin. Their shape does not seem to be forced by the southern boundary, which would be an unwanted modeling effect. The triangular resonant area hypothesized by Campos Morais and Abecasis (1978), imposed by the breakwater sections outside the harbour basin, it not recognized and not expected to occur.

The most notable, consistent difference is that the frequencies at which these several modes are most apparent in Triton output are typically lower (higher

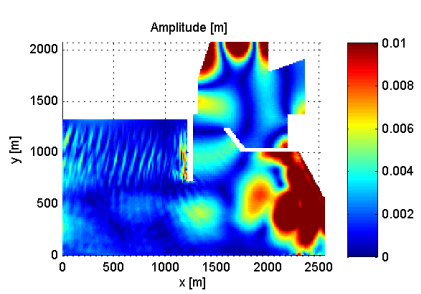

(a) Amplitude from Triton at $T = 86.8\,\mathrm{s}$

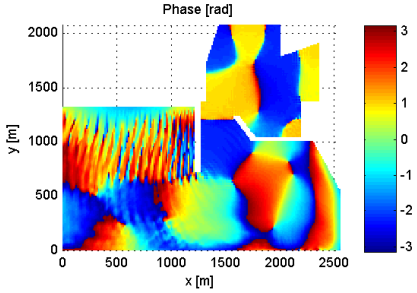

(b) Associated phase from Triton

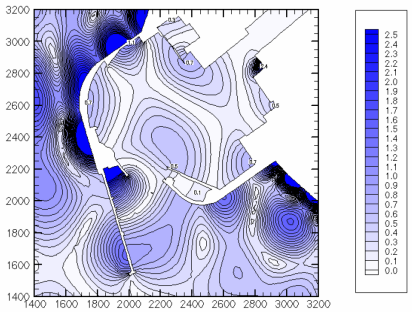

(c) Amplitude ratio at $T = 80\,\mathrm{s}$ from Avilez Valente (2007)

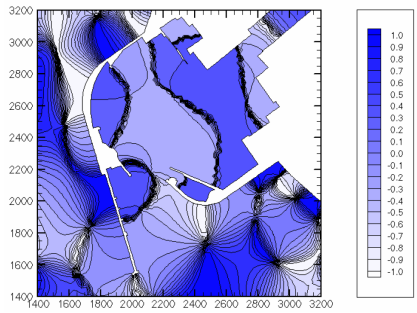

(d) Associated phase from Avilez Valente (2007)

Figure 6.4: Examples of a basin eigenmode resulting the presented approach (using Triton run LG06) and compared to results from Avilez Valente (2007)

eigenperiods) than those identified by Avilez Valente (2007). This is most probably due to the difference in sea level. Whereas Avilez Valente (2007) used mean sea level (CD+2 m) the models run in Triton are based on CD+0 m, resulting in lower propagation velocities and higher eigenperiods. This discrepancy is most pronounced in shallow areas, like the harbour basin. It must however be noted that this difference might be attributable to an imperfectly modeled dispersion, underestimating the wave celerity.

Another important difference is the shape of the harbour entrance and the exclusion of the docks beyond the primary harbour basin (dock 1 and 2, see Figure 4.7) in LG06. This has a distinct effect on the locations of nodes and anti-nodes. The rearside of the present model induces an anti-node whereas in reality dock 1 would induce a pattern on its own. Furthermore, especially based on Avilez Valente (2007), it can be concluded that a node is often induced at the narrow harbour entrance.

The discrepancy of the Triton model versus the results of Avilez Valente (2007) illustrates the sensitivity of the basin shape. Although comparable modes are present, the position of nodes and anti-nodes is not identical. It would therefore be beneficial to make a more detailed run using Triton and perform a more suitable validation on the present approach.

The position of nodes and anti-nodes is most important when assessing the impact of these seiches on a moored vessel. A ship placed in an anti-node will be

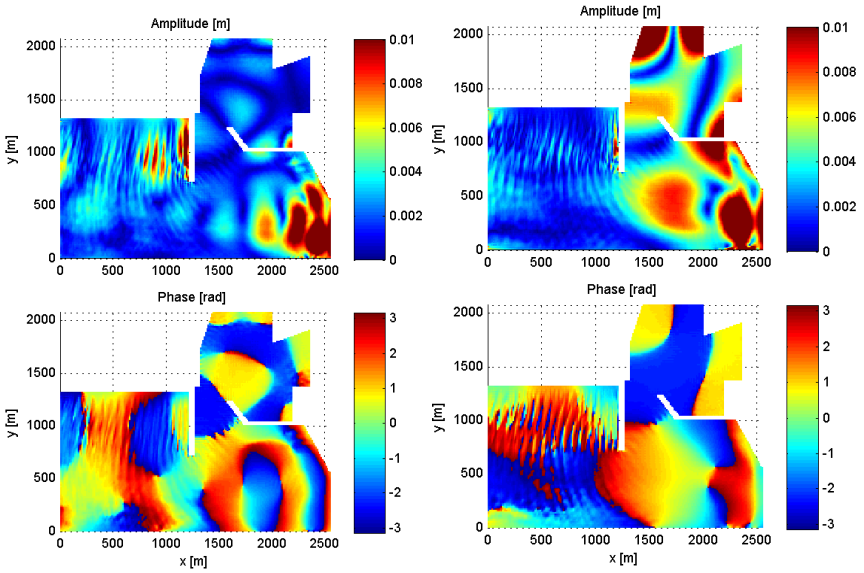

(a) At $T = 77.8\,\mathrm{s}$ (b) At $T = 138.3\,\mathrm{s}$

Figure 6.5: Examples of basin eigenmodes inducing a node in the proximity of berth A, with a frequency within the range of vessel motion natural frequencies (from LG06)

affected by the waterlevel elevation, thus experience a heaving motion as a result of this eigenmode. This motion is generally not relevant for vessel mooring. When a ship is placed in a node, by definition the amplitude of this eigenwave at that the vessel's position will be zero. However (as briefly mentioned above), the influence of the wave will not be negligible. In fact, the ship is essentially placed on a slope. Furthermore, at a node the water velocities will be highest. This heavily affects the moored vessel. Depending on the orientation of the ship with respect to the anti-nodes, the wave period and natural period of the vessel motion, a ship placed in a node will therefore experience a surge and pitch or sway motion.

Figure 6.5 shows that a node at the berth is likely to occur. This can thus be relevant for the moored vessel.

6.4 Wave induced current

An important phenomenon found from run LG05 is an eddy-like cell developing between the beach and the leeside of the breakwater. This cell and its development throughout the run are shown in Figure 6.6. These figures consider a 24 s-averaged velocity field, i.e. the primary waves are, for the greater part, filtered out of the results.

It can be seen that a return current is induced almost immediately from first wave impact on the beach. This current subsequently expands in magnitude and extent. Within half an hour the velocity generated at the beach, i.e. the energy source, seems to stabilize. Velocities at this location reach over 1 m/s. The

vortex and jet still extend, until eventually the current reaches the northern breakwater, creating smaller side-vortices as well.

The current shown can be attributed to set-up caused by incident waves on the shore. Although output shows a mere 7 cm set-up nearshore, the velocity amplitude agrees with previous measurements and simulations thereof by Triton, performed by Van der Hout (2009). It is noted that the set-up might be underestimated by using a partially reflecting boundary; this boundary allows energy to pass out of the domain whereas dissipation of energy does not. Finally, the set-up has used a Chézy friction coefficient of 65. Whereas this is applicable for sandy beaches, it is too smooth for a flow-breakwater interaction. The extent and velocity of the current found near the berth might therefore be overestimated by Triton.

Considering that the area of high velocity is a zone shielded from incident waves by the northern breakwater, the location of the eddy seems plausible. With respect to reality, the difference of the orientation of the southern breakwater due to the numerical model set-up (briefly noted in Chapter 5) must be kept in mind. The deflection of the eddy occurring in reality may therefore be different; its tail might not be directed to berth A and its relevance in reality might be less.

To ascertain the natural cause of the current, possible numerical shortcomings of the model inducing such a current are explored. First, bearing in mind the experimental state of Triton and therefore its lack of robustness, it can be suggested that the velocity found is due to a numerical instability induced by the model boundary. However, it seems that the source of energy is not located at the boundary, as these adjacent cells show low amplitude velocities. The source is in the domain itself thus not an instability due to the boundary definition.

Another numerical cause might be due to the open boundary at the southern end of the domain. As discussed earlier, this boundary shows an oddly low energy content. This might indicate that this boundary is in fact partially reflecting energy. An excess of energy might then be found adjacent to the southern breakwater, i.e. between the beach and the northern breakwaters tip. This energy, not being able to leave the domain, would then cause the eddy shown. However, Figure 6.2, showing the energy content of the domain, does not show high values in this area.

It is therefore concluded that the eddy-like velocity field found is a possible actual phenomenon, induced by the incident waves on the shore. Its relevance is evident from Figure 6.6e, where its current is found at the location of berth A (at $(x, y) \approx (1300,980)$) after approximately 2 hours. The records at berth A are shown in Figure 6.7. The current due to the eddy-like velocity field is clearly recognized. It magnitude is in the order of 0.2 m/s and its direction oscillates. As discussed, the orientation of the eddy with respect to berth A might be different from reality due to the schematizations simplification.

The aforementioned conclusion might possibly be substantiated by studying morphological changes near the berth and along the southern breakwater or by interpreting pilot experiences, not performed within this study. The magnitude of the current should be measured to see whether it has an impact in reality.

Finally, on the southern boundary, a small and local incident velocity can be seen (Figure 6.6). It is believed this velocity is a numerical artifact. Its cause can be found in the treatment of the boundary settings by Triton: for a closed boundary, a constant depth is assumed upon which a typical kh-value is

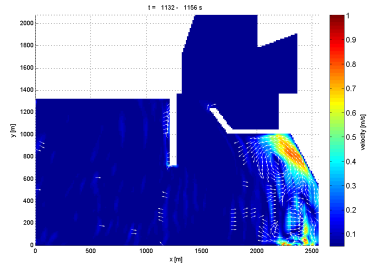

(a) At $t = 1132$–$1156\,\mathrm{s}$

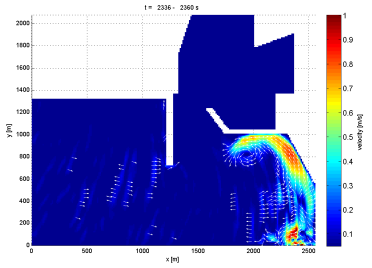

(b) At $t = 2336$–$2350\,\mathrm{s}$

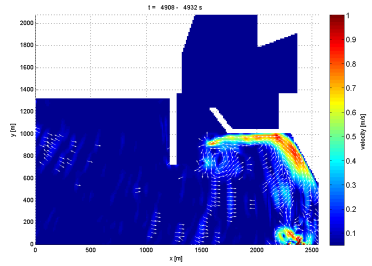

(c) At $t = 4908$–$4932\,\mathrm{s}$

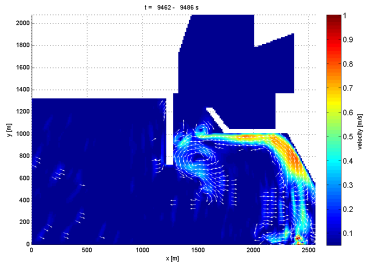

(d) At $t = 9462$–$9486\,\mathrm{s}$

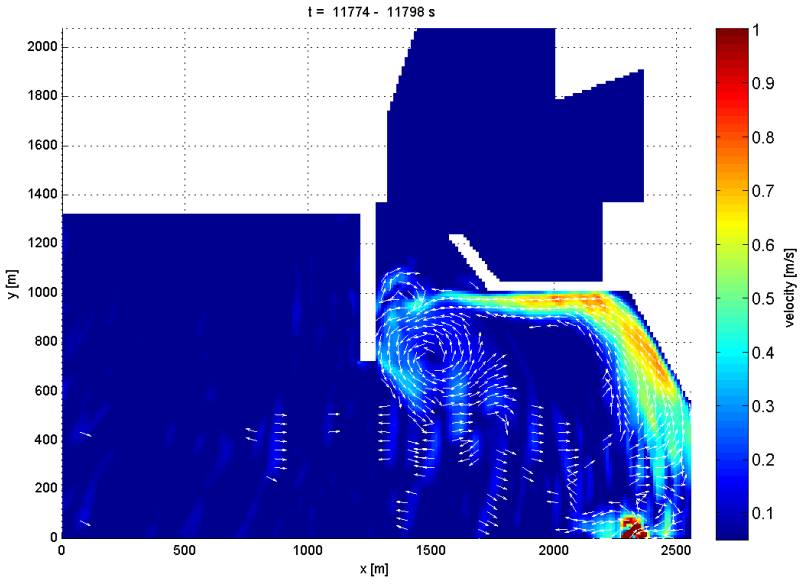

(e) At the end of the run, $t = 11774$–$11798\,\mathrm{s}$

Figure 6.6: Averaged velocities showing the development of the eddy between the beach and the southern breakwater (LG05), with colours indicating amplitude and arrows denoting velocity direction

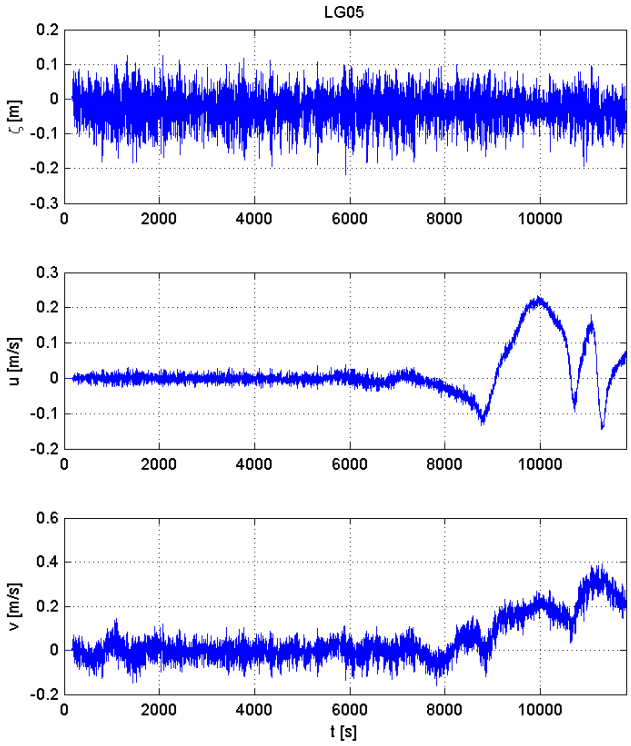

Figure 6.7: The waterlevel elevation and velocities at berth A, during run LG05

calculated. It is expected this depth is taken as the first depth point encountered along the boundary, in this case at $x, y = 0, 0$. This value is not appropriate when approaching the beach. A solution would be to define this boundary as various, shorter boundaries, each assuming a kh-value. It can however be seen that the effect of this local velocity on the area of interest is negligible.

6.5 Summary

Berth A in the Port of Leixões is shown to be well protected from primary waves. Low frequency waves are shown to have a relatively strong influence.

It can be seen that the LF band energy content has a significant component due to the harbour oscillations. From the spatial spectral analysis it follows how the eigenmodes in the wavefield at berth A depend on the dimensions and entrance orientation of the harbour basin. The harbour basin is the source of the eigenmodes found at berth A and must therefore be included in the numerical model. The triangular resonant area hypothesized by Campos Morais and Abecasis (1978) is not found in the analyses and not expected to occur.

An eddy-like current which had not been identified in previous research possibly occurs. The precise influence of this current on the ship has, due to the limited available time, not been established. The proper modeling of the beach and the distance from the beach to the northern breakwater – a difference of the present model compared to the physical model – is of importance with respect to the assessment of the current mentioned.

Chapter 7

Conclusions and recommendations

Recapping the goals of this thesis

The goals of the present project can be summarized as follows.

1. To assess the applicability of a numerical model chain as a generic method for the determination of moored vessel motions in actual harbour applications, taking into account its accuracy as well as workability.

2. To provide an understanding of the inoperativeness issue at berth A of the Port of Leixões.

For this purpose, a validation of the complete numerical chain has been performed. Furthermore, a numerical model was set up and studied including the main harbour basin of Leixões. It can be concluded that both of the aforementioned goals have been attained, although further development of the model chain is much needed. Below, the generic and case-related aspects of this project will be elaborated on succesively

7.1 Numerical method chain

7.1.1 Conclusions

Determining the motions of a moored vessel in a harbour is a complex matter, as is well known and thoroughly described in Chapter 1. The significant effect of non-linear waves requires the use of advanced numerical models.

It has been shown that the method used in the present study is able to adequately model this matter. However, it is not regarded a suitable tool for engineering purposes. These core conclusions will be elaborated on in the following paragraphs.

Potential of method

The numerical method chain Triton-Harberth-Quaysim has been applied completely within this project. The relevant wave dynamics (diffraction, shoaling,

etcetera) and vessel dynamics are included adequately. An exception can be found in the transmission of wave energy through the breakwater. This might or might not have a significant contribution but is not included.

The method includes primary as well as bound and free low frequency (LF) waves, harbour oscillations and currents. These are shown to be in correspondence with expectations from theory or, regarding seiches, results of previous research.

Considering bound waves, Triton adds, as a non-linear model, a significant accuracy, as bound waves shoal more profoundly than primary waves. Taking these into account with a potential theory model, e.g. PHAROS, would therefore induce an important underestimation of LF energy.

Another added value of this wavemodel is that all wave processes are modeled simultaneously: primary and low frequency waves, harbour oscillations and flows. This enables an assessment to be based to a lower extent on assumptions; after all, one does not have to neglect one of the phenomena occurring in reality. Moreover, information on the relative phases of different force contributions are retained.

An added value of Harberth, although not relevant for the validation performed within the present project is the inclusion of reflections off a quaywall. Quaysim, subsequently, as a time-domain model, is able to describe non-linear mooring line forces. This too expectedly induces a more accurate result when applied to an actual case.

Despite the above, the results of the validation (see Chapter 3) do not provide sufficient confidence to apply the method on the case study of berth A. The sensitivity for the mooring line characteristic break elongation must be mentioned in this respect. The precise lay-out of the mooring system, too, may be the base of the divergent results. Further research must be performed to substantiate or reject these hypotheses.

From the above, the potential of the model chain is clear. The complete method has shown its applicability in laboratory cases previously. The present project, as well as Van der Wel (2011), assess the applicability of Triton in complex cases. Nevertheless, using the method as an engineering tool for an a priori assessment is highly discouraged.

The method as an engineering tool

An engineer's aim is to solve a problem, to supply a suitable design. In establishing a solution, numerical models are an important tool, possibly the most important. Extensive calibration, however, is often not possible due to a lack of measurements, time or know-how. Nor can excessively time-consuming computations be performed. A method used does need to provide sufficiently accurate results to serve as a base for a design. The method used within the present project has been shown to be applicable. However, it is not fit to serve as an engineering tool.

The importance of low frequency waves, in turn, complicates the analyses of the wavefield results. Due to the realization of surface elevation timeseries using random phases, a highly deviating spectrum results (further treated in Appendix C). Overall energy will agree but the distribution along the frequencies will deviate, making the identification of eigenmodes doubtful. Accounting for

this, statistically sound conclusions must be based on a long run or more runs with different phase seeds.

Above all, the lack of workability of the present method from an engineering perspective is due to the wave propagation model Triton. Its accuracy, not unlike other Boussinesq or non-hydrostatic models, is limited. For primary waves, Triton is applicable up to $kh \approx 3$–4. In case of an interest in LF waves, a more restrictive limit of $kh < 1$ for primary waves applies.

Most decisive, however, is the lack of practical workability of Triton. Although two working models have been run with success and were analyzed within the present report, completing such a run is not quite straightforward. An often occurring error is an unresolved bug in the implemented boundary condition. Furthermore, imposing another wave condition can induce the occurrence of an error, even if the model set-up has worked previously. This has limited the research within this project. Running various models, placing the analyzed results in context turned out practically impossible.

Another flaw was found using open boundaries, which appear to impose a nodal point. Although this is believed to have induced a local error only during the runs used in the present report, it might be more significant in other applications.

A second pressing restriction has been found in the high simulation times, in accordance with previous applications of Triton (Boeyinga, 2010). The present application in an actual harbour required a large domain having sufficient resolution to resolve the primary waves. Additionally, as mentioned above, the interest in low frequency energy necessitated to simulate long periods of time. In the present project, a run length of approximately 3.2 hours was chosen. The Triton computation thereof took approximately 7 days. For engineering purposes, this is too time consuming by far, especially considering the probability of an error occurring, causing the computation to terminate early or late in the computation.

The subsequent models do not provide a reliable result without decent care either. Quaysim, although a relatively user-friendly and quick model, demands a calibration as the vessel schematization and the mooring line lay-out are components for which the model is highly sensitive. Without this calibration, results remain inconclusive.

7.1.2 Recommendations

- Further steps towards practical applications of Triton are regarded of little use as long as the lack of boundary robustness has not been resolved. Most importantly, the numerical implementation of the partially reflecting boundary needs severe adjustment. Furthermore, the flaw recognized along open boundaries is recommended to be solved.

- The computational cost of Triton can be reduced by developing a version running multi-threated. This will likely allow the Triton model's input to be calibrated more properly, as is usually done within coastal engineering practice.

- It is regarded valuable to apply Triton to more isolated case-related studies, e.g. to use intermediate steps rather than to apply Triton in practice

too soon. Examples of benchmark tests suitable to hydraulic and coastal engineering can be found in Demirbilek et al. (2010) providing theoretical solutions or measurements to compare with. Other methods too can be assessed using these benchmark cases.

- An important recommendation is to assess the use of another wave model. It has been shown that the field of application requires Boussinesq or non-hydrostatic models. Various exist and should be taken into consideration, e.g. SWASH and Bouss-2D. It must be noted however, that none of these models guarantees a stable simulation. The connection of the chosen model to Harberth and Quaysim or comparable diffraction and motion models must be assessed subsequently. More measurements might be beneficial in this assessment.

- It could be considered to deviate from this chain method and to allow an assembly of more established numerical models, each assigned to a particular wave phenomenon. Rather than including all processes in a single wave model as performed in the present thesis, this would require a more elaborate set-up of models but would possibly not demand the computational cost of a Boussinesq model. Guidelines must then be developed on how to determine vessel motions in complex harbour geometries using this assembly of models. As an example it can be suggested to combine SWAN, Delft3D-flow and PHAROS or XBeach using suitable directives to obtain an indicative wavefield at a berth.

- The validation of Harberth and Quaysim within the method chain must be further elaborated on as well. It is recommended to use different case measurements. The measurements used within the present thesis suffer an excessive amount of LF energy, causing a discrepancy in the wave input for Harberth. A different case might thus ensure an improvement thereof.

- Much can be gained by a validated means of analyzing the wavefield results. The influence of LF waves and the uncertainty of the result spectra in this frequency band are relevant in a seiching assessment. In this regard, validating the spatial spectrum analysis developed within this thesis by measurements or a comparison to PHAROS might be useful. This method might be further developed by using a wavelet approach, enabling the analysis of non-stationary signals and showing the actual excitation of harbour eigenmodes. Secondly, the application of wave splitting (see e.g. Bakkenes (2010)) to the wave model results might be beneficial. As all sorts of virtual probe alignments are available from numerical modeling, this might show the actual source of the LF energy at a berth by providing its main direction.

7.1.3 Summary

The method used in the present report is appropriate but needs much further development to be applicable by engineers or consultants in practice. A major focus therein is the lack of robustness and the computational cost of Triton. Furthermore, alternatives of the method are recommended to be further developed.

It has been concluded that the physical scale model measurements have suffered restrictions. Furthermore, numerical modeling using such an advanced model as in the present project is difficult. This is why the most reliable assessment is made using a combination of these two types of modeling. When keeping in mind the scale effects, physical modeling can show most completely the relevant physics. It can furthermore serve to calibrate or validate numerical models. These, in turn, can provide valuable additional computations.

7.2 Case study of berth A of the Port of Leixões

7.2.1 Conclusions

Including the harbour basin of the Port of Leixões and focusing on low frequency waves have evidently provided an added value to the assessment of the wave climate at berth A. Whereas this berth is sufficiently protected from primary waves, the relative occurrence of LF waves is clearly shown.

It can be seen that the LF band energy content has a significant component due to the harbour oscillations. Furthermore, it follows from analysis of the measured motions that the important, horizontal motions (sway and surge) are sensitive for particularly these frequencies. The importance of the correct modeling of these seiches is thus proven.

From the spatial spectral analysis that has been developed within this thesis it has been shown that and how the eigenmodes in the wavefield at berth A depend on the dimensions and entrance orientation of the harbour basin. The harbour basin is the source of the eigenmodes found at berth A and must therefore be included in the numerical model.

Triton solves these harbour oscillations implicitly and takes into account in a realistic manner their incident energy. After all, bound waves are included properly and their shoaling is simulated correctly. The spatial spectral analyses further shows no evidence of an occurrence of the triangular mode suggested by Campos Morais and Abecasis (1978) (see Figure 4.8); this is therefore not expected to be of importance.

Another finding from the wave model results is the possible occurrence of an eddy-like current which had not been identified in previous research. The precise influence of this current on the ship has, due to the limited available time, not been established. The alternately south- and northwards directed flow might excite a surge motion. Further measurements and modeling is thus recommended.

The proper modeling of the beach and the distance from the beach to the northern breakwater – different compared to the physical model – is of importance with respect to the assessment of the current mentioned. This emphases again the effects of the restriction of physical models.

At this point, determining the ship motions at berth A is within reach. Due to the limited confidence in the results obtained from Quaysim and, therefore, in this model, this has not been performed within the present thesis report.

7.2.2 Recommendations

- The amount of low frequency energy has been limited in the present thesis to bound wave energy. This is in accordance with previously performed research by Rosa Santos (2010); Van der Wel (2011) in which incident free LF waves were neglected. Although it can be assumed from Herbers et al. (1995b) that the contribution of distant LF energy is not significant, trapped LF waves can be relevant along the Leixões coast. Analyses of tidal gauge data can, to a limited extent, provide an improvement or validation of the assumption taken.

- To assess trends in mooring line forces, comparable with or complementing to the work of Rosa Santos et al. (2009) and in order to provide possible solutions to the inoperativeness problem, various mooring cases can be simulated in Quaysim or an alternative motion model. This does not require additional Triton runs. Pretension, different fender types and mooring masters, for example, can easily be applied and their relative impact can be estimated.

- To attain a more comprehensive view on the downtime conditions, new runs can be made using Triton or another applicable model considering different wave conditions, their probability of occurrence and effect on vessel motion. Within this project this has been pursued but consistently led to errors, seizing the computation. Due to the limited available time, these could not be resolved within the project. Nevertheless, Triton does have this potential, especially when the boundary condition issues are solved, as recommended in Section 7.1.2. As Rosa Santos et al. (2008b) have assessed several wave conditions as well (consider table B.1), this might provide comparison measurement data.

- Analyses of other vessel sizes and types are subsequently easily performed, without the need of re-running the wave model. Again, this shows an advantage of using numerical models.

- It is further recommended to take into account in more detail the harbour basin lay-out, especially the harbour entrance. It is recognized this has an effect on the location of nodes and anti-nodes of the occurring seiches. It must be considered to perform these simulations using a different model, as Triton easily introduces numerical instabilities. One should, however, consider the absolute wave height of these eigenwaves to assess their influence on vessel motion.

- In order to validate or reject the predicted possible occurrence of an eddy-like current, flow measurements are recommended in the vicinity of berth A and/or along the southern breakwater. An analysis of the influence of this current can, alternatively, be made studying morphodynamical changes based on bathymetrical surveys. Other numerical models might provide an insight in the occurrence of the eddy current as well, e.g. Delft3D-flow, as the current is not significantly caused by LF waves. A fourth, very indicative method to assess this is by using pilot experience.

- Another recommendation is to estimate the transmission of waves through the breakwater, if possible as a function of frequency. Previous research

has indicated the occurrence of this transmission. The actual effect thereof on vessel motions might be identified, after which future research can include or justly exclude the transmitted wave.

- Finally, it must be noted that prototype measurement complements the presently available data. As physical model tests might suffer from dimension restrictions or scale effects, prototype measurements do not. These are thus strongly recommended.

7.2.3 Summary

The assessment of the wavefield at berth A of the Port of Leixões indicates a significant contribution due to harbour oscillations. From their wave height and the location of their nodes, it is expected that these seiches affect the moored vessel motions. Including the basin in future research, reducing physical basin effects, is thus concluded to be essential.

Appendix A

Elaboration on related physics

This chapter is used to introduce some additional physics relevant when modeling coastal areas and harbours.

A.1 Low frequency waves

A special interest is given to low-frequency (LF) waves. This arises from the overlapping range of these and natural frequencies of some degrees of freedom of a moored vessel, see Section 2.3. The applicability of LF waves in coastal zones is described in Herbers et al. (1994, 1995a,b); Ligteringen and Moes (2001); Reniers (2010); Reniers et al. (2010); Rosa Santos (2010); Van Dongeren et al. (2003).

LF waves can have the following origins.

1. Ocean storms.
2. An earthquake at the ocean floor.
3. The set-down beneath wave groups, so-called bound long waves.

The main interest in this project is in the latter.

A rule of thumb for the wave height of the bound long waves in shallow water is given by Ligteringen and Moes (2001).

$$H_{\mathrm{s,lf}} = 0.08 \left(\frac{T_{\mathrm{p}} H_{\mathrm{s}}}{h} \right)^2 \tag{A.1}$$

in which the factor 0.08 has the unit $\mathrm{m/s^2}$.

The concept of set-down waves is best introduced by a bichromatic wavefield, consider Figure A.1. The superposition of two waves with different frequencies leads to interference, visible — both in time and space — as an amplitude modulation, an alternation of high and low amplitude wave groups. This modulation is commonly referred to as the wave envelope.

A real ocean wavefield is a superposition of numerous wave components with their individual amplitudes, frequencies, phases, directions and celerities. These

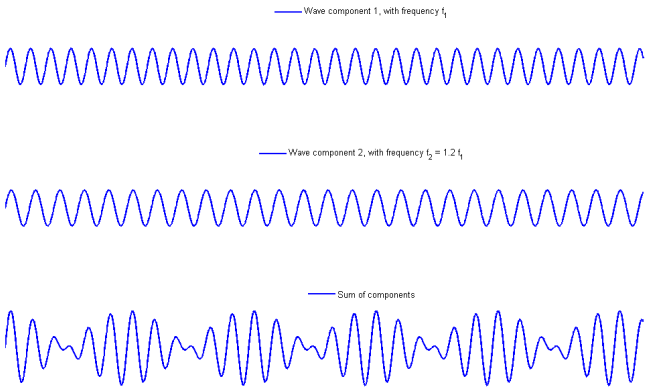

Figure A.1: Envelope due to the superposition of two waves

superposed waves compose a very irregular wave field. In this irregular wavefield too, an alternation of groups of higher waves and of lower waves is visible. This alternation is the origin of bound waves. This is also indicated by a strong correlation of measured energy levels of infragravity waves and swell (Herbers et al., 1995a, his reference Munk (1949)).

Shear forces S_{xx} and S_{yy} within the water volume subject to waves are maximum under high waves and minimum under low waves. The described envelope therefore induces a modulation of high and low shear forces. The gradient due to the alternating groups, i.e. dS_{xx}/dx and dS_{yy}/dy, causes local set-downs and set-ups. Since the wave groups are moving, they thus induce a bound long wave with a length equal to the amplitude modulation envelope and traveling at the propagation velocity of the envelope (Equation A.2b), i.e. of their carrier waves — opposed to free waves, which conform to the dispersion relation (Equation A.2a). These different celerities approach symptotically in shallow water.

$$c = \frac{\omega}{k} = \sqrt{\frac{g}{k}\tanh(kh)} \tag{A.2a}$$

$$c_g = \frac{\partial\omega}{\partial k} = \left(\frac{1}{2} + \frac{kh}{\sinh(2kh)}\right)\sqrt{\frac{g}{k}\tanh(kh)} \tag{A.2b}$$

$$\tag{A.2c}$$

Longuet-Higgins and Stewart (1962) have assessed the shear forces discussed above and found Formulae A.3.

$$S_{xx} = \left(n + n \cdot \cos^2\theta - \frac{1}{2}\right) E_w \tag{A.3a}$$

$$S_{yx} = S_{xy} = (n \cdot \sin\theta\cos\theta)\, E_w \tag{A.3b}$$

$$S_{yy} = \left(n + n \cdot \sin^2\theta - \frac{1}{2}\right) E_w \tag{A.3c}$$

In which E_w denotes the primary wave energy. In case of wave groups long compared to the water depth and colinear primary waves, these shear forces induce an average waterlevel elevation (Longuet-Higgins and Stewart, 1962, Equation 3.26)

$$\bar{\zeta} = -\frac{\left(2n - \frac{1}{2}\right)}{\rho(gh - c_g^2)} E_w \tag{A.4}$$

where the overbarred $\bar{\zeta}$ denotes averaging over one wave cycle.

It has been shown that this bound long wave has a phase lag of 180 ° with respect to the amplitude envelope (Reniers et al., 2010, his reference Biesel (1952)).

Sand (1982) describes the influence of directionality of the carrier waves. Herbers et al. (1995a) too emphasize the importance of this directionality as analysis showed that the directional spectrum of infragravity waves is usually broad and sensitive to incident swell propagation directions. Sand (1982) concludes that the long-wave amplitude in natural wave fields is clearly smaller than in plane wave trains, even for small difference angles $\Delta\theta$ between the short-wave components. In shallow water there seems to be a reduction of low-frequency amplitude with a factor of typically 5–10 due to the directionality of the carrier waves. This factor decreases with increasing water depth.

According to Sand (1982), the LF wave amplitude can be estimated through

$$a_{LF} = G \cdot \frac{H_s^2}{16} \tag{A.5}$$

where G is a transfer function that can be calculated and is given in Figure A.2. The significant long wave height $H_{s,lf}$ is, subsequently, 3–4·a_{lf} (Sand, 1982). An estimation can thus be made reading this figure, at which a reasonable assumption for the difference frequency is $\Delta f/f = 0.2$ (Sand, 1982, his reference Sedivy (1978)).

Van Dongeren et al. (2003) presents a formula to calculate the bound wave energy due to a primary wave pair through the difference-interaction coefficient D, Equation A.7 (adapted from Van Dongeren et al., 2003, Eq.18). The total bound energy can subsequently be calculated by integrating over all primary components, Equation A.6 (Van Dongeren et al., 2003, Eq.17). In practice, the continuous spectrum will be discretized and the formulae will be adapted accordingly.

$$E_{bnd}(f_{bnd}) = 2\int_{f_{bnd}}^{\infty}\int_0^{2\pi}\int_0^{2\pi} D^2(f_1, f_2, \Delta\theta) E(f_1, \theta_1) E(f_2, \theta_2) d\theta_2 d\theta_1 df_1 \tag{A.6}$$

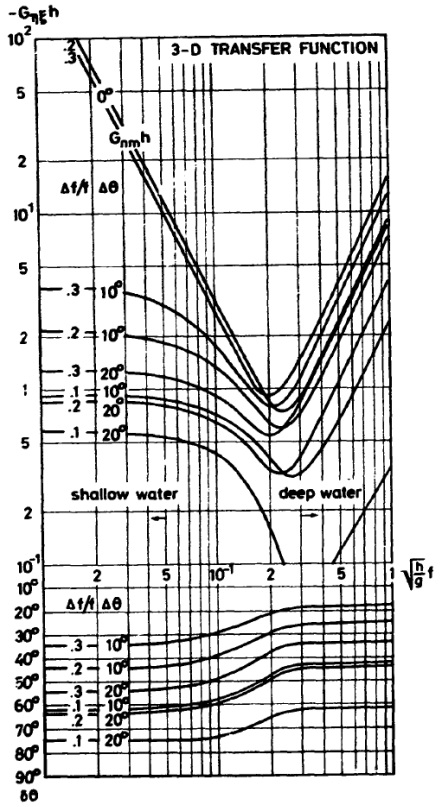

Figure A.2: The directional transfer function G for a wave group consisting of two frequencies $f_1 = f$ and $f_2 = f + \Delta f$ with angle $\Delta\theta$ between one another. Lower part indicates long wave direction of travel, θ_{bnd}, for short waves with $\theta_1 = -\theta_2$ (Sand, 1982)

with

$$\begin{aligned} D(f_1, f_2, \Delta\theta) = & \frac{g k_1 k_2 \cos(\Delta\theta + \pi)}{8\pi^2 f_1 f_2} \frac{\cosh(k_{\text{bnd}} h)}{\cosh(k_1 h)\cosh(k_2 h)} \\ & - \frac{g f_{\text{bnd}}}{(g k_{\text{bnd}} \tanh(k_{\text{bnd}} h) - 4\pi^2 f_{\text{bnd}}^2) f_1 f_2} \\ & \cdot \left[f_{\text{bnd}} \left(\frac{16\pi^4 f_1^2 f_2^2}{g^2} - k_1 k_2 \cos(\Delta\theta + \pi) \right) \right. \\ & \left. - \frac{1}{2} \left(\frac{-f_1 k_2^2}{\cosh^2(k_2 h)} + \frac{f_2 k_1^2}{\cosh^2(k_1 h)} \right) \right] \end{aligned} \tag{A.7}$$

with $\Delta\theta \equiv |\theta_1 - \theta_2|$, $f_{\text{bnd}} \equiv f_2 - f_1$, and $\vec{k_{\text{bnd}}} \equiv \vec{k_1} - \vec{k_2}$. Furthermore, $\phi_{\text{bnd}} \equiv \phi_2 - \phi_1 + \pi$ and $\theta_{\text{bnd}} \equiv \arctan(\vec{k_{\text{bnd}}}\hat{y}/(\vec{k_{bnd}}\hat{x}))$.

The formula of Van Dongeren et al. (2003) is essentially similar to the formula presented by Herbers et al. (1994, Eq. A5) and Hasselman before him. The difference is that Van Dongeren et al. (2003) is corrected to consider pressures at the surface whereas Herbers et al. (1994) is based on pressures at the sea floor.

The bound LF wave in deep water has negligible height for many applications — in the order of centimeters — but increases rapidly as the waves travel into shallow water. This shoaling effect in fact is more pronounced for bound waves than for free waves. Whereas shoaling of free waves is described by Greens law, $a \propto d^{-0.25}$, for a shoaling bound wave the amplitude is proportional to $d^{-0.25}$ to $d^{-2.5}$.

A.1.1 Free LF waves

When the carrier break, for example at the beach surf zone, their energy dissipates. The bound waves, however, are released as free waves. These then either escape offshore as so-called leaky waves, if the angle of incidence is small — $|f_2^2 \sin\theta_{2,0} - f_1^2 \sin\theta_{1,0}| < (f_2 - f_1)^2$ (Herbers et al., 1995a) — or are trapped in the surf zone by refraction, if the angle of incidence is large. These mechanisms are illustrated by Figure A.3. The trapped, so-called edge waves, propagate back and forth between the shoreline and a depth h_{t} given by Equation A.8

$$h_t = \frac{g}{|\omega_2^2 \sin\theta_{2,0} - \omega_1^2 \sin\theta_{1,0}|} \cdot \text{atanh}\left(\frac{(\omega_2 - \omega_1)^2}{|\omega_2^2 \sin\theta_{2,0} - \omega_1^2 \sin\theta_{1,0}|} \right) \tag{A.8}$$

for $|f_2^2 \sin\theta_{2,0} - f_1^2 \sin\theta_{1,0}| > (f_2 - f_1)^2$ (Herbers et al., 1995a).

Note that the leaky waves unshoal conform Greens law, see Figure A.4, and reflected waveheights can therefore exceed the incident waveheight. This was already hypothesized by Longuet-Higgins and Stewart (1962). According to Herbers et al. (1995a), this causes free waves to dominate the infragravity band well outside the surf zone.

Another phenomenon at the surf zone generating long waves is the variation of the sea level due to the breaking of individual carrier waves, which can be seen as a local hump in the mean sea level. When multiple breaking zones occur a long-period water oscillation is created. This mechanism is called surf-beat

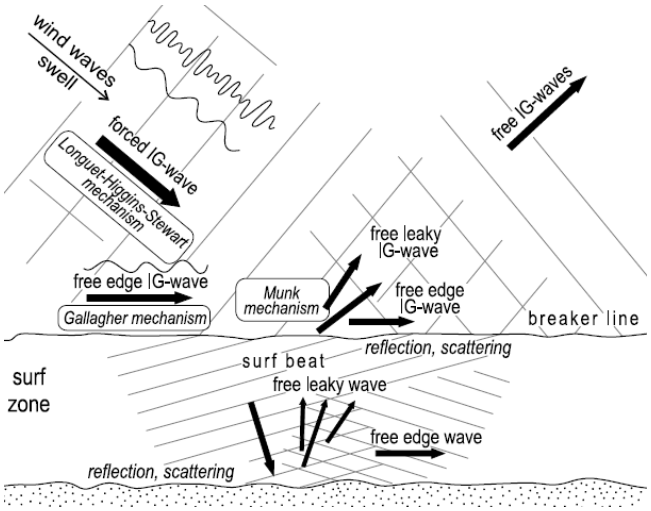

Figure A.3: Generation mechanisms for free LF waves at the shoreline

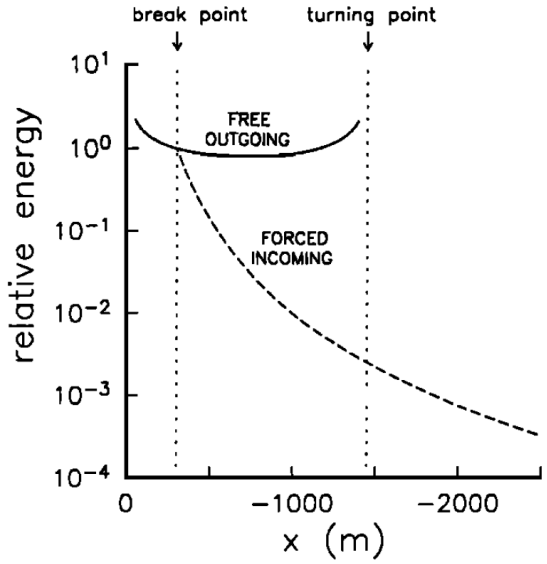

Figure A.4: Schematic of infragravity wave generation on a plane beach (slope 0.01) by nonlinear interaction of two swell components with frequencies and deep-water incidence angles of 0.09 Hz, -25 ° and 0.11 Hz, -30 °. The forced, shoreward propagating infragravity wave with the difference frequency 0.02 Hz is nearly resonant in shallow water and strongly amplified — dashed line. While the incident swell components are dissipated through breaking, the forced infragravity wave is released as a free wave, reflects from the beach seaward — solid line. Well outside the surf zone the weakly depth dependent outgoing free wave is much more energetic than the incoming forced wave. (Herbers et al., 1995a, figure 2a)

(Van Rijn, 2011). Another explanation of this phenomenon can be found in (Herbers et al., 1995a, his references Bowen (1978); Symonds (1982)), stating that slow oscillations in the wave setup associated with variations of the breakpoint location of incident swell wave groups can also drive infragravity waves. An assessment of the surfbeat mechanism is beyond the scope of this project.

Bound or free LF wave can amplify in an open basin, even if the length of the bound wave does not exactly match a resonant wave length of the basin (Van der Molen, 2006).

Finally, bound LF waves can can release as LF waves as well due to discontinuities in bathymetry and geometry (Van der Wel, 2011, his reference Bowers 1977).

Free LF energy can have remote, even transoceanic sources. This is likely when an observed low-energy swell is combined with a directionally narrow, shoreward propagating infragravity wavefield (Herbers et al., 1995a). Herbers et al. (1994, 1995a,b); Reniers et al. (2010) have assessed the relative importance of free waves with respect to bound waves. Herbers et al. (1995a) found that infragravity motions observed in depths of 8–200 m comprise both forced waves that are accurately predicted by second-order nonlinear wave theory (Equation A.6) and — usually more energetic — free waves radiated from shore (Herbers et al., 1995b). Furthermore, as the infragravity wavefield is likely to be directionally broad compared to the carrying swell, it is expected to be trapped to shore through refraction, as discussed above (Herbers et al., 1995a). However, for highly energetic wave climates the incident bound LF waves can be expected to dominate.

A.2 Velocities and pressure profile along the vertical

Surface waves induce a current in the water of which the nonuniform vertical profile is given by the following formulae, (Journée and Massie, 2001b).

$$u_x = \hat{\zeta}\omega k_{\mathrm{x}} \frac{\cosh\left(k(h+z)\right)}{\sinh(kh)} \cos(\vec{k}\binom{x}{y} - \omega t) \tag{A.9a}$$

$$u_y = \hat{\zeta}\omega k_{\mathrm{y}} \frac{\cosh\left(k(h+z)\right)}{\sinh(kh)} \cos(\vec{k}\binom{x}{y} - \omega t) \tag{A.9b}$$

$$u_z = \hat{\zeta}\omega \frac{\sinh\left(k(h+z)\right)}{\sinh(kh)} \sin(\vec{k}\binom{x}{y} - \omega t) \tag{A.9c}$$

In case of shallow water ($kh \to 0$), the horizontal velocities at the bottom are nonzero and nearly uniform over depth. The induced velocities are then approximated by the formulae below.

$$u_x = \hat{\zeta}\omega \frac{k_{\mathrm{x}}}{kh} \cos(\vec{k}\binom{x}{y} - \omega t) \tag{A.10a}$$

$$u_y = \hat{\zeta}\omega \frac{k_{\mathrm{y}}}{kh} \cos(\vec{k}\binom{x}{y} - \omega t) \tag{A.10b}$$

$$u_z = \hat{\zeta}\omega \left(1 + \frac{z}{h}\right) \sin(\vec{k}\binom{x}{y} - \omega t) \tag{A.10c}$$

When forces on a vessel are calculated using panel theory, the pressures and veloicities on these panels are based on these vertical profiles.

A.3 Reflection parameters

Considering a harbour geometry one must appropriately model the breakwaters and beaches. The reflection off these boundaries can be approximated and subsequently put in the numerically imposed boundaries, e.g. in Triton.

Please note that Triton uses an instantaneous reflection parameter since it is a time-domain model. In the formulae below, however, $C_{\mathrm{R}} \equiv |\frac{H_{\mathrm{r}}}{H_{\mathrm{i}}}|$, i.e. the reflection ratio is a fraction of the reflected and incident wave heights, inherently spectral quantities. It is noted this discrepancy must be evaluated more thoroughly. The formulae below do however serve as a rough estimation of the reflection coefficients which calibration must provide more applicable values.

The reflection ratio of a wave reflected by a rubble mound breakwater is given by Muttray et al. (2006, Eq.7)

$$C_{\mathrm{R}} = \left(1.3 + 3d\frac{2\pi}{L_0}\right)^{-1} \tag{A.11}$$

Alternatively, Equation A.12 (Verhagen et al., 2009) can be used, involving the breaker parameter ξ and a roughness coefficient γ_{f} depending on the type of breakwater armour.

$$C_{\mathrm{R}} = \tanh(a\xi_{\mathrm{m\text{-}1,0}}^{b}) \tag{A.12a}$$

$$\text{with } a = 0.167\left(1 - \exp(-3.2\gamma_{\mathrm{f}})\right) \tag{A.12b}$$

$$b = 1.49(\gamma_{\mathrm{f}} - 0.38)^2 + 0.86 \tag{A.12c}$$

The reflection ratio of a beach can be estimated using the relation below.

$$C_{\mathrm{R}} = 0.1\xi^2 \tag{A.13}$$

Appendix B

Description of physical research

Physical model research considering berth A and its berthing properties has been performed at the Hydraulics Laboratory of the Hydraulics, Water Resources and Environment Division of the University of Porto's Faculty of Engineering (FEUP). The basin used is 28 by 12 meters large and at maximum 1.20 m deep.

A physical model study of the northern breakwater considering its overtopping has also been performed (Veloso Gomes et al., 2009) but will not be treated in this chapter.

B.1 Phases and starting points

Two phases are distinguished, shown in Figure B.1. Although the figure illustrating phase 1 does display the northern breakwater, this phase used an empty basin with only the berthing lay-out represented. Further starting points of the phase 1 model used by Rosa-Santos are listed below.

1. Froude scaling with a geometric scaling factor of 1:100.
2. A simplified geometry: the northern breakwater was not represented.
3. Uniform water depth with bottom level at CD-16 m.
4. A dissipating beach installed in the wave tank with a slope of approximately 14%, having some correspondence with the actual beach (Rosa Santos, 2012b).
5. Colinear, head-on waves, using a Jonswap spectrum with peak enhancement factor $\gamma = 3.3$.
6. Approximately 600 waves for each performed simulation.
7. Linearized and calibrated mooring line and fender stress-strain (σ,ϵ-) relations (refer to Rosa Santos et al., 2010a).
8. 65 t breaking strength of mooring lines (Rosa Santos et al., 2009), 640 kN (Rosa Santos et al., 2008b).

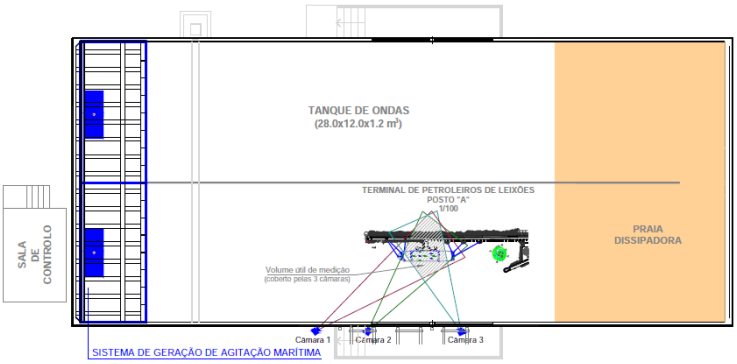

(a) Phase 1

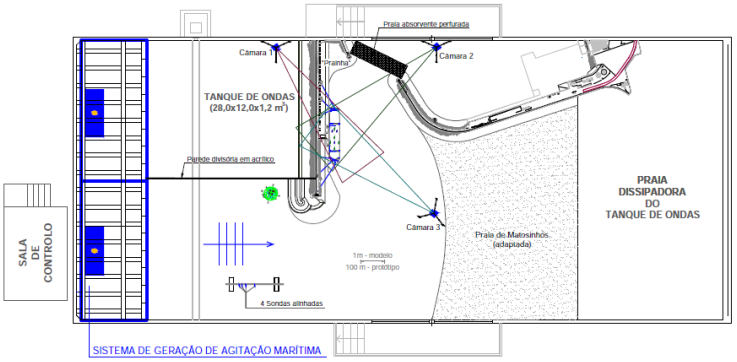

(b) Phase 2

Figure B.1: Overview of physical modeling phases (from Rosa Santos, 2010)

During phase 1, vessel motions were recorded using Qualisys as well as an in-house developed stereoscopic vision system. Whereas Qualisys uses three infrared cameras, the latter uses two normal video cameras and is developed and tested to be used for prototype measurements (Malheiros et al., 2009).

Phase 2 does include the harbour lay-out to a certain extent. During this phase a porous/absorbent object was put at the entrance to the inner harbour basin to reduce reflections and thus to mimic the harbour basin that was not completely incorporated. During this phase, overtopping over and transmission through the breakwater were not reproduced correctly.

B.2 Tested conditions

Rosa Santos has performed extensive physical research, comprising various wave conditions. Tests included irregular sea states with incident significant wave heights of 1.0, 1.5, 2.0 and 2.5 m during phase 1 and 3.0 and 4.5 m during phase 2. Primary waves were defined using a Jonswap spectrum, bound waves were then superposed as will be discussed below.

It was not intended to reproduce a particular storm or selected wave conditions since prototype motions measurements were not available (Rosa Santos, 2012b).

The effect of the tidal state has also been investigated. Moreover, mooring alternatives were physically studied, altering the lay-out (usual/asymmetrical versus recommended/symmetrical, see Figure B.3), the pretension forces on the breast lines (increasing from 10–12 t to 25–27 t) and the friction coefficient (increasing from 0.11–0.13 to 0.45–0.48).

Due to a lack of time not all test have been analyzed or published on yet. Table B.1 shows the various tests published on and references to the relevant articles.

B.3 Reflection absorption of the wavemaker

The wavemaker at the Hydraulics Laboratory of FEUP includes dynamic wave absorption (Malheiros et al., 2009) to absorb reflected waves and to minimize basin-induced eigenwaves. The efficiency of the absorption is frequency dependent, as shown in Figure B.2. Note that the frequency axis is on model scale, using Froude scaling and the applied geometrical scale (1:100) these frequencies must be divided by 10 to obtain prototype values (Van der Wel, 2011).

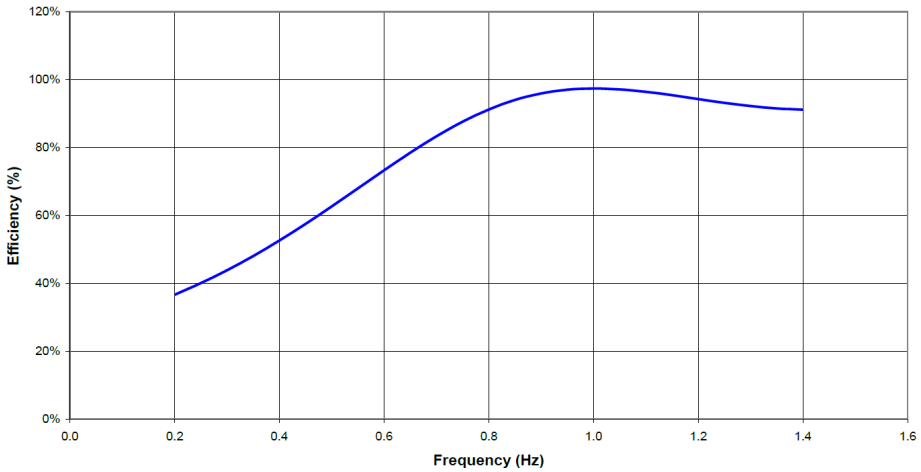

Figure B.2: Efficiency of dynamic wave absorption (Rosa Santos, 2010, p.440)

B.4 Inclusion of bound waves

FEUPs wavemaker (like many others) is based on linear wave theory. Therefore, when simulating shallow to intermediate waters it is required to apply a bound wave compensation to reduce spurious free long waves in the wave basin. These spurious secondary waves are similar in amplitude to the bound waves, but 180 ° out of phase. If not reduced, they will propagate in the basin causing interference patterns and results will be distorted.

The wavemaker at FEUP is designed by HR Wallingford and this bound wave compensation is introduced directly by the system; the user does not have access to the code used for this purpose (Rosa Santos, 2012b).

Table B.1: Conditions tested in physical model phases of which results are discussed in literature, with a: Rosa Santos et al. (2010b,c), b: Rosa Santos et al. (2008b), c: Rosa Santos et al. (2009), d: Rosa Santos et al. (2010a), e: Rosa Santos (2012c) and f: Malheiros et al. (2009). Low and high friction denote a coefficient of 0.11–0.13 and 0.45–0.48 respectively; base pretension denotes 100–120 kN on all lines while during extra pretension tests 245–265 kN was imposed on the breast lines; MSL and HT denote CD+2 m and CD+4 m respectively. The tests discussed in Section B.7 and on which the validation in Chapter 3 is based are indicated in blue.

Phase		1														2			
Layout		Symmetrical		Asymmetrical															
Pretension		Base								Extra						Base		Extra	
Friction		Low						High		Low				High		Low	High	Low	High
Waterlevel		MSL	HT	MSL		HT		MSL		MSL		HT		MSL		HT			
H_s [m]		2.0		1.5	2.0	1.5	2.0	1.5	2.0	1.5	2.0	1.5	2.0	1.5	2.0	3.0			
T_p [s]	8	a,b	a,b				a,b												
	10	a,b	a,b	c	c	c	a,b,c	d	d	c,d	c,d,f	c	c	d	d	a,d	a,d	a,d	a,d
	12	a,b	a,b	c	c	c	a,b,c	d	d	c,d,e	c,d	c,f	c	d	d	a,d	a,d	a,d	a,d
	14	a,b	a,b	c	c	c	a,b,c	d	d	c,d,e	c,d	c	c	d	d	a,d	a,d	a,d	a,d
	16			c	c	c	c	d	d	c,d,e	c,d	c	c	d	d	a,d	a,d	a,d	a,d
	18			c	c	c	c	d	d	c,d	c,d	c	c	d	d	a,d	a,d	a,d	a,d
	20															a,d	a,d	a,d	a,d

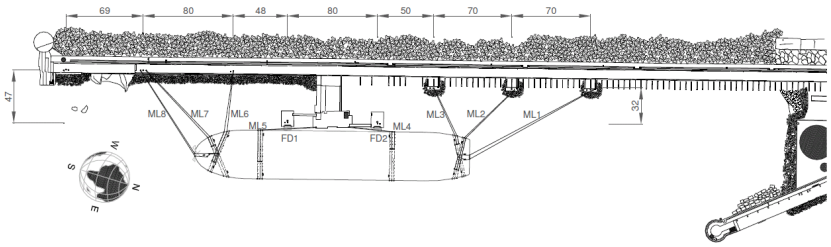

(a) Asymmetrical — usual — mooring line lay-out at berth A

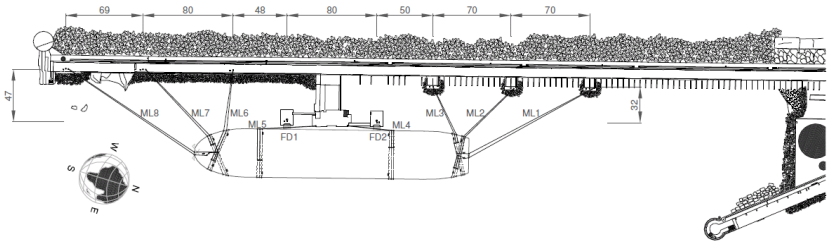

(b) Symmetrical mooring lay-out based on OCIMF (2008)

Figure B.3: Overview of physical modeling phases (from Rosa Santos et al., 2008b); mooring lines 3 and 6 are breast lines, lines 4 and 5 are spring lines

All physical tests performed in the mentioned studies apply this bound wave compensation (Rosa Santos, 2012a). The LF wave conditions generated were not calibrated (Rosa Santos et al., 2010b).

Recently, Rosa Santos has been able to deduce the imposed paddle positions and waterlevel elevation from this system and has reconstructed the timeseries.

B.5 Design vessel

The design vessel is based on the biggest oil tanker that regularly demands Leixões oil terminal berth A. The maximum loading condition, at 105,000 DWT, is assumed. The models natural periods of oscillation, displacement, draft and metacentric height were calibrated by placing concrete weights. These and other main characteristics of the modelled vessel are given in Table B.2.

B.6 Mooring lay-out

The characteristics of the mooring lines and fenders are given in Table B.3, distinguishing the usual, asymmetric lay-out and the symmetric lay-out based on recommendations by OCIMF (2008) as shown in Figure B.3.

B.7 Analysis of used data

The tests of which data was acquired and, therefore, on which the validation in this thesis will be based used the following conditions.

- Phase 1 set-up.

Table B.2: Design vessel properties (Rosa Santos et al., 2010a)

Characteristic	Full-scale	Model scale
Displacement [kg]	122,714,000	119.721
Length overall [m]	245.1	2.451
Length between perpendiculars [m]	236.0	2.360
Beam [m]	43.0	0.430
Maximum draft [m]	14.1	0.141
Vertical position of the centre of mass [m]	12.5	0.125
Transverse metacentric height [m]	5.83	0.058
Longitudinal position of the centre of buouyancy from stern [m]	128.4	1.284
Roll natural period in deep water conditions [s]	12.5	1.250

Table B.3: Characteristics of mooring lines and fenders, length at full scale and model-scale stiffness taken from Rosa Santos et al. (2008b); angles read from figure B.3 with 0 ° pointing starboard and increasing counterclockwise; asy and sym denoting asymmetrical and symmetrical lay-out respectively

Mooring line/Fender ID	length full scale [m]	stiffness model [N/m]	approximate angle [°]
ML1	150	16.9	-60
ML2	90	34.1	-44
ML3	55	49.8	+23
ML4	55	49.3	+84
ML5	82	34.4	-87
ML6	82	34.3	-7
ML7	90	34.1	+43
ML8; asy	167	6.5	+56
ML8; sym	120	31.0	+32
DF1	n.a.	86.5	n.a.
DF1	n.a.	85.6	n.a.

- MSL (CD+2 m).
- The asymmetrical mooring layout.
- Extra pretension on breastlines.
- Low friction coefficient on fenders.
- Waves of $H_s = 1.5$ m and with periods T_p of 12, 14 and 16 s.

These test are indicated in blue in Table B.1.

Imposed waterlevel elevations

Recently, Rosa Santos has been able to regenerate the timeseries of paddle deflection and hereby imposed waterlevel elevation used in the physical model tests. As discussed in Section B.4, these were calculated within the wavemakers control and this was previously essentially regarded as a black box.

The spectra of these timeseries, see Figure B.4 and Table B.4, show an incredible amount of LF energy, both compared to expectations based on Longuet-Higgins and Stewart (1962) and Van Dongeren et al. (2003) and to the discussion of the incorporation of LF energy given in Rosa Santos (2010). According to Rosa Santos (2012b), the issue is the evaluation of the spurious free long waves. These should be subtracted from the timeseries, i.e. the large amount of LF energy in the timeseries is due to the additional long wave energy to account for spurious waves.

Table B.4: Low-frequency waves imposed during tests

Test condition T_p [s]	12	14	16
$H_{m0,lf}$ [m]	0.46	0.68	0.93
$T_{p,lf}$ [s]	103.9	119.4	136.5

The determination of LF components by the wavemakers system will not be elaborated upon further in this thesis. It is however important to conclude that the imposed wave record contains this amount of LF energy.

Measured waterlevels

In the spectra of the measured wave elevation (of which that obtained from probe 1 are given in Figure B.5) it can be recognized that some distinctive peaks occur. With the basins second transversal eigenmode at 22.2 mHz and the third lateral eigenmode at 6.6 mHz some of these peak might be attributable to basin oscillations. It is remarkable however that this latter mode has only low energy content at probe 4.

Furthermore, other peaks cannot be related to eigenmodes this easily, e.g. the peak found at 16 mHz. Taking into account Appendix C, this might be due to the realization of the spectrum and the variation of LF energy around the expected value. However, imposed waterlevel elevations seem to contain sufficient energy throughout the LF range, as shown earlier.

Table B.5 shows that the overall amount of LF energy is significant for all performed tests. Mainly based on this observation, it is concluded that eigenmodes

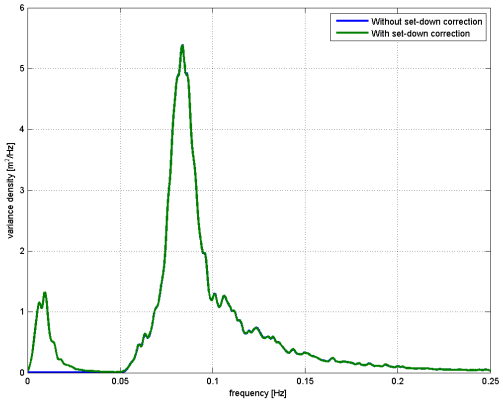

(a) $T = 12\,\mathrm{s}$

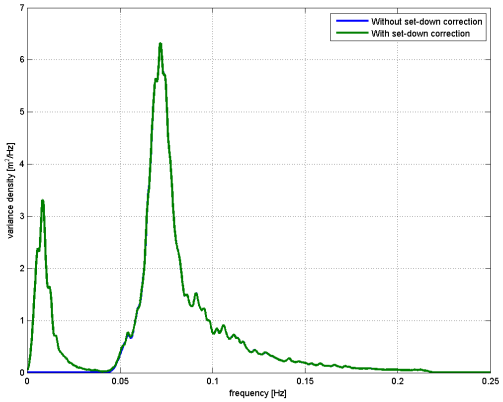

(b) $T = 14\,\mathrm{s}$

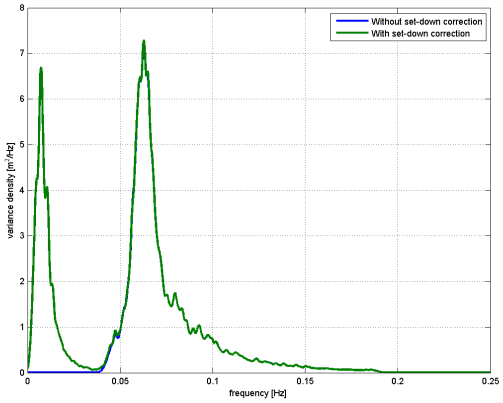

(c) $T = 16\,\mathrm{s}$

Figure B.4: Spectra of imposed waterlevel elevation without (blue) and with (green) bound wave compensation

Table B.5: Mean measured wave properties at probes 1–4

Test condition T_p [s]	12	14	16
$H_{s,full}$ [m]	1.56	1.60	1.58
$T_{p,full}$ [s]	12.27	13.71	15.92
$T_{m\text{-}1,0,full}$ [s]	12.09	14.20	16.72
$T_{m0,1,full}$ [s]	10.69	12.29	14.06
$T_{m0,2,full}$ [s]	10.24	11.66	13.28
$H_{s,lf}$ [m]	0.17	0.23	0.27
$T_{p,lf}$ [s]	122.36	73.46	68.76
$T_{m\text{-}1,0,lf}$ [s]	80.91	75.63	85.96
$T_{m0,1,lf}$ [s]	59.60	54.07	50.88
$T_{m0,2,lf}$ [s]	53.00	48.97	45.35

are expected to have occurred during the measurements but unambiguously determining the modes triggered is difficult.

Measured ship motions

The spectra and significant amplitudes of the vessel's six degrees of freedom are given in Figure B.5. It can be noted that surge (with an amplitude of approximately 1.2–1.6 m) has been the most critical during these measurements, as PIANC dictates surge motion should not exceed 2.5 m.

As expected, it can be seen that the horizontal motions (surge, sway and yaw) are typically in the LF wave range, 40–100 s, whereas the vertical motions are coinciding with the primary wave frequency range. In the roll and heave spectra two ranges of high energy can be noted, possibly indicating two natural frequencies of the moored vessel system in these degrees. The surge spectrum shows two ranges of high energy as well, indicating a correlation with the spectra of sway and yaw, which both have a relatively narrow response range. The coupling of these latter three motions is not unusual and often occurs as an effect of the interaction with the fender.

Measured mooring forces

The forces along the mooring lines and on the fenders result in the spectra shown in Figure B.6. It can be seen that the spring lines, mooring line 4 and 5, show a relatively high correlation to surge and sway whereas other mooring line force spectra show the narrow energy peak that occurs in the yaw motion. This can be expected through the mooring line layout, as the spring lines are close to the center of and almost perpendicular to the vessel.

The forces along the stern, breast and head lines are typically 110–330 kN. Forces along mooring line 1, relatively parallel to the mooring structure, are typically low whereas the mooring lines most perpendicular to the vessel experience typically higher forces. The fenders experience forces of approximately 800 kN.

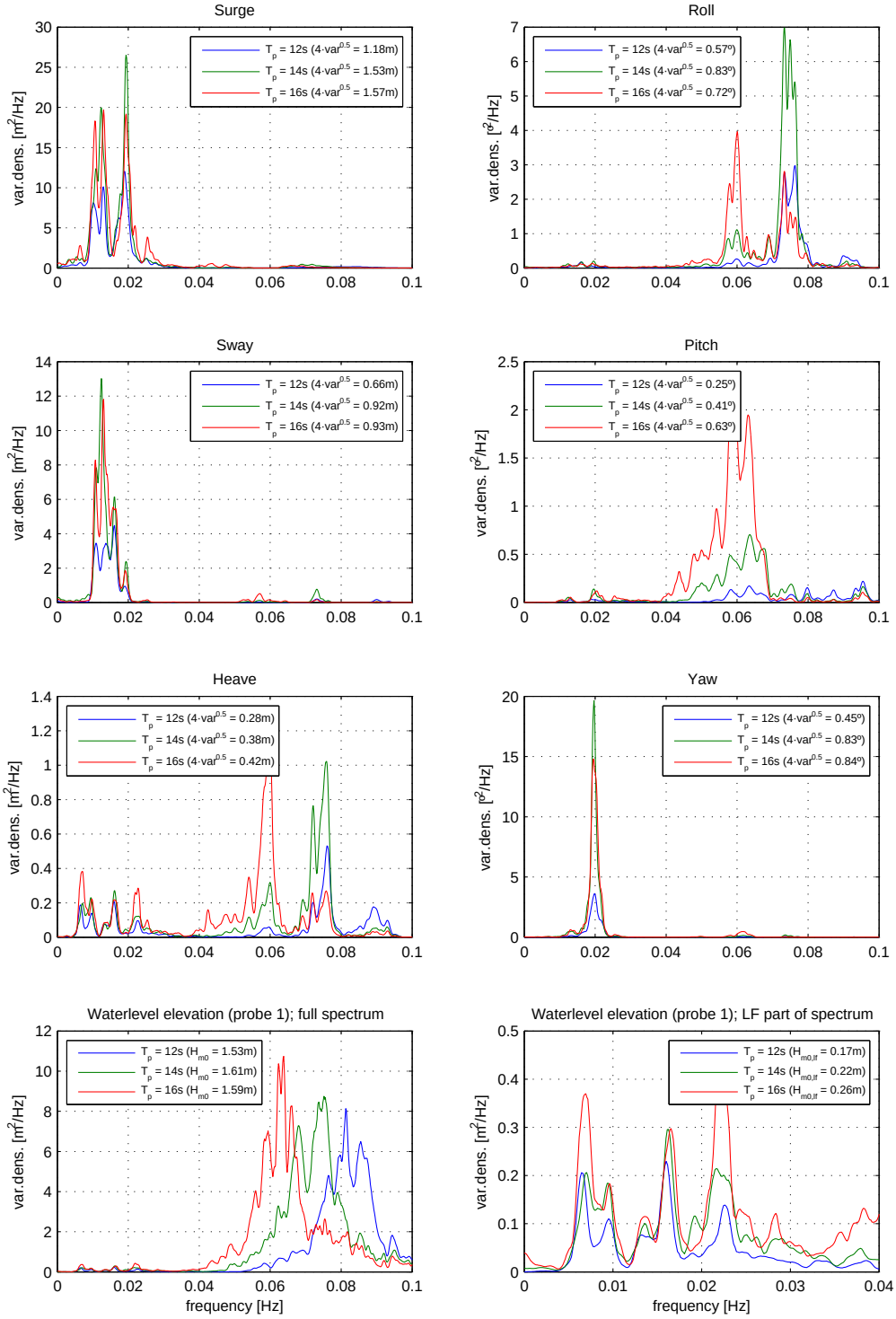

Figure B.5: Vessel motion spectra and spectra of waterlevel elevation at probe 1

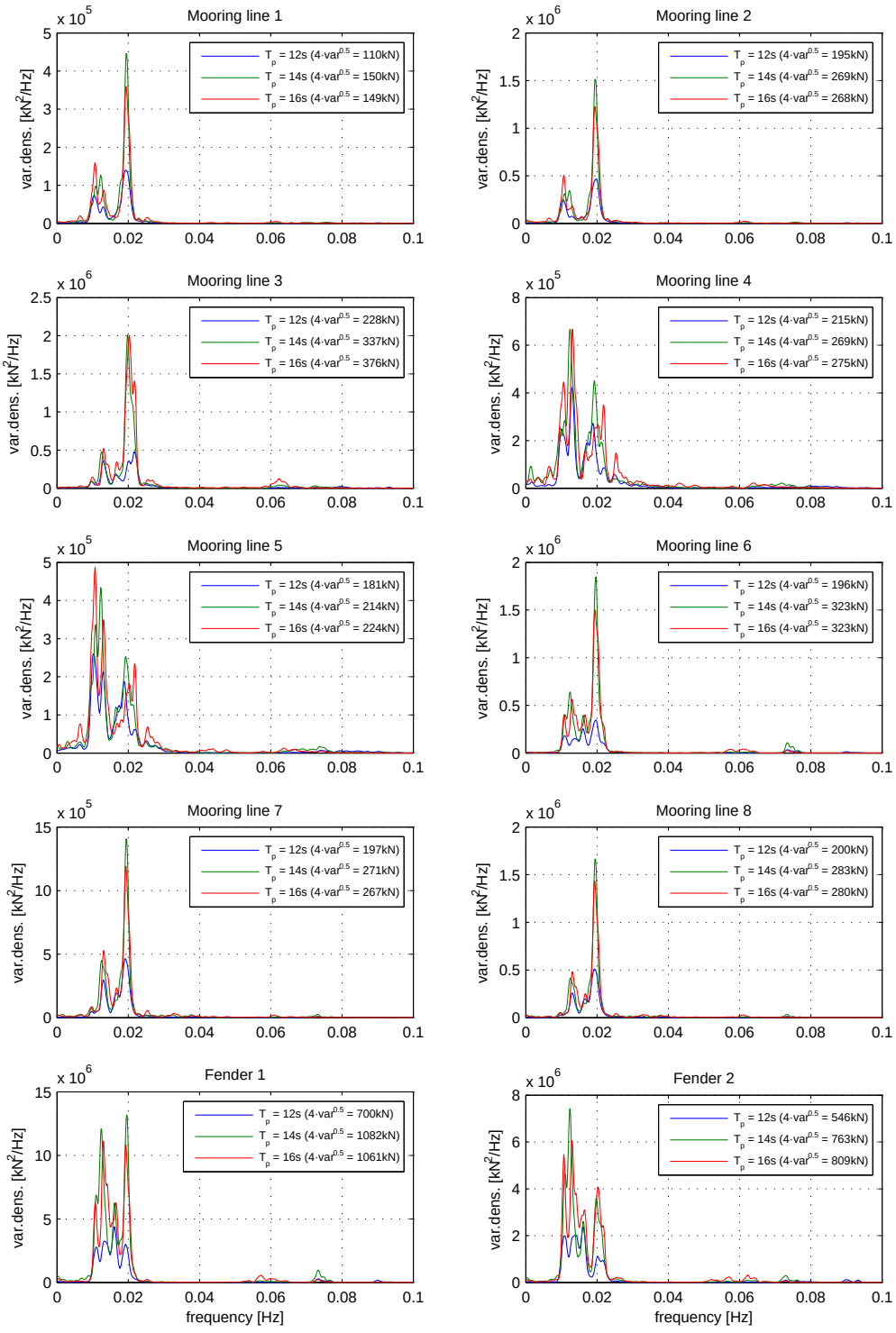

Figure B.6: Forces measured during phase 1; mooring lines 4 and 5 are the spring lines, mooring lines 3 and 6 are the breast lines

Appendix C

Uncertainty due to spectrum realization

When interpreting a generated timesignal, or any measured timesignal for that matter, one must be aware of the uncertainty within the obtained spectrum. For a sound statistical analysis a very long timeseries is beneficial, comprising innumerous waves for all frequencies of interest. A wave record long enough ensures that an amplitude-modulated wave appears in the spectrum-domain with its mean amplitude, which is representative. If a wave record is too short, possibly only the low-amplitude or the high-amplitude part of the modulated wave are included, thus resulting in a non-representative spectral energy. The energy found at the LF tail of the spectrum is therefore highly dependent on the time frame recorded or, equivalently, on the phases of wave components.

Generally, simulations are of a length in which higher-frequency waves occur sufficiently often to assure a consistent spectrum realization, e.g. 2 hours. For a sound statistical analysis for LF waves, however, these simulations are too short and they suffer a great uncertainty. In case of bound LF waves, this uncertainty is due to the realization of the carrier waves directions and phases determining the bound wave energies and phases.

To quantify this, an analysis has been made using colinear waves with varying seeds for the phase generation.

T_p	14 s
H_m0	1.5 m
h	18 m
T	7000 s
dt	0.1 s
$DSPR$	0
phase seed	1–250

It can be seen the primary wave spectrum is generated each realization with sufficient consistency, the energy content differs insignificantly and wave periods are low-spread. The LF wave spectrum however, is found to be very phase-dependent. Wave heights vary by approximately 5%. The wave periods $T_\mathrm{m0,1}$ and $T_\mathrm{m0,2}$ are reasonably consistant too, varying approximately 5%. The peak period and $T_\mathrm{m\text{-}1,0}$ are higly varying and therefore an unusable indicator.

Table C.1: Variance in a spectrum realization: full spectrum — 0–0.25 Hz

		mean	min	max	σ	$\frac{\sigma}{\text{mean}}$[%]
$H_{\text{m0,full}}$	[m]	1.5014	1.5006	1.5026	0.0003	0.000
$T_{\text{p,full}}$	[s]	13.999	13.972	14.028	0.0053	0.038
$T_{\text{m-1,0,full}}$	[s]	13.9	13.4	15.3	0.33	2.4
$T_{\text{m0,1,full}}$	[s]	11.911	11.899	11.928	0.0049	0.041
$T_{\text{m0,2,full}}$	[s]	11.343	11.337	11.351	0.0025	0.022

Table C.2: Variance in a spectrum realization: LF part of spectrum — 0–0.04 Hz

		mean	min	max	σ	$\frac{\sigma}{\text{mean}}$[%]
$H_{\text{m0,lf}}$	[m]	0.096	0.083	0.11	0.0052	5.5
$T_{\text{p,lf}}$	[s]	606	50	$7.0{\cdot}10^3$	966	159
$T_{\text{m-1,0,lf}}$	[s]	300	191	617	68	23
$T_{\text{m0,1,lf}}$	[s]	88	76	104	5.1	5.9
$T_{\text{m0,2,lf}}$	[s]	68.3	60.5	78.6	2.9	4.4

Moreover, when going into the spectrums individual values it is found that the deviation is enormous, see Figure C.1, showing a relative standard deviation of approximately 100% between 0–0.04 Hz. Although the mean value coincides with the imposed variance density, an individual realization differs significantly, as is plotted. Peaks found in one realization contain only low energy or possible do not contain any energy in other realizations. This LF range especially is relevant as it coincides with harbouroscilations as well as (moored) vessel eigenfrequencies.

This analysis shows that the interpretation of peaks within the spectrum, aimed at identifying harbour eigenmodes or — in case of force or motion spectra — mooring system eigenmodes, is not as straightforward as one might think. A certain peak might well be an eigenmode. It might however also be an artifact due to the finite-time realization of the spectrum using random phases. Equally, an eigenmode might be underestimated due to a low energy in the input wave at its frequency.

An obvious solution of this problem is longer simulation periods but this results in impractical simulation times. Another solution might be to evaluate the response over input per frequency rather than merely the output. Alternatively, a careful selection of a realization to ensure a small deviation from the imposed spectrum or at least to ensure that certain frequencies are well included might be worthwhile.

An elaboration of the above is beyond the scope of the present thesis.

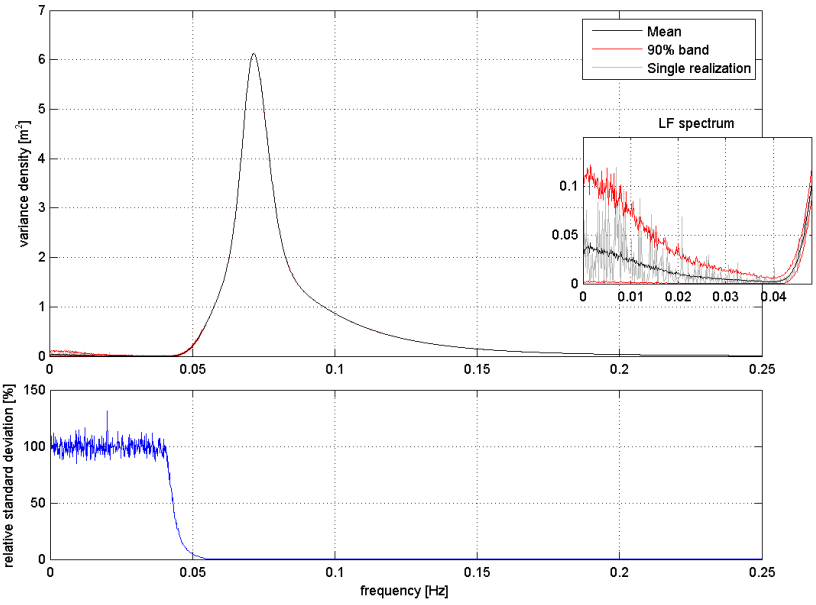

Figure C.1: The spread of the input spectrum due phase realizations using different seeds and the subsequent relative deviation, based on 250 realizations

Appendix D

Additional remarks

This chapter is written in cooperation with Dr.eng. Paulo Rosa Santos [1] and was added to this report after submission, August 2013. It presents an elaboration of discussions in earlier chapters and includes additional considerations, in response to remarks made by Paulo Santos during and after my project. It thus refines the earlier version of this report and offers a more complete discussion to successive students or other readers. I want to express my thanks to Paulo Santos for taking the time and effort to point out and solve incompletenesses in this report.

D.1 Low-frequency energy in the wavemaker's signal during physical studies

In Sections 3.2.1 and B.7, it is recognized that the low-frequency waveheight $H_{\mathrm{m0,lf}}$ measured at the probes 1–4 during physical model study phase 1, is high compared to theory. Moreover, frequency analysis of the wavemaker's displacement too, shows high low-frequency contents.

It must be noted that the displacements considered in Section B.7 are not the actual wavemaker displacements. They are the displacements solely based on the incident wave, not taking into account active reflection correction. The actual displacements are not recorded. Using the given time series on the numerical model boundary straight-forwardly will thus not reproduce the physical model test and has therefore not been pursued.

The high amount of low-frequency energy in the physical model is striking. Generally, an explanation to occurrence thereof in a scale model basin might be found in one of the following origins of low-frequency energy.

- Spurious low-frequency (free and bound) waves, occurring when using 1^{st} order wave steering.
- Evanescent waves along the basin length.
- Reflections at the wavemaker boundary, occurring when no use is made of an active reflection correction (or numerical equivalent).

[1] University of Porto, Portugal; Faculty of Engineering (FEUP)

- Resulting from a conservative approach, accounting for free low-frequency waves (e.g. trapped edge waves or low frequency waves of distant origin).

The present study does not identify the cause of the high amount of low-frequency energy, for this further research is needed. It seems beneficial for future interpretation to know if the wavemaker's code is indeed conservative.

Another suggestion is to assess the other sources of low-frequency energy (e.g. trapped edge waves) present at Leixões. Although, based on Herbers et al. (1995b) a first estimation of incident free low-frequency energy is to be in the order of 3–4% of the primary wave energy, a better resemblance to the physical tests might be found.

D.2 Schematization issues

D.2.1 Reflection at wave maker

In the validation, Chapter 3, the reflection of wave energy at the numerical boundary within Triton needs to simulate the reflection at the wavemaker during physical model tests.

The wavemaker used is calibrated both at HR Wallingford and, after installation, at FEUP. Before each study, wave conditions are calibrated in the experimental facility as well. A set-down compensation is used to avoid a "laboratory effect" that results from the use of first order wave generation theory in shallow waters when reproducing sea states. The reflection of the wavemaker is indicated in Section B.3.

Within Triton, two parameters can be used to adapt the implementation of the incident wave boundary: ω_{implicit} and ω_{explicit}. The latter is a measure of how strict the boundary condition is imposed, with $0 < \omega_{\text{explicit}} < 1$. The lower the value, the less strict it the boundary is, the more it is open or permeable for outgoing waves. Using a value of 0.10 for this parameter in simulations during this thesis, an open boundary for outgoing waves has been pursued. This value has been chosen using experience from Deltares' Triton users. The numerical implementation this boundary, like most within Triton, uses an indicative wave period, for which the primary, peak wave period had been chosen. The evaluation of this boundary condition using wave splitting was not possible within this project. Nor can the percentage of energy that is still re-reflected be indicated in comparison to the physical model's wavemaker.

Overall, both the numerical and physical boundary show a similar property, to be absorbent most perfectly for a certain frequency and gradually more reflective for other frequencies.

D.2.2 Basin length

Some reference figures and data in articles were misinterpreted. In these figures, the wavemaker is included in the basin length. Therefore, the dimension of the distance between wave maker paddles and beach (water line) is not 27 m or 28 m (full tank length) but 20 m. The comparison with a numerical model performed in Chapter 3 (Figure 3.6), should have been executed taking into account the appropriate basin length.

Considering a 20 m basin length and taking into account the 14% beach slope, longitudinal eigenmodes can be expected at 3.1, 6.3, 9.4 and 12.5 mHz. An evaluation of the measured spectrum indicates the occurrence of these eigenmodes; especially the 2nd and 3rd mode, some measurements show the 1st mode. This enforces the note that eigenmodes complicate the interpretation of model results.

D.2.3 Reflection coefficients

The reflection coefficients used have not been calibrated during my project. Rather, I have used the calibration executed by Van der Wel (2011) on the measurements of the Phase 2 physical model. He has found that the coefficients of 2% for the beach and 40% for breakwater boundaries provide the most accurate results.

Measurements performed by Rosa Santos (2010), however, show a wave index of 14.3% at the beach, indicating that the primary wave energy in my model results is likely to be underestimated. The coefficients he has specified, having a value of 12–18% should be adopted.

Futhermore, whereas the 40% reflection coefficient is appropriate for breakwater slopes, it is not for quay walls. The choice of this coefficient value is a result of earlier set-ups, trying to get the numerical model running. For the sections of the harbour basin in which a vertical wall is present, higher coefficients should be adopted. In order to adress the occurrence of seiching, a numerical model with basin coefficients of 100% was used. In this thesis report it is noted that the appropriate amount of reflected wave energy should be between the results of my two models, having 40% and 100% reflection respectively. In this way, an adequate interpretation of the results has been persued, without the need of running a new model (for which here was no time).

Within Triton, reflection coefficients are set along with a normative wave period (as mentioned in Section 2.2.4). For this, the primary (i.e. peak) wave period was chosen. It is commonly assumed by Triton developers that the reflection ratio will be higher for waves of different periods or oblique waves. Regarding low-frequency waves, it is expected that 100% of the wave energy will be reflected. However, literature is not available. Boeyinga (2010) has used Triton and found that the wave phase of the reflected wave is modeled incorrectly (refer to his thesis report for details). Again, the validation of this reflection coefficient could not be included in this thesis scope. It is assumed that the reflection of low-frequency waves is approximately 100%; which is in the same order as in reality.

D.2.4 Beach slope

The beach within the case study as well as the validation study is schematized to minimize the chance of Triton becoming instable: therefore the beach has not been modeled up to the waterline. Rather, the computational domain ends at approximately 2 m waterdepth. Modeling beaches is possible in Triton using a set-up module. However, this easily induces instabilities. Futhermore, the beach modeled and used in the validation (Chapter 3) is too steep. The beach modeled in the case study, however, was based roughly on admiralty charts and its schematization serves the purpose of this study.

D.2.5 Berth schematization in Harberth and Quaysim

The schematization of the berth (fenders, mooring line positions etc.) within this project is based on available literature (tables, AutoCAD drawings and other figures) as well as set-up files I received from Martin van der Wel. It is well possible this set-up is not perfect. It has been attempted to include viscous damping by altering the quadratic damping values; however no more accurate results were found. Furthermore, the fender reaction force could be included in Quaysim.

Regrettably, a full calibration of the berth characteristics using data provided in Rosa Santos (2010) could not be performed due to the limited amount of time available. The calibration performed in this MSc project is limited and the increase in parameters is high. To obtain more accurate results in the future, further calibration is recommended with an emphasis on the added value of a numerical method combined with physical measurements.

D.3 Resonance patterns

A tool was developed and used to get some insights in the resonant patterns, beyond evaluating individual spectra.

The schematization used has a drawback since the waterlevel used was CD+0 m, coinciding with the level of lowest astronomical tide at the Port of Leixões. This is another result of the process in which making the model work was the first challenge and an adaptation to a different waterlevel was not dealt with until later. It is straightforward to apply but as rerunning the model takes approximately a week, the time constraint of this project did not allow this.

The waterlevel does have accordance to reality and taking into account this low water level (discussed in Section 6.3), an evaluation was possible. After all, the intent was to obtain insights in the occurance of seiching, nodal patterns and to see if boundary conditions were imposing seiches.

The results show similarity to Avilez Valente (2007). I do acknowledge the accordance of one of the modes found with the hypothetical resonant area of Campos Morais and Abecasis (1978). However, I think there are many other modes with equal relevance to berth A. The conclusions in Chapter 7 perhaps should pronounce this more clearly.

Another conclusion is that it is of importance to model the harbour entrance correctly (Section 7.2.2). The given schematization was used to overcome instability issues of the numerical model, often occurring at the corners of the boundary segments. The shape of this entrance is however important due to the proximity to the berth.

Bibliography

P. Avilez Valente. Estacção de passageiros e complexo náutico do molhe sul do porto de Leixões. October 2007.

H.J. Bakkenes. Observation and seperation of bound and free low-frequency wave in the nearshore zone. MSc Thesis, Delft University of Technology, June 2010.

H.B. Bingham. A hybrid Boussinesq-panel method for predicting the motion of a moored ship. *Coastal Engineering*, 40:21–38, 2000.

J. Boeyinga. Boussinesq-type wave modelling in port applications. MSc Thesis, Delft University of Technology, May 2010.

M. Borsboom, N. Doorn, J. Groeneweg, and M. Van Gent. A Boussinesq-type wave model that conserves both mass and momentum. 2000.

J. Bosboom and M.J.F. Stive. *Coastal Dynamics I.* VSSD, January 2012.

C. Campos Morais and F. Abecasis. Storm surge effects at Leixões. *Fourteenth Coastal Engineering Conference, Copenhagen*, 1978. Memória n. 503, Tema D.

W.E. Cummins. The impulse response function and ship motions. *Symposium on ship theory at the Institut für Schiffbau der Universität Hamburg*, October 1962. Report 1661.

J. De Bont, W. Van der Molen, J. Van der Lem, H. Ligteringen, D. Mülestein, and M. Howie. Calculations of the motions of a ship moored with moormaster units. *Coastal Engineering*, 2010.

M.P.C. De Jong and M.J.A. Borsboom. Shallow water initiative (HAWAI), WP1: Nearshore wave modelling. Report, January 2007. H4643.

M.P.C. De Jong, M.J.A. Borsboom, J.A.M. De Bont, and B. Van Vossen. Evaluation of an extended operational Boussinesq-type wave model for calculating low-frequency waves in intermediate depths. *Proceedings of the ASME 2011 30th International Conference on Ocean, Offshore and Arctic Engineering OMAE2011*, 06 2011.

M.P.C. De Jong, M.J.A. Borsboom, and J. Dekker. Calculation of low-frequency waves in shallow water and comparison to common practice in diffraction methods. In *Proceedings of the 28th International Conference on Ocean, Offshore and Arctic Engineering*, 2009.

Z. Demirbilek, A. Zundel, and V. Panchang. Benchmark tests for harbor wave agitation models. *Ports symposium*, 2010.

T.H.C. Herbers, S. Elgar, and R.T. Guze. Infragravity-frequency (0.005-0.05 Hz) motions on the shelf. part I: Forced waves. *Journal of Geophysical Oceanography*, 24:917–927, April 1994.

T.H.C. Herbers, S. Elgar, and R.T. Guze. Generation and propagation of infragravity waves. *Journal of Geophysical Research*, 100:24,863–24,872, December 1995a.

T.H.C. Herbers, S. Elgar, R.T. Guze, and W.C. O'Reilly. Infragravity-frequency (0.005-0.05 Hz) motions on the shelf. part II: Free waves. *Journal of Geophysical Oceanography*, 25:1063–1079, June 1995b.

L.H. Holthuijsen. *Waves in Oceanic and Coastal Waters*. Cambridge University Press, 2007.

J.M.J. Journée and W.W. Massie. *Introduction in Offshore Hydromechanics (OT3600)*. Delft University of Technology, March 2001a.

J.M.J. Journée and W.W. Massie. *Offshore Hydromechanics*. Delft University of Technology, first edition, January 2001b.

H. Ligteringen and J. Moes. Motions of moored ships in long waves. 2001.

M.S. Longuet-Higgins and R.W. Stewart. Radiation stress and mass transport in gravity waves, with application to 'surf beats'. April 1962.

P. Malheiros, P. Rosa Santos, A. Paulo Moreira, P. Costa, F. Veloso Gomes, and F. Taveiro Pinto. Robust and real-time motion capture of rigid bodies based on stereoscopic vision. *3rd international conference on integrity reliability and failure, Porto/Portugal, 20-24 July 2009*, July 2009. Ref: S0215_ P0429.

M. Muttray, H. Oumeraci, and E. Ten Oever. Wave reflection and wave run-up at rubble mound breakwaters. *International Conference on Coastal Engineering, San Diego*, 2006.

OCIMF. *Mooring Equipment Guidelines*. Witherby Seamanship International, 3 edition, 2008.

J.A. Pinkster. *Low frequency second order wave exciting fores on floating structures*. PhD Thesis, Delft University of Technology, 1980.

A.J.H.M. Reniers. Lecture coastal dynamics 2. Collegerama, May 2010. CT4309 lecture May 18th, Delft University of Technology.

A.J.H.M. Reniers, M.J. Groenewegen, K.C. Ewans, S. Masterton, G.S. Stelling, and J. Meek. Estimation of infragravity waves at intermediate water depth. *Journal of Coastal Engineering*, 57:52–61, 2010.

P. Rosa Santos. *Análise da Interacção de Navios com Dispositivos de Acostagem e Amarração. Estudo em Modelo Físico do Posto "A" do Terminal de Petroleiros do Porto de Leixões*. PhD Thesis, Faculdade de Engenharia da Universidade do Porto, July 2010.

P. Rosa Santos. Data leixoes model test. Personal communication, March 2012a.

P. Rosa Santos. Leixoes model test. Personal communication, June 2012b.

P. Rosa Santos. Notes. Personal communication, February 2012c.

P. Rosa Santos, F. Veloso Gomes, F. Taveira Pinto, J. Alfredo Santos, Guedes Soares, N. Fonseca, A. Paço, A. Paulo Moreira, P. Costa, P. Malheiros, and E. Brógueira Dias. Influence of the use of mooring line pretension on the behaviour of a moored oil tanker. *Proceedings of International Conference in Ocean Engineering, ICOE 2009, IIT Madras, Chennai, India, 1-5 Feb. 2009*, February 2009.

P. Rosa Santos, F. Veloso Gomes, F. Taveira Pinto, and E. Brógueira Dias. Influence of the friction forces at the ship-fenders' interface on the behaviour of a moored oil tanker. *Proceedings on the Third International Conference on the Application of Physical Modeling to Port and Coastal Protection*, 2010a.

P. Rosa Santos, F. Veloso Gomes, F. Taveira Pinto, and E. Brógueira Dias. Physical Modelling of Leixões Oil Terminal - Portugal. 2010b.

P. Rosa Santos, F. Veloso Gomes, F. Taveira Pinto, and E. Brógueira Dias. Physical Modelling of Leixões Oil Terminal - Portugal. Presentation, Port Infrastructure Seminar 2010, June 2010c.

P. Rosa Santos, F. Veloso Gomes, F. Taveira Pinto, E. Brógueira Dias, and H. Guedes Lopes. Improving operational conditions at Leixões oil terminal - Portugal. *COPEDEC VII, 2008, Dubai, UAE*, 2008a.

P. Rosa Santos, F. Veloso Gomes, F. Taveira Pinto, C. Guedes Soares, N. Fonseca, J. Alfredo Santos, A. Paulo Moreira, P. Costa, and E. Brógueira Dias. Physical model study of the behaviour of an oil tanker moored at a jetty. *Coastlab08 - Bari*, 2008b.

S.E. Sand. Long waves in directional seas. *Coastal Engineering*, 6:195–208, 1982.

C. Soler. Swell and wave-groups at Saldanha bay. MSc Thesis, Delft University of Technology, April 2006.

A.J. Van der Hout. Two-dimensional wave breaking in Triton, comparison of computational results to physical scale model measurements of waves breaking on an artificial surf reef. Report, March 2009. H5150.20.

W. Van der Molen. *Behaviour of moored ships in harbours*. PhD Thesis, Delft University of Technology, 2006.

W. Van der Molen. Mike 21 - Harberth — moored ship response modelling in harbours, April 2007a.

W. Van der Molen. Triton - Harberth — moored ship response modelling in harbours, April 2007b.

W. Van der Molen, M. Rossouw, D. Phelp, K. Tulsi, and L. Terblanche. Innovative technologies to accurately model waves and moored ship motions. In *Science real and relevant conference*. CSIR, 2010.

W. Van der Molen and I. Wenneker. Time-domain calculation of moored ship motions in nonlinear waves. *Coastal Engineering*, 2008.

M. Van der Wel. The behaviour of a moored oil tanker in the port of Leixões, Portugal. MSc Thesis, Delft University of Technology, May 2011.

A. Van Dongeren, A. Reniers, and J. Battjes. Numerical modeling of infragravity wave response during DELILAH. *Journal of Geophysical Research*, 108(C9), September 2003.

G. Van Oortmerssen. *The motions of a moored ship in waves.* PhD Thesis, Delft University of Technology, 1976. Publication No. 510.

L.C. Van Rijn. *Principles of Fluid Flow and Surface Waves in Rivers, Estuaries and Oceans.* Aqua Publications, 2011.

F. Veloso Gomes, F. Taveira Pinto, E. Brogueira Dias, and H. Guedes Lopes. Two-dimensional physical modeling of the northern breakwater of Leixões harbor, Portugal: Case study. *Journal of waterway, port, coastal, and ocean engineering*, November 2009.

F. Veloso Gomes, F. Taveira Pinto, and P. Rosa Santos. Berthing characteristics and the behaviour of the oil terminal of Leixões Harbour, Portugal. 2005.

H.J. Verhagen, K. d'Angremond, and F. Van Roode. *Breakwaters and closure dams.* VSSD, 2nd edition, 2009. ISBN 978-90-6562-173-3.

I. Wenneker. Wave forces on moored ships - coupling of boussinesq-type wave model Triton with diffraction model DELMULTI (TUD). Report, November 2006. WL|Delft Hydraulics H4585.20.

I. Wenneker and M. Borsboom. A novel cartesian cut-cell approach, 2005.